Transport Properties and Modification of the Flux Pinning in Single Crystal Bismuth Cuprate Superconductors

by

Janet Ann Cutro

B.S.. Rensselaer Polytechnic Institute (1979)
M.S., Columbia University (1984)

Submitted to the Department of Physics
in partial fulfillment of the requirements for the degree of

Doctor of Philosophy

at the

MASSACHUSETTS INSTITUTE OF TECHNOLOGY

June 1997

Signature of Author .....
Department of Physics
6 May 1997

Certified by .....
Terry P. Orlando
Professor of Electrical Engineering
Thesis Supervisor

Certified by .....
Mildred S. Dresselhaus
Institute Professor
Thesis Supervisor

Accepted by .....
Professor George F. Koster
Chair, Departmental Committee on Graduate Students

Transport Properties and Modification of the Flux Pinning in Single Crystal Bismuth Cuprate Superconductors

by

Janet Ann Cutro

Submitted to the Department of Physics
on 6 May 1997, in partial fulfillment of the
requirements for the degree of
Doctor of Philosophy

Abstract

Two studies on single crystals of the high temperature cuprate superconductor $Bi_2Sr_2CaCu_2O_8$, performed in 1988 and 1990-91 respectively, are presented in their original timeframe. Results are reviewed in a present day context at the end of the thesis.

Detailed measurements of the angular and temperature dependence of the magnetic field-induced resistive transition are reported. Resistance is observed in the sample for small values of applied field ($\approx$ 100 Oe) even at low current densities ($<$ 10 A/cm^2). This suggests that the resistive transition does not directly reflect the upper critical field of the superconductor, but is complicated by flux-flow effects. The angular dependence of the resistive transition cannot be fit by any standard model for anisotropic fields in superconductors, and anisotropic ratios as large as 50 are found for fields applied perpendicular and parallel to the **c**-axis of the crystal, indicating a large difference in the viscosity for flux motion in the two directions. Current-voltage characteristics for fields applied parallel to the **c**-axis are linear for low currents at temperatures above 77 K. The shape remains relatively unchanged until the field is within about 20° of the a-b planes, where there is a sudden change to more threshold-like behavior.

It has been suggested that the extreme anisotropy of the strongly layered high-temperature superconductors poses intrinsic limitations to the critical current, arising from a short correlation length along the vortex axis (pancake vortices). In the second set of experiments, this possible materials limitation is addressed through the introduction of irradiation induced defects. A comparative study is presented of the flux pinning in single crystal $Bi_2Sr_2CaCu_2O_8$ before and after irradiation by H^-, He^-, Ne^-, and Ar^+ at incident energies in the MeV range. Irradiation conditions were chosen to hold the total calculated vacancy production by each ionic species approximately constant, and the crystals were sufficiently thin as to assure nearly complete penetration. A significant increase in the pinning energy is found after irradiation by the heavier ions, while light ion (H^-, He^+) irradiations result in pinning energies comparable to those of unirradiated crystals. As a result of higher pinning energies, critical currents were observed to persist at markedly higher temperatures and fields. The Ar^+ dose dependence of the magnetization J_c exhibits a temperature independent but field dependent peak, which is indicative of a classical matching effect. The inter-vortex spacing at the matching field is not consistent with an estimate of defect spacing based upon a model of damage by vacancy pro-

duction. It is suggestive rather of the presence of a lower density of relevant defects which act as effective pinning centers, such as would result from a small fraction of high energy recoil events producing damage cascades, rather than simple vacancies. Calculations of recoil energy spectra quantitatively support the existence of cluster-like defects in heavier ion irradiated samples. The dominance of low energy recoils in primary knock-on spectra of H^+ and He^+, however, implies a predominance of point defects in light ion irradiated samples. Spatially extended defects can interact with longer sections of the vortices and lead to a higher pinning energy.

Thesis Supervisor: Terry P. Orlando
Title: Professor of Electrical Engineering

Thesis Supervisor: Mildred S. Dresselhaus
Title: Institute Professor

Acknowledgments

The length of this project, with its many interruptions and leaves of absence, makes it especially challenging to thank everyone properly or in the right order. I have had three outstanding advisors while at MIT, but I feel it fitting to start at the end and work my way backwards. I would first like to thank Professor Terry Orlando for taking on an unexpected student, and having the patience to allow me to continue to work intermittently on this thesis, in spite of many indications that it would never be finished. I greatly admire Terry for his uncommon and obvious sense of integrity, as well as his surreptitious sense of humor, and agile mind. He also has a gift for teaching classes with a flair worth missing sleep for, with or without the bribery of doughnuts. I am deeply grateful to him for taking my chapters from under his office door, and will always remember his kindness to me.

Professor David Rudman was the principle advisor of this project from its inception through the experimental stages, publications, and the beginning of the writing of this thesis. I thank him for countless acts of generosity in the process of introducing me to the unfamiliar field of high-temperature superconductivity. His support was instrumental to the success of this project. He also taught me that legendary feats of experimental and presentational prowess are possible, armed with a Coke (caffeinated, of course) in one hand. I am sincerely grateful to Dave for continuing to advise this project through my leaves of absence and even from Colorado after his departure from MIT. It was also my unexpected pleasure to be properly congratulated by the old gang after my defense, because Dave made sure they heard the news.

To my collaborators at what is now Lucent Technologies, I express my heartfelt thanks. Drs. Bruce van Dover, Lynn Schneemeyer and Alice White opened their facilities to me and gave generously of their time, expertise and encouragement. They are experimentalists extraordinaire and extraordinary people. I especially thank Bruce for sharing his lab and carefully developed experimental techniques with me, and Lynn for her unsurpassed skills in growing state-of-the-art crystals. I thank Dr. Mike Gyorgy for the use of his balance and vibrating

sample magnetometer. Bruce and Lynn also gave me patient instruction and help with tiny fragile samples and huge resilient frustrations. P.S. The roses were absolutely beautiful!

Prior to the beginning of this project, the late Professor David Adler made it possible for me to come to MIT, and advised and supported me through the beginning of my academic career in amorphous silicon research. I thank him for lively political discussions, the best group dinners to ever dishevel a Chinese restaurant, and a host of other contributions to my professional and personal well-being. His door was always open and his enthusiastic devotion to physics never interfered with his attention and affection for the people around him.

Professors Millie Dresselhaus and Takashi Imai carefully read and commented upon this thesis, and offered criticism which was of great value to me. I also thank Millie especially for rejoining my thesis committee after my long absence from MIT, and simply for setting an outstanding example for women in science.

At the very beginning of this project, Dr. Jenh-Yih Juang patiently taught me how to do "magnet runs". Juang was always calm and encouraging, and he tried to teach me not to worry about the small stuff. I've almost got it, Juang.

At the Francis Bitter National Magnet Lab, I would like to thank Bruce Brandt, Larry Rubin and Jean Morrison for helping to make magnet runs go as smoothly as possible.

I especially thank Professor George Koster for providing me with funding from the Physics Department during some crucial transitions in my student career, and Peggy Berkowitz and Pat Solakoff for their willing and kind help throughout.

Over the time I spent at MIT, I greatly enjoyed the company of my fellow students and friends. It has been many years, and so at the risk of leaving someone out I thank, for discussion and companionship, Mary Matthiesen, Katy Barmak, Kevin Coffey, Lenny Rubin, Dave Dombrowski and John Kucera. Before that, in Dave Adler's group I benefited greatly from

the knowledge and camaraderie of Pat Cullen, Camille Fuleihan, Jean-Jacques Hajjar, Angela Odoardi (Mickunas), and my very dear and current friend, Kathleen Tokuda.

Outside of MIT, I have been warmly supported by the love of my family and friends, especially my parents, grandparents, brothers, Ann L., my cousin Lucy, Lin-Lin, Nancy, Anabel, Tom Y., Margie W., Edmund, Lee W., Ellen, Sandi, Greta, Ron, Dora, Koren, and my newest and most delightful relatives, Nina, Moriah, and Galen. I thank my old friends from RPI, IBM and Columbia who have checked in on me from time to time, and who are not mentioned by name only because the list would fill a new chapter. To my new friends, especially those who share my house with me, thanks for enduring my recent preoccupation with the completion of this project, to the exclusion of things like keeping the electricity on.

I give special thanks to the very dear Ted Scourtis, who has waited patiently for the imminent return of romance and music to our lives.

I owe a profound debt of gratitude to my best friend and fellow ex-IBM engineer, Dr. Anne Balant-Campbell, who never let me doubt that I would graduate.

Finally to my grandmother, the late Risa Marinacci, whose love and encouragement I will carry with me always, I dedicate this work.

Contents

List of Figures

List of Tables

Chapter 1

Introduction

1.1 Preview and Chronology

In this thesis I present two sets of experiments upon single crystals of the high temperature cuprate superconductor $Bi_2Sr_2CaCu_2O_8$. The first is a preliminary investigation of the angular dependence of the magnetic field-induced resistive transition. This study was done in 1988, about one year after the famous "Woodstock for Physicists" APS meeting. Our results showed an astounding lack of flux pinning in this material above 77 K, and an anisotropic in-field transition that could not be explained with any conventional model of the upper critical field.

The second set of experiments was not begun until late in 1990, after an extended leave of absence by the author from MIT. In the interim, the scientific community had recognized that the high temperature superconductors did not conform to the conventional understanding of the superconducting state in a magnetic field. Furthermore, it had become clear that low critical currents posed serious limitations to the possible applications of these materials. In an attempt to address these limitations, the second set of experiments examines the modification of the flux pinning in $Bi_2Sr_2CaCu_2O_8$ after being subjected to irradiation by various ions. These experiments were completed in 1991. Now in the Spring of 1997, following another extended leave of absence by the author, this thesis is presented.

1.2 Background and Preliminary Results

The discovery by Bednorz and Muller[1] in 1986 of the high temperature cuprate superconductor $La_{2-x}Ba_xCuO_4$ astonished the scientific community and marked the beginning of a new era in superconductivity. Once it was firmly established that the critical temperature in this compound was indeed near 35 K, researchers around the world raced to synthesize related compounds that might show superconducting behavior at even higher temperatures. In 1987, critical temperatures were measured[2] in $YBa_2Cu_3O_7$ around 90 K, for the first time exceeding the boiling point of nitrogen. The possibility of using liquid nitrogen as a coolant, because of its low cost and ready availability, opened the door to widespread commercial applications of the high temperature superconductors.

When it was found by chemical substitution that the copper oxide planes in the structure of $YBa_2Cu_3O_7$ were responsible for superconductivity, the development of a whole family of copper-oxide type II superconductors quickly followed. The bismuth based compounds, $Bi_2Sr_2CaCu_2O_8$ and $Bi_2Sr_2Ca_2Cu_3O_{10}$, with critical temperatures of 90 K and 110 K respectively, were first synthesized[3–5] in 1988. Still higher critical temperatures were found in the thalium cuprates, including $Tl_2Ba_2CaCu_2O_8$, $TlBa_2Ca_2Cu_3O_9$, and $Tl_2Ba_2Ca_2Cu_3O_{10}$, with critical temperatures of 105 K, 115 K, and 125 K, respectively. The highest critical temperature measured to date is 134 K, in the compound $HgBa_2Ca_2Cu_3O_8$.

Intense efforts to understand the physics of the high temperature (HTC) superconductors began immediately, and proceeded interactively with equally concentrated efforts to develop the technological potential of these materials. High critical temperatures and estimated upper critical fields exceeding 100 T pointed to enormous potential for applications. Some limitations were however evident. Unlike conventional metallic superconductors, the new materials are ceramics. This poses tremendous technological obstacles to the process of making wires from them. In addition, the current carrying capacity was quickly found to be disappointingly low. As the first experiments of this thesis were beginning, this second limitation was known to exist in La_2BaCuO_4 and $YBa_2Cu_3O_7$. Little or nothing was then known about the properties of the subsequently discovered cuprate superconductors. Single crystals of $YBa_2Cu_3O_7$, however, were

known to have higher critical currents than bulk polycrystalline samples, which was explained by the presence of "weak links" at the grain boundaries.

In the simplest terms, the motivation in 1988 for the first set of experiments of this thesis was to investigate the properties of what was then the newest member of the cuprate family of HTC superconductors. Structurally, these materials were known to be composed of layers, with $Bi_2Sr_2CaCu_2O_8$ having the highest anisotropy of the cuprates yet discovered. We set out to measure the detailed anisotropy of the upper critical field of single crystal $Bi_2Sr_2CaCu_2O_8$, knowing only the behavior of the resistance as a function of temperature in zero field, and preliminary results of the x-ray structural analysis.

Our results, while extremely interesting, were not consistent with the conventional definition of the upper critical field. In conventional superconductors, the upper critical field is defined as the field which returns the sample to 50% of its extrapolated normal state resistance, and the shape of the transition is relatively step-like. In $Bi_2Sr_2CaCu_2O_8$ we find instead an onset of resistance across the sample for fields as low as 100 Oe, even for currents as small as 10 A/cm^2 and for temperatures as low as 77 K. The shape of the transition depends strongly on the orientation of the crystal in the magnetic field, leading to anisotropy ratios as large as 50 for fields applied parallel and perpendicular to the copper oxide planes respectively. Unlike $YBa_2Cu_3O_7$, the detailed anisotropy of the transition can not be fit by the conventional effective mass model of the upper critical field. We attribute the observed field-induced resistance to flux flow* of an unprecedented magnitude. The anisotropy reflects large differences in the flux-flow viscosity with respect to crystal directions, and is not interpreted to be a direct measure of the upper critical field. The angular dependence of the transition suggests that flux motion is impeded when crossing planes. Measurements conducted several degrees below 77 K** reveal the appearance of more threshold-like behavior, especially for fields oriented near the planes, perhaps implying the existence of finite critical currents at lower temperatures.

*This early interpretation of flux flow was later found to be more correctly described in terms of "flux creep".

**In 1988 commercial He flow cryostats were not available and it was significantly more difficult to conduct measurements over a wide temperature range. It was, however, relatively easy to obtain data a few degrees below 77 K by pumping on liquid nitrogen.

These results suggested a vortex state with virtually no pinning at temperatures above 77 K, while some degree of pinning was indicated at lower temperatures. Palstra[6] later found the in-field resistivity to be activated over several orders of magnitude. Critical currents in $Bi_2Sr_2CaCu_2O_8$ were soon widely recognized to be insignificant at temperatures above 20 K and fields greater than a few hundredths of a tesla. As these effects were observed in single crystals in this case, the extremely low critical currents could not be attributed to weak links at grain boundaries, but had to be accepted rather as an intragranular phenomenon. Thus, in addition to the materials processing problems posed by weak links, a more intrinsic obstacle to high-temperature superconductor (HTC) applications had appeared.

Evidence for unusual vortex behavior was in fact not limited to results of $Bi_2Sr_2CaCu_2O_8$, but was soon found to exist to varying degrees in all of the HTC cuprate superconductors, including both single and non-single crystal materials. It was noted that these effects became more pronounced with the degree of structural anisotropy of the material, which accounted for the huge magnitude of the dissipation measured in $Bi_2Sr_2CaCu_2O_8$. Attention rapidly focused on the fundamental physics of vortex behavior in high temperature superconductors, and especially as to how it might differ from the traditional theories of flux motion. Simultaneously, efforts intensified to find a way to improve critical currents in light of these developing new theories.

1.3 Motivation for Irradiation Experiments

In the approximately two years between the first and second sets of experiments of this thesis, the consideration of vortex dynamics in the new superconductors generated much study and controversy. Disagreement focused in particular on the origin of an "irreversibility line" in the H-T plane, below which irreversible vortex behavior was observed, and above which vortices seemed to move virtually freely. There was general agreement that there were several key features distinguishing the HTC cuprates from conventional superconductors, namely, the high

critical temperatures, short coherence lengths, and weak interplanar couplings. The first two of these clearly act to diminish effective flux trapping by defects and therefore the critical current. The observation of the thermally activated resistivity and the relaxation of the magnetization pointed to a mechanism of "thermally activated flux creep" to account for the large dissipation at high temperatures. Flux (Bitter) decoration experiments and the response of the vortices to forced oscillation in a magnetic field suggested that the vortex lattice "melts" at some temperature which is well below T_c, perhaps in fact at the irreversibility line. While anisotropy had to be folded into these models, completely new models were emerging, including the flux liquid theories of Nelson[7–9] and the pancake vortices proposed by Clem,[10] that considered the anisotropy to be fundamental in determining HTC vortex behavior. This raised the issue of a possible intrinsic limitation to the critical current, arising alternatively because vortices are either very short or very flexible, in either case due to the weak interplanar couplings.

As these models were in the early stages of development, in the absence of an established theory it was hoped that these limitations could be overcome by the introduction of extrinsic defect structures by various methods. Irradiation of conventional superconductors had been shown under some conditions to result in an increase in the critical current density. This technique is particularly appropriate to the high temperature superconductors with respect to easily creating defects of a size comparable to the short coherence lengths, which was expected to result in a higher pinning force on the vortices.

Because of its extreme anisotropy, $Bi_2Sr_2CaCu_2O_8$ is an excellent system in which to consider whether weak interplanar couplings pose intrinsic limitations to the enhancement of flux pinning. Yet, in the hope of more quickly achieving technologically viable results, irradiation efforts prior to the work at hand had focused almost entirely on $YBa_2Cu_3O_7$. Ironically, it was soon to be shown that the bismuth system was far more amenable to solutions of the weak link problem in non-single crystal applications than any of the other high temperature cuprates. Specifically, after the current work was underway, it was reported that long wires and tapes had been fabricated of $Bi_2Sr_2CaCu_2O_y$ and $Bi_{2-x}Pb_xSr_2Ca_2Cu_3O_y$, some having critical current densities in excess of 10^5 A/cm^2 at 4.2 K and 30 T.[11] Because of these results, atten-

tion was about to refocus on the bismuth cuprates that continues up to the present. Today, the development of the technology of long superconducting tapes is dominated by the bismuth cuprates, because low angle grain boundary processing methods in these materials enable high critical currents. The irradiation method is very relevant to the improvement of critical currents in these tapes at higher temperatures and fields. As the current work began, however, interest in $Bi_2Sr_2CaCu_2O_8$ was at an all time low.

Experiments of irradiation in superconductors have historically been very empirical, due to the complex nature of the damage induced by this method. Furthermore, many of the early irradiation experiments on high temperature superconductors suffered from a lack of clean, reproducible starting materials, widely varying ranges of penetration depths in the samples, and the omission of same-sample comparisons before and after irradiation. Success in significantly raising the critical current in high temperature superconductors was not achieved until 1989, when van Dover et al.[12] reported a factor of 100 improvement to 6 x 10^5 A/cm^2 at 77 K and 0.9 T of a $YBa_2Cu_3O_7$ single crystal after irradiation with fast neutrons. In 1990 similar improvements were obtained[13,14] after irradiation by 10^{16} protons/cm^2 at an incident energy of approximately 3 MeV. The use of high quality single crystals was key in achieving and analyzing these results. In addition, these experiments demonstrated that the conveniently available technology of ion beams could produce results similar to the comparatively scarce and somewhat more hazardous method of neutron irradiation. Yet, in spite of such promising results of significantly increased critical currents at 77 K and 1 T, the irreversibility line was found to be unaffected. The relevant pinning centers were agreed to be point defects.

In the only irradiation experiment on single crystal $Bi_2Sr_2CaCu_2O_8$ prior to the current work, Palstra[15] found that the introduction of defects by He^- in the MeV range produced only slight increases in the pinning energy. He concluded that the physics of pinning in this material is dominated by the high anisotropy, leading to a short correlation length along the vortex axis.

1.4 Results of Irradiation Experiments

In the second set of experiments, we consider the question of whether the irreversibility line is a structural feature, or if it may be moved by the introduction of irradiation induced defects. Since proton irradiation was successful in improving the critical current of single crystal $YBa_2Cu_3O_7$, one of our experiments is to irradiate $Bi_2Sr_2CaCu_2O_8$ under similar conditions. However, since He^+ irradiation was unsuccessful in single crystal $Bi_2Sr_2CaCu_2O_8$, which, by analogy to proton irradiation is likely to produce primarily point defects, we also examine the generation of defect structures other than point defects to act as pinning centers. This approach recognizes the importance of the role of anisotropy and investigates the possibilities of pinning longer segments of the vortices with extended defects. To this end we conduct a systematic study, comparing critical currents before and after irradiation by H^+, He^+, Ne^+, and Ar^+.

We extend and improve upon previous efforts in the following ways. Uniform, homogeneous, reproducible single crystals are used, in order to isolate, as much as possible, the effects of induced damage from the intrinsic defect structure. Same-sample comparisons are made to rule out complications arising from sample variations. The crystals are sufficiently thin as to assure nearly complete penetration of the ions through the sample. In order to more clearly resolve the effects of flux pinning of the different types of defects introduced by various ions, the irradiation conditions are chosen to hold the total vacancy production by each ionic species approximately constant.

We present results of the in-field resistive transition, transport current-voltage characteristics and magnetization J_c as a function of temperature, before and after irradiation by H^+, He^+, Ne^+, and Ar^+ of single crystal $Bi_2Sr_2CaCu_2O_8$. We have further examined the Ar^+ dose dependence in our crystals of the magnetization J_c at different temperatures. The effects we see for light ion irradiation are consistent with results reported by Palstra et al.,[15] that is, fluences up to 4×10^{14} cm^{-2} He^+ at 2 MeV on single crystals produced only modest improvements in the pinning energy. After irradiation by the heavier (Ne^+ and Ar^+) ions, however, we observe significant increases in the pinning energies and critical currents, which we attribute to the introduction of spatially extended defects. Arrhenius plots of the resistive transition show that

the activation energy changes by a factor of 2.3 for Ar^+ as opposed to only 1.45 for H^+. Our data imply that heavier ion irradiation, unlike light ion damage, results in an upward shift of the irreversibility line.

Transport J_c's show two to five-fold improvements after Ne^+ and Ar^+ irradiation but after irradiation by H^+ or He^+ the critical current either fails to improve or degrades. The shape of the current-voltage characteristic is concave upward, approaching linearity at higher temperatures and fields. Heavier ion irradiation suppresses the voltage for all measurement conditions and retards the transition to linear behavior. After light ion irradiation, however, the voltage developed at a given temperature, field and current is generally higher than in the unirradiated sample.

The magnetization J_c shows significant improvement after heavier ion irradiation as well. At low temperature the increases in J_c after irradiation by Ne^+ and Ar^+ are on the order of factors of two, roughly consistent with the improvements observed in transport. More impressively, a markedly decreased sensitivity to elevated temperature and field is evident after Ne^+ and Ar^+ irradiation, which is not observed after irradiation by H^+ and He^+. The temperature at which the critical current becomes immeasurably small ($< 10^4$ A/cm^2) is unaffected by light ion irradiation; for a field of 1 T critical currents diminish to zero above roughly 15 K - 20 K, whereas finite critical currents are measurable at temperatures as high as 30 K after heavy ion irradiation. This is consistent with the observed increases in the pinning energies and indicates that an upward shift in the irreversibility line occurs only for the case of the heavier ion damage.

We attribute the improved pinning in heavy ion irradiated samples to the presence of large or clustered defects resulting from damage cascades of high energy recoils of primary knock-on atoms. The dominance of low energy recoils in light ion bombardment, on the other hand, most probably results in a predominance of point defects, as was inferred for results of proton irradiation in $YBa_2Cu_3O_7$.[13,14] Due to the short correlation length along the vortices in $Bi_2Sr_2CaCu_2O_8$, the spatial extent of pinning centers is particularly important in effecting stronger defect-vortex interactions which lead to higher pinning energies. This is in contrast to results in the more three dimensional $YBa_2Cu_3O_7$ system, where point defects were found to

be effective pinning centers.

The Ar^+ dose dependence of the magnetization J_c exhibits a temperature independent peak, which is indicative of a classical matching effect, for which the average defect spacing is equal to the vortex spacing. A simple estimate of the defect spacing based upon a model of damage by vacancy production is far too low to account for the field dependence of the observed peaks. This is suggestive of the presence of a lower density of relevant defects which act as effective pinning centers, such as would result from a small fraction of high energy recoil events producing larger defects, rather than simple vacancies.

Calculations of recoil energy spectra quantitatively support the above supposition of cluster-type defects in heavier ion irradiated samples. The spectra for H^+ and He^+ are practically identical, showing a predominance of low energy recoils, whereas both Ne^+ and Ar^+ show a small but significant fraction of events occurring above 10 KeV. These higher energy events are known to induce recoil cascades and produce cluster-type damage in HTC layered superconductors, as compared to the low energy recoils which are more likely to produce point defects.[16,17]

These results demonstrate the potential to improve pinning in $Bi_2Sr_2CaCu_2O_8$ with spatially extended defects in order to overcome two-dimensional (pancake vortex) effects. Civale et al. have produced long columnar defects in $YBa_2Cu_3O_7$ by GeV Sn^- irradiation which illustrate this effect.[18] It is most likely that our ≈ 3 MeV Ne^+ or Ar^+ irradiation of $Bi_2Sr_2CaCu_2O_8$ would produce cluster-type defects rather than columnar defects (which require ionization energy loss rates exceeding 2 KeV/Å, i.e. incident energies at fractions of GeV). Increases in pinning have also been achieved using fast neutron irradiation,[19–21] a process which features a high proportion of high energy recoil events.[16] In conclusion, novel microstructures in $Bi_2Sr_2CaCu_2O_8$ can lead to increased vortex-defect interaction energies and thus higher critical currents at higher temperatures and fields.

In the past several years since these experiments were completed, the fundamental reexamination of the physics of vortices has led to a more integrated and detailed picture of vortex behavior in high temperature superconductors. Advances in the pinning of vortices have proceeded interactively with the increased understanding of new regimes of vortex behavior, as for

example in the case of columnar defects. At the end of this thesis, we discuss these advances, and place the work at hand in the present day context of continuing progress in flux pinning in high temperature superconductors.

1.5 Outline

The chronology of this thesis, as described in the first section, affects the order of presentation in the following way. Since the first set of experiments on the angular dependence represent some of the earliest results of $Bi_2Sr_2CaCu_2O_8$ available, they are presented before the literature review. In fact, they are part of the literature which motivated the second set of experiments. Therefore, Chapter 2 presents the results of the angular dependence of the magnetic field-induced resistive transition.

Chapter 3 reviews the relevant literature up to 1990-91, the time frame of the work at hand. It is divided into three parts, the first of which gives an overview of the literature that will be surveyed, and how the early work on angular dependence fits into this progress. The second section reviews early theories of vortex behavior in high temperature superconductors. Starting from a brief review of the traditional theory of vortices, models of thermally activated flux creep, vortex glass, flux liquid, and pancake vortices are surveyed. This section concludes with a discussion of the irreversibility line. The third section reviews irradiation in superconductors. First the main results of irradiation in conventional superconductors are summarized. The process of damage production by energetic particles is then briefly explained. Following this, the subject of irradiation in high temperature superconductors is introduced. Then, because very few results on $Bi_2Sr_2CaCu_2O_8$ were available, irradiation of $YBa_2Cu_3O_7$ is extensively discussed, leading to a specific examination of proton irradiation of single crystal $YBa_2Cu_3O_7$ at incident energies near 1 MeV. These experiments are closely related to the work of this thesis. Finally, the limited number of results of irradiation of thin films of $Bi_2Sr_2CaCu_2O_8$ are reviewed, concluding with the one single crystal experiment of Palstra.[15]

Chapter 4 describes the experimental procedures of the preparation and measurement of samples for irradiation. The reader is directed to the first section for a concise explanation of the design of this experiment and in particular to the flowchart of Figure 4.1. The next two sections describe the sample growth and handling procedures. Next, the methods of attaching electrical contacts and mounting the samples for measurement and irradiation are described. Following that is a detailed discussion of the measurement techniques and apparatus. Finally, the last section explains precisely how the irradiation conditions were chosen. Calculations of vacancy densities and damage profiles, which lead to the selection of equivalent damage doses are presented.

In Chapter 5 the results of the irradiation experiments are presented. The effects of irradiation upon the resistive transition, transport current voltage characteristics and the magnetization J_c are discussed. The implications of the Ar^+ dose dependence of the critical current with respect to defect structure are examined. The supposition of cluster-type defects in heavier ion irradiated samples is explored through the calculation of recoil energy distributions in $Bi_2Sr_2CaCu_2O_8$. In the final section we present the summary and conclusions of this work as they were understood at the time these experiments were completed. The reader is directed to this section for a concise synopsis of our results, rather than to the end of Chapter 6.

In Chapter 6 we review the continued progress in the field between the completion of our experiments and the presentation of this thesis. The work at hand is then placed in the context of these recent developments. This chapter does not contain a comprehensive summary of this work, (see Chapter 5) but focuses rather on those parts of it which relate to recent progress which has occurred since the completion of the experiments presented in this thesis.

1.6 References

1. J.G. Bednorz and K.A. Muller, Z. Phys. B **64,** 189 (1986).

2. M.K. Wu, J.R. Ashburn, C.J. Torng, P.H. Hor, R.L. Meng, L. Gao, Z.J. Huang, Y.Q. Wang, and C.W. Chu, Phys. Rev. Lett. **58**, 908 (1987).

3. H. Maeda, Y. Tanaka, M. Fukutomi, and T. Asano, Jpn. J. Appl. Phys. **27**, L209 (1988).

4. R.M. Hazen, C.T. Prewitt, R.J. Angel, N.L. Ross, L.W. Finger, C.G. Hadidiacos, D.R. Veblen, P.J. Heany, P.H. Hor, R.L. Meng Y.Y. Sun, Y.Q. Wang, Y.Y. Xue, Z.J. Huang, L. Gao, J. Bechtold, and C.W. Chu, Phys. Rev. Lett. **60**, 1174 (1988).

5. C.W. Chu, J. Bechtold, L. Gao, P.H. Hor, Z.J. Huang, R.L. Meng, Y.Y. Sun, Y.Q. Wang, and Y.Y. Xue, Phys. Rev. Lett. **60**, 941 (1988).

6. T.T.M. Palstra, B. Batlogg, L.F. Schneemeyer, and J.V. Waszczak, Phys. Rev. Lett. **61**, 1662 (1988).

7. D.R. Nelson, Phys. Rev. Lett., **60**, 1973 (1988).

8. D.R. Nelson, and S. Seung, Phys. Rev. B **39**, 9153 (1989).

9. D.R. Nelson, J. Stat. Phys., **57**, 511 (1989).

10. J.R.Clem, Phys. Rev. B **43**, 7837 (1991).

11. K. Heine, J. Tenbrink, and M. Thoner, Appl. Phys. Lett., **55,** 2441 (1989); N. Enomoto, *3rd Int. Conf. Supercon.*, Sendai, Japan, Nov. 1990.

12. R. B. van Dover, E. M. Gyorgy, L.F. Schneemeyer, J.W. Mitchell, K.V. Rao, R. Puzniak, and J.V. Waszczak, Nature (London) **342**, 55 (1989).

13. R. B. van Dover, E. M. Gyorgy, A.E. White, L.F. Schneemeyer, R.J. Felder, and J.V. Waszczak, Appl. Phys. Lett. **56**, 2681 (1990).

14. L. Civale, A.D. Marwick, M.W. McElfresh, T.K. Worthington, A.P.Malozemoff, and F.H. Holtzberg, Phys. Rev. Lett. **65**, 1164 (1990).

15. T.T.M. Palstra, B. Batlogg, L.F. Schneemeyer, and J.V. Waszczak, Phys. Rev. B **43,** 3756 (1991).

16. M. A. Kirk and H. W. Weber, in *Studies of High Temperature Superconductors*, edited by A. V. Narlikar (Nova Science, New York, 1992), Vol. **10**.

17. A. D. Marwick, private communication.

18. L. Civale, A. D. Marwick, T. K. Worthington, M. A. Kirk, J. R. Thompson, L. Krusin-Elbaum, Y. Sun, J. R. Klem, and F. Holtzberg, Phys. Rev. Lett. **67**, 648 (1991).

19. W. Kritscha, F.M. Sauerzopf, H.W. Weber, G.W. Crabtree, Y.C. Chang, and P.Z. Jiang, Europhys. Lett. **12**, 179 (1990).

20. W.Gerhauser, H.W. Neumuller, W. Schmidt, G. Ries, G. Saemann-Ischenko, H. Gerstenberg, and F.M. Sauerzopf, Physica (Amsterdam) C **185-189**, 2273 (1991).

21. H.W. Weber and G.W. Crabtree, in *Studies of High Temperature Superconductors*, edited by A. V. Narlikar (Nova Science, New York, June 1991), Vol. **9**, and references therein.

Chapter 2

Early Work On Angular Dependence

The reader should note that this chapter is written as if it were 1988 to capture the importance of this work in its original timeframe. In Chapters 3 and 6 we will comment on the great deal of progress that has been made since, in understanding the nature of flux motion in high T_c materials.

2.1 Introduction

Our in-field transport measurements of single crystal $Bi_{2.2}Sr_2Ca_{0.8}Cu_2O^*_{8+\delta}$ began as an experiment to determine the angular and temperature dependence of the upper critical field, H_{c2}, of this [then recently discovered] non-rare earth based cuprate superconductor. For more than two decades prior to the discovery of the high temperature superconductors, much theoretical and experimental study had focused on H_{c2} in dirty type-II superconductors. Within the Ginzburg-Landau[1] formalism, the theory relating H_{c2} to fundamental microscopic electronic parameters such as the density of states at the Fermi level, N(0), the resistivity $\rho_n(T_c)$, the Fermi surface area, S, and T_c, had been extensively developed, as for example by of the work of Abrikosov and Gor'kov[2], and Werthamer, Helfand, and Hohenberg.[3] In the high T_c materials, early success in applying the GLAG (Ginzburg-Landau-Abrikosov-Gor'kov) theory promised direct comparison

*A note on the specific stoichiometries quoted in different parts of this thesis can be found in section 4.2, third paragraph.

with detailed measurements of critical properties, because H_{c2} can be related to the coherence length within the GLAG formalism.

The anisotropy of the upper critical field, $H_{c2}(\theta)$, offers considerable insight into the physics of the material. Working from the linearized Ginzburg-Landau equations, relations describing the detailed angular dependence of H_{c2} arising from different origins of critical field anisotropies have been developed. Anisotropy may arise from bulk properties of the system, as in the effective mass model[4], which incorporates the conductivity anisotropy, or from the mechanism of surface superconductivity. In the effective mass model the angular dependence of H_{c2} is given by

$$H_{c2}(\theta) = \frac{\Phi_0}{2\pi\xi_\perp^2}(\cos^2\theta + \varepsilon^2\sin^2\theta)^{-1/2},$$

where Φ_0 is the flux quantum, $\xi_\perp$ is the coherence length perpendicular to the **c**-axis, θ is the angle between the **c**-axis and the applied magnetic field, and $\varepsilon = \sqrt{m/M}$, where m and M are the effective masses perpendicular and parallel to the **c**-axis respectively. For the phenomenon of surface superconductivity, Tinkham[5] found the angular dependence to be given by

$$\left|\frac{H_{c2}(\theta)\sin\theta}{H_{c2}(\perp)}\right|^2 + \left|\frac{H_{c2}(\theta)\cos\theta}{H_{c2}(\parallel)}\right|^2 = 1,$$

where $H_{c2}(\parallel) = H_{c3}$, the enhanced surface superconductivity, $H_{c2}(\perp)$ is the bulk value of the upper critical field, and θ is the angle between the surface of the sample and the applied magnetic field. The resistive transition in an applied magnetic field of $Bi_{2.2}Sr_2Ca_{0.8}Cu_2O_{8+\delta}$ single crystals, however, proved to be highly unusual, and could not be interpreted within these theories of $H_{c2}(\theta)$.

Our results, while extremely interesting, are not consistent with the conventional definition of the upper critical field. We find instead that there is an onset of resistance across the sample for fields as low as 100 Oe, even for current densities as small as 10 A/cm^2 and for temperatures as low as 77 K. The shape of the resistive transition depends strongly on the orientation of the crystal in the magnetic field, leading to anisotropy ratios as large as 50 for fields applied perpendicular and parallel to the **c**-axis of the crystal. These results

reflect the anisotropic nature of the flux-flow resistivity in these materials, and are not a direct measure of the upper critical field of the material. To further explore these unusual flux-flow effects we made a preliminary investigation of the anisotropy and temperature dependence of the in-field current-voltage characteristics of $Bi_{2.2}Sr_2Ca_{0.8}Cu_2O_{8+\delta}$ single crystals.

The phenomenon of flux flow was well known in traditional superconductors as the limiting factor in determining the critical current. Far below the "depairing critical current", at which the kinetic energy of the current becomes equal to the electron pair condensation energy, a type-II superconductor starts to dissipate energy due to the motion of the penetrated fluxons under the influence of the Lorentz-like force, $\mathbf{F}_L = \mathbf{J} \times \mathbf{B}$. However, in conventional superconductors, at low currents vortices are prevented from moving by an additional force. This "pinning" force, $\mathbf{F}_p$, is due to structural imperfections that provide normal or partially normal regions in the material where it costs less energy to place the (necessarily) normal vortex cores; hence they are "pinned" on these sites. As the current is increased, eventually $\mathbf{F}_L = \mathbf{F}_p$, and flux flow and dissipation begin as the critical current is reached. As will be seen, our H_{c2} measurements of $Bi_{2.2}Sr_2Ca_{0.8}Cu_2O_{8+\delta}$ indicate that even well below T_c and for very low fields and current densities, flux flow occurs with virtually no threshold in this material and that there is therefore no apparent pinning of vortices.

2.2 Experimental

2.2.1 Crystal structure

The study of single crystals offers many experimental advantages: the structure can be precisely determined by x-ray analysis, the influence of grain boundaries upon the electrical characteristics is eliminated, and anisotropic properties can be measured directly. Figure 2.1 shows the crystal structure of $Bi_2Sr_2CaCu_2O_8$. It is orthorhombic with lattice parameters of $\mathbf{a} = 5.414$ Å, $\mathbf{b} = 5.418$ Å, and $\mathbf{c} = 30.89$ Å.[6,7] The nearly square copper-oxide planes are diagonally inset into the unit cell and the vertical structure consists of pairs of these coupled copper-oxide planes separated by Sr and Bi oxides. Chemical substitution has shown that the copper-oxide planes

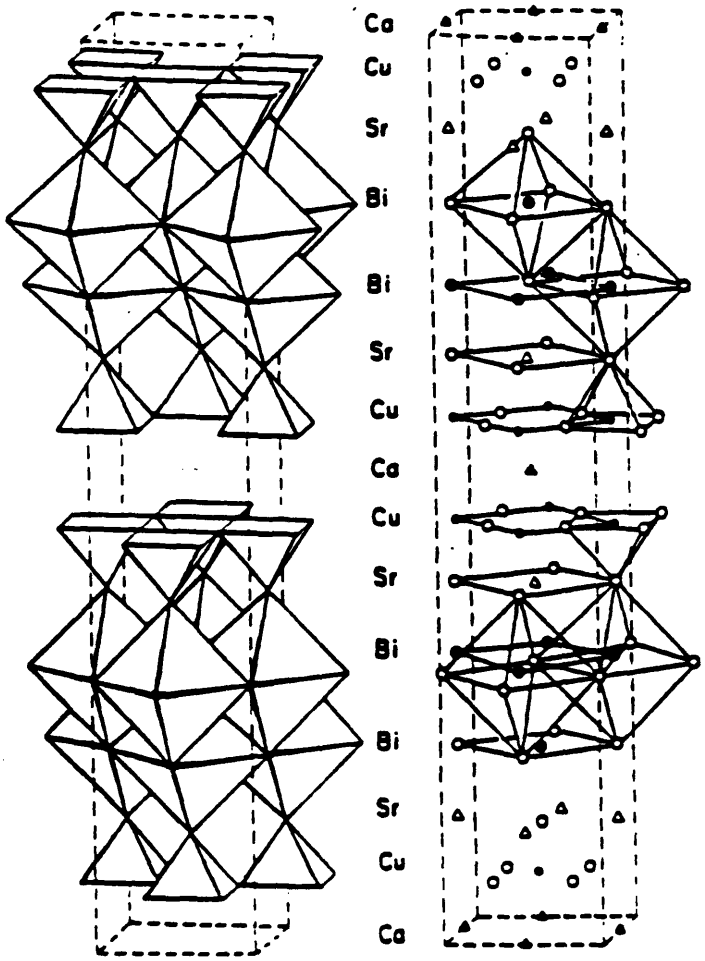

Figure 2-1: The structure of $Bi_2Sr_2CaCu_2O_8$, sometimes called Bi-2212.

are responsible for superconductivity, and the copper valence is controlled by doping in the Bi-O layers. Structurally, this compound differs from $YBa_2Cu_3O_7$ in several respects.[7,8] The Cu-O chains in $YBa_2Cu_3O_7$ are replaced by Bi-O edge-shared tetrahedra, perhaps leading to more two-dimensional-like behavior. The pair of Cu-O superconducting planes are apparently more weakly coupled than in $YBa_2Cu_3O_7$, as suggested by the higher anisotropy in the resistivity of this material.[9] Finally, unlike $YBa_2Cu_3O_7$, there is no twinning in the a-b plane in this system.

2.2.2 Sample Growth

Single crystal samples for this study were grown from alkali chloride fluxes.[10] The indicated stoichiometry, $Bi_{2.2}Sr_2Ca_{0.8}Cu_2O_{8+\delta}$, was determined from x-ray structure refinement. Pre-reacted Bi-Sr-Ca-Cu-O mixtures were prepared from high purity Bi_2O_3, $SrCO_3$, $Ca(OH)_2$ and CuO by slow heating to 800-850°C with intermediate grinding steps. These mixtures are generally not single phase. Appropriate quantities consisting of 10-50 wt% of this pre-reacted starting material were then thoroughly mixed with alkali halide salts (e.g., NaCl, KCl) or salt mixtures and placed in various types of crucibles. These were heated above the melting temperature of the salt or salt mixture, and cooled at rates of 1-10°C/h. In a typical experiment, a 20 wt% mixture of Bi-Sr-Ca-Cu-O in KCl was heated rapidly to 875°C, held at that temperature for 1 hour, and then cooled at 10°C/h to 760°C. Crystals of $Bi_{2.2}Sr_2Ca_{0.8}Cu_2O_{8+\delta}$ form with a plate-like morphology, mainly on top of the salt, although crystals were observed within the solidified charge. Crystals were separated mechanically from the solidified melt, and the adherent salt was easily washed from the crystals with no apparent loss of superconductivity in the sample. The best crucible used to contain the melts was platinum, which reproducibly yielded high quality crystals with no evidence of platinum incorporation.

2.2.3 Contacts

Single crystal samples had typical dimensions of $\sim$ 1 x 2 x 0.001 mm^3, with the **c**-axis normal to the plate, allowing easy angular separation in transport and magnetic measurements. Low resistance contacts, non-rectifying and of moderate mechanical stability, were reproducibly made

by attaching fine Ag wires with Ag cement to Ag pads sputtered onto the crystals. Post-oxygen anneals were not made after Ag pads were sputtered.

2.2.4 Characterization

Measurements of the resistive transition as a function of the applied magnetic field were made at the Francis Bitter National Magnet Laboratory (FBNML) using a standard four-point probe technique. A constant dc current was passed through the sample and the resistance was measured as a function of applied field. The measuring currents were kept to less than 10 A/cm^2 to prevent experimental artifacts such as contact heating or suppression of T_c due to the low critical current density from confusing the interpretation of the results. Alternatively, current-voltage characteristics could be measured using a variable current source while holding the applied field constant. The sample temperature was measured in zero field using both platinum and carbon-glass resistance thermometers, and was controlled in field with a capacitance thermometer. Temperature control of better than 0.1 K can be achieved with this technique. The temperature-controlling sample holder and most of the equipment necessary for the measurements were provided by the FBNML. For angular dependent measurements, the cryostat was placed on a rotating table to vary the direction of the applied field relative to the c-axis of the sample. This required the use of a split-coil solenoid (Helmholtz coil) with a maximum field of 8 Tesla. The angular resolution was better than half a degree. As will be seen in the following discussion, the large anisotropies in these samples makes this degree of angular resolution necessary.

2.3 Results and Discussion

Figure 2.2 shows the temperature dependence of the resistivity as a function of magnetic field for fields parallel and perpendicular to the c-axis of the crystal. The zero-field curve shows the high quality of the sample; the sample resistance goes to zero at 84 K. However, in the presence of a small applied magnetic field the sample exhibits non-zero resistance even for temperatures

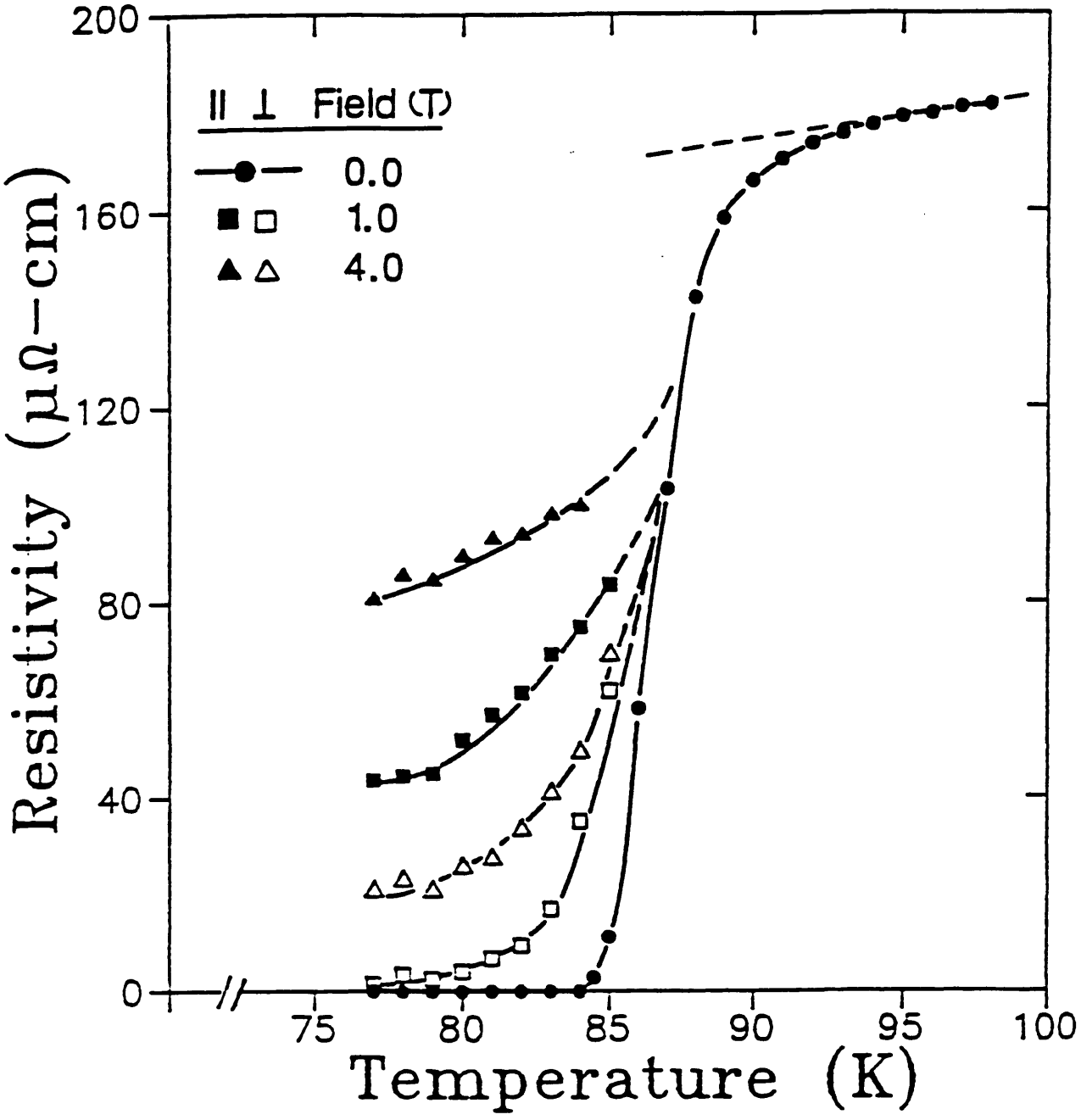

Figure 2-2: Change in the temperature dependence of the resistive transition as a function of applied magnetic field for single crystal $Bi_{2.2}Sr_2Ca_{0.8}Cu_2O_{8+\delta}$. Field is applied both parallel to (solid points) and perpendicular to (open points) the **c**-axis of the crystal. Lines are to guide the eye only.

far below T_c. This behavior is in sharp contrast to the resistive transition of a traditional superconductor which, in the presence of an applied field, simply moves to lower temperature with little broadening. Details of the low field current-voltage characteristics[11] of these samples verify the absence of any threshold current for the onset of resistance in this temperature regime for fields greater than 100 Oe.

The angular dependence of the field-induced resistive transition is shown in Fig. 2.3 for a sample temperature of 83 K. The resistance is normalized to the extrapolated normal state resistance of the sample at the measurement temperature, as indicated by the dashed line in Fig. 2.2. As described above, resistance is immediately developed upon application of the field. The shape of the transition remains essentially unchanged until the field is oriented to within 30° of the a-b planes, and the shape changes rapidly only when the field is within 10° of the a-b plane. The transition shape is distinctly different from the field broadened transitions typically observed in $YBa_2Cu_3O_7$ single crystal samples,[12] and supports our view that the resistive transition represents a flux-flow-induced voltage regime, and is not a direct measurement of the critical field transition of the superconductor.

The detailed angular dependence of the applied field anisotropy for the resistive transition is shown in Fig. 2.4. Here we plot the field required to return the sample to 15% (open circles) and 30% (closed circles) of the normal-state resistance as a function of the field direction. This is equivalent to taking a horizontal cut in Fig. 2.3 at R/R_n values of 0.15 and 0.30, and is the standard criterion used to define the upper critical field in traditional anisotropic superconductors.[13] The anisotropies between perpendicular and parallel orientations (with respect to the **c**-axis of the crystal) are 50 and 30, respectively, for these two definitions. This is a much larger anisotropy than has been reported for either the critical field or critical current of other high temperature superconductors.[14] Note that the narrowness of the angular dependence emphasizes the need for accurate field alignment in any measurement of the anisotropic properties of this material.

We have attempted to fit this angular dependent data with both the effective-mass model[4]

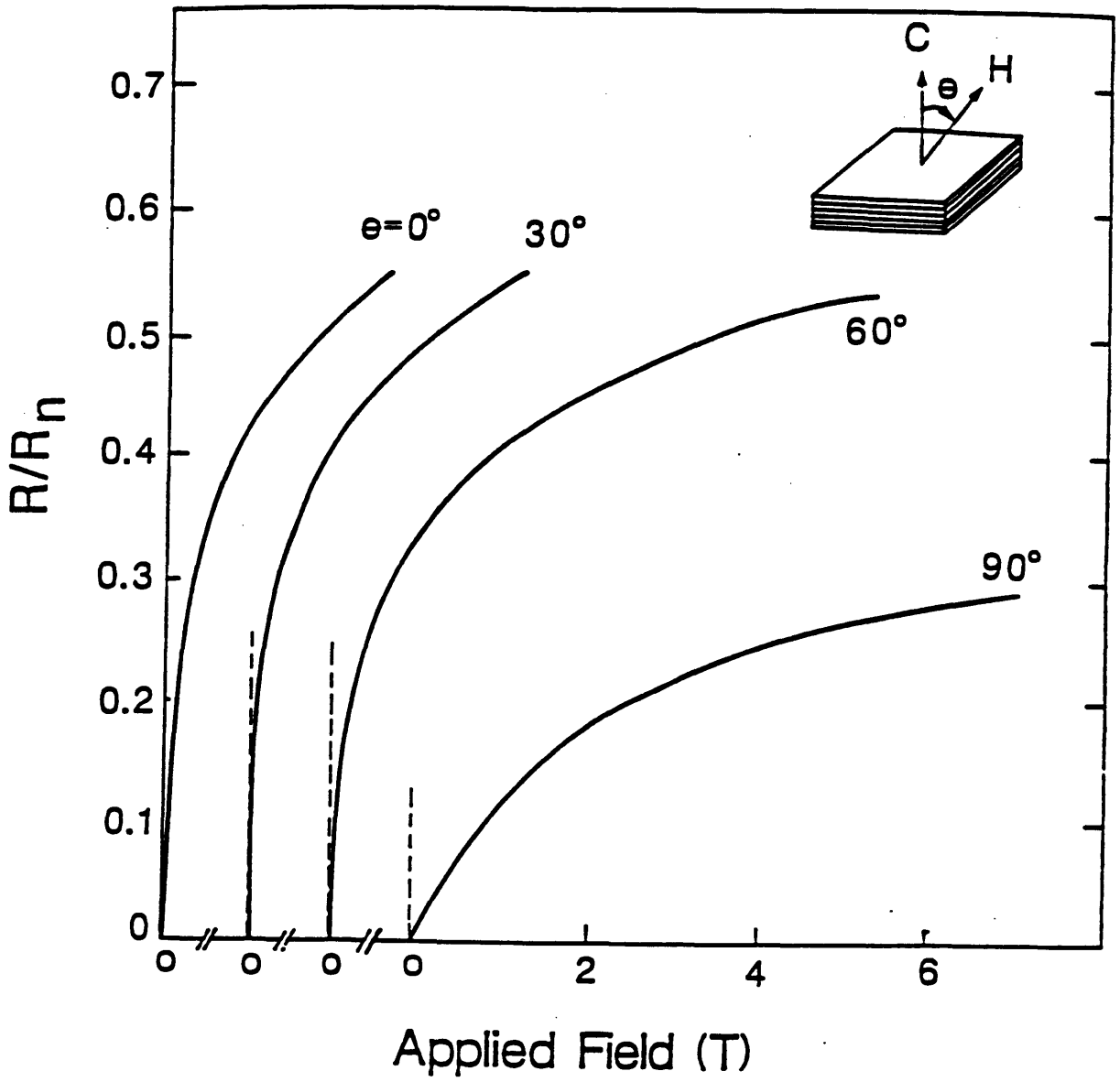

Figure 2-3: Resistive transition as a function of applied field for various field orientations relative to the crystal c-axis. Measurement temperature was 83 K. Resistance has been normalized to the extrapolated normal state resistance at that temperature.

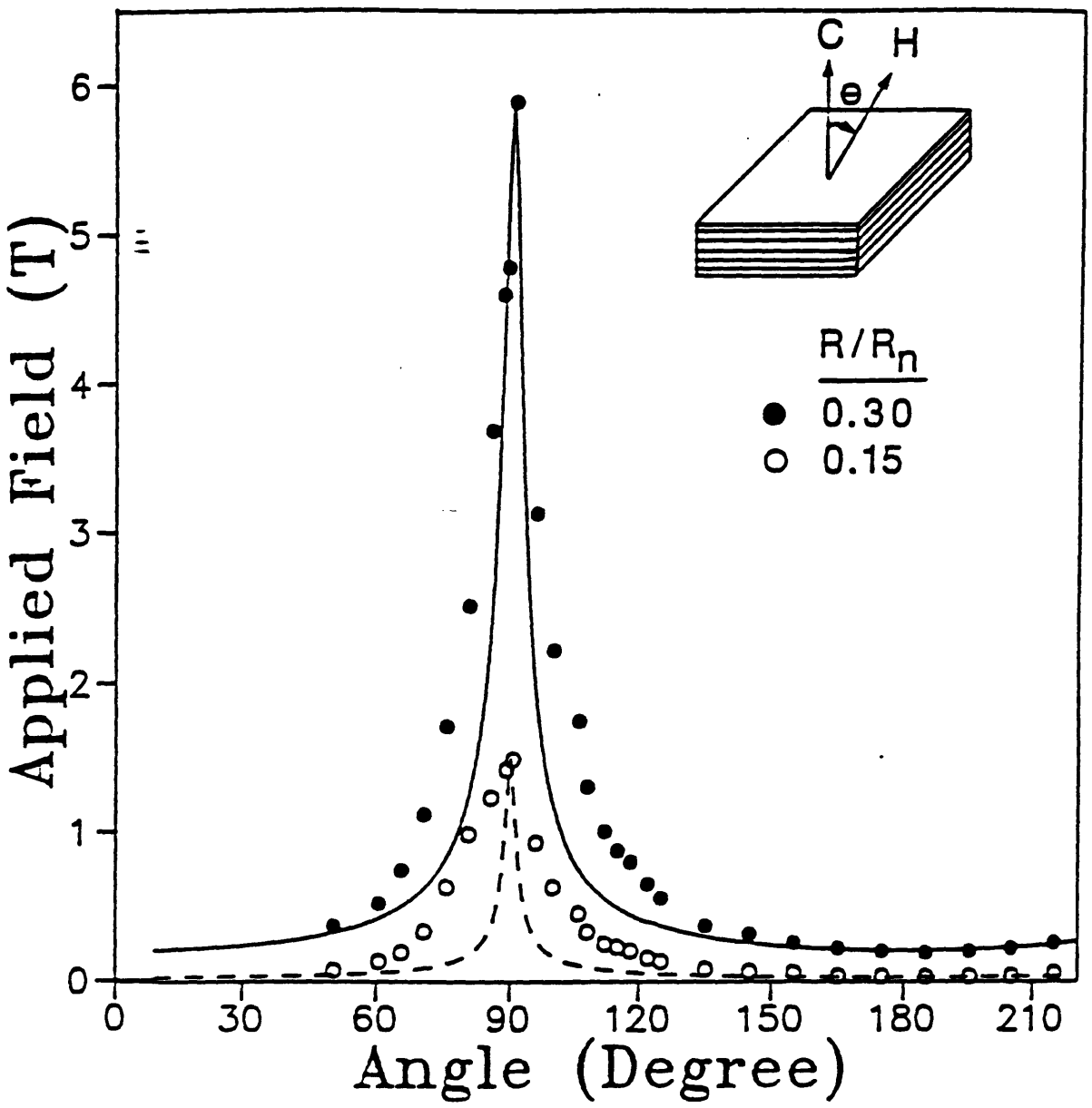

Figure 2-1: Angular dependence of the field-induced resistive transition for two values of the normalized resistance, R/R_n, measured at 83 K. Lines represent fits to the data using the effective-mass model for anisotropic superconductivity.

and Tinkham's thin film formula[5] for critical field anisotropy of superconductors. The curves shown in Fig. 2.4 are fits to the data using the effective-mass model with the anisotropy ratio as the only input parameter. (For such large values of anisotropy the effective-mass model and Tinkham's model are indistinguishable on this scale.) While neither model accounts for the data well, the agreement between the fit and the data improves for larger R/R_n values. Recent results by Palstra, Batlogg, Schneemeyer, and Cava[15] on $Bi_{2.2}Sr_2Ca_{0.8}Cu_2O_{8+\delta}$ single crystals show similarly poor fits to the effective-mass model when the criterion for the transition is chosen as $R/R_n = 0.3$, but show greatly improved fits for $R/R_n = 0.5$, continuing the trend we have observed. For comparison, in both traditional superconductors[13] and $YBa_2Cu_3O_7$ single crystals[14,16] the angular dependence of the resistive transition in an applied field can be fit with the effective-mass model relatively independent of the value of R/R_n chosen, indicating that the upper critical field phase boundary is being measured directly. Our results for $Bi_{2.2}Sr_2Ca_{0.8}Cu_2O_{8+\delta}$ indicate that the resistive transition at the phase boundary is modified by flux-flow effects. We speculate that at low values of R/R_n the onset of resistance may result primarily from flux flow, while higher values of R/R_n may probe the phase boundary.

The observed anisotropy in Fig. 2.4 corresponds to large differences in the flux-flow viscosity for the two field directions. The corresponding directions of flux flow with respect to the crystal structure are illustrated in Fig. 2.5, with flux motion occurring in the a-b plane for $\mathbf{H} \parallel \mathbf{c}$ and normal to the a-b plane for $\mathbf{H} \perp \mathbf{c}$. In the simple model for flux flow[17] the viscosity parameter β is defined by

$$\frac{\rho_f(t, B, \theta)}{\rho_n} = \frac{1}{\beta(t)} \frac{B}{H_{c2}(t, \theta)}$$

where ρ_f is the flux-flow resistivity, ρ_n is the normal state resistivity, B is the flux density in the superconductor (corresponding to the applied magnetic field), H_{c2} is the upper critical field, and $t = T/T_c$. In the Bardeen-Stephen[18] model $\beta(t)=1$, while a more sophisticated dirty limit calculation by Gor'kov and Kopnin[19] (based on the kinetic equation of Eliashberg) yields a more complicated temperature and field dependence. While the full temperature and field dependence of ρ_f has not been calculated, it is clear that the flux-flow resistivity is at least indirectly related to the upper critical field H_{c2}.

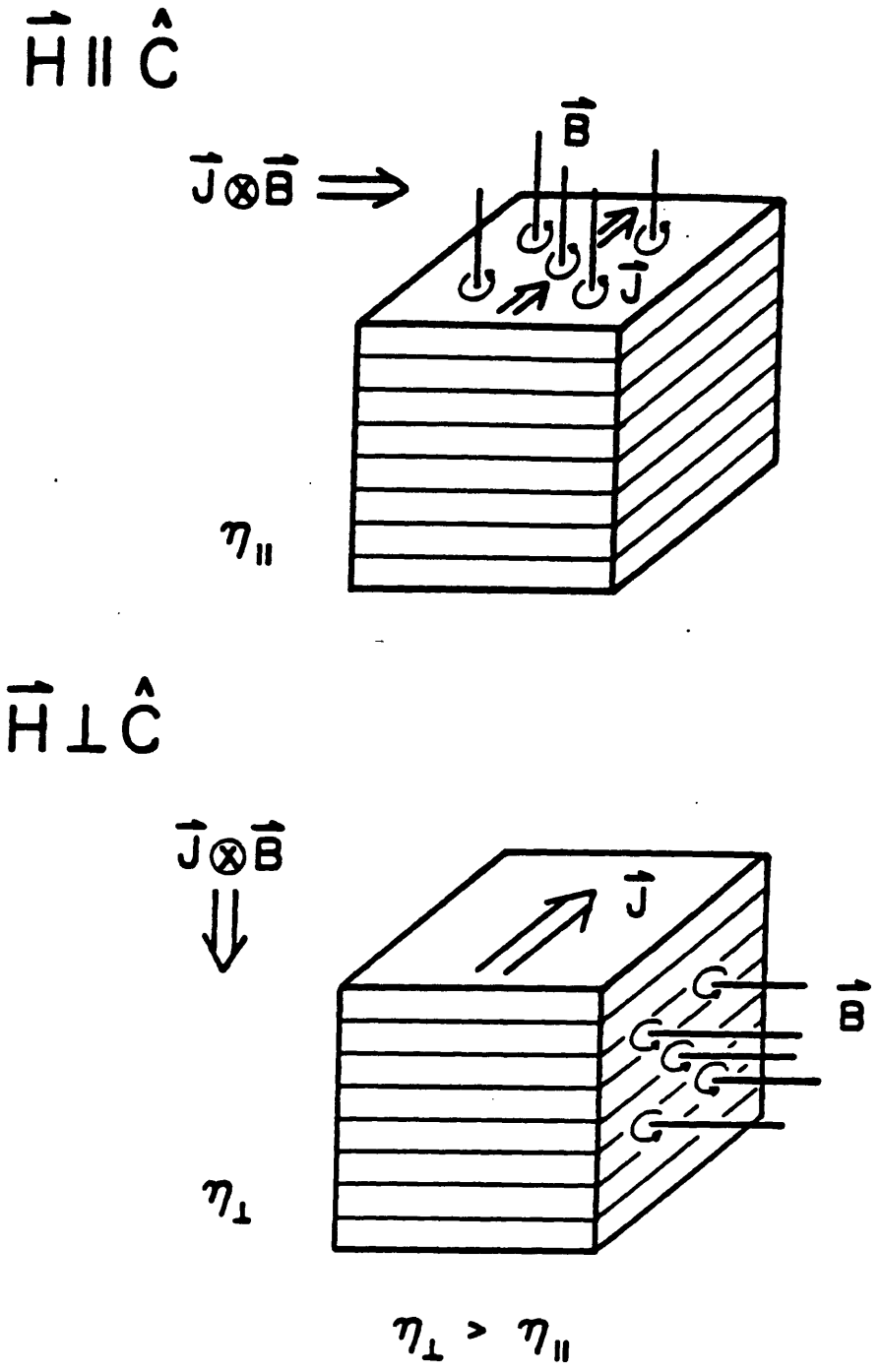

Figure 2-5: Crystal structure in relation to anisotropic viscosity for flux motion occurring in the a-b plane ($\mathbf{H} \parallel \mathbf{c}$) and normal to the a-b plane ($\mathbf{H} \perp \mathbf{c}$).

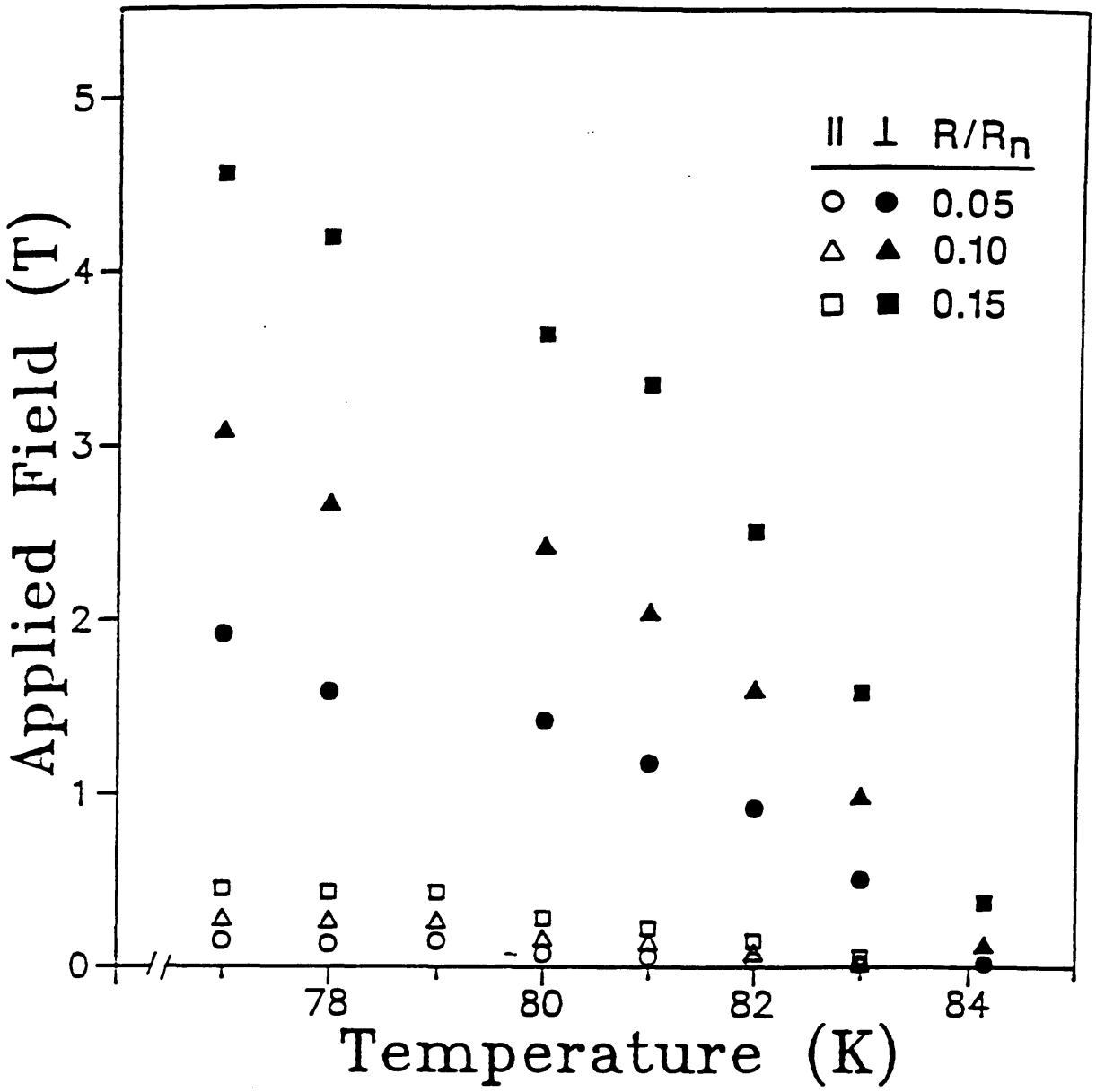

Figure 2-6: Temperature dependence of the field-induced resistive transition for three different values of R/R_n. Field direction is parallel to (open symbols) and perpendicular to (closed symbols) the **c**-axis of the crystal.

Figure 2.6 shows the temperature dependence of three different R/R_n values for fields parallel and perpendicular to the **c**-axis of the crystal. There is a strong negative curvature for the perpendicular field direction in all cases. This result is different from other reports of the critical field in this material, where a linear temperature dependence was found for both field orientations.[15,20] Although the curve shape is suggestive of two-dimensional effects for which $H_{c2} \propto (1\text{-}t)^2$, the curves cannot be fit by a parabolic temperature dependence.

In measurements conducted within several degrees of T_c, we did not observe any evidence of pinning for any field direction, i.e. no indication of a finite critical current. However, near 77 K, a threshold appears. The field-induced resistive transition at several temperatures down to 69 K is shown in Fig. 2.7, for fields perpendicular and parallel to the **c**-axis. In a typical sample, as the temperature is lowered, the threshold appears first for $\mathbf{H} \perp \mathbf{c}$, and then becomes evident at lower angles and finally for $\mathbf{H} \parallel \mathbf{c}$, indicating that the strongest/weakest pinning exists for fields applied along the a-b planes/**c**-axis, corresponding to flux motion normal to/in the a-b planes. It should be noted that the specific curve shape of the resistive transition is also sample dependent. For the particular sample shown in Fig. 2.7 no signal was observed out to 8 T for $\mathbf{H} \perp \mathbf{c}$ at 69 K. Although the full temperature dependence is yet to be determined, it is clear from these preliminary data that the onset of resistance is a strong function of temperature as well as orientation.

To further investigate pinning and flux flow effects at low thresholds, preliminary in-field current-voltage measurements were made, as a function of temperature and angle. Figure 2.8 shows an I-V result measured at 83 K and $\mathbf{H} = 0.19$ T for **H** parallel and perpendicular to the **c**-axis. At these orientations and all angles in between (not shown), the current-voltage characteristics are linear. (Slopes at intermediate orientations fall in between and decrease monotonically with θ.) This is indicative of Bardeen-Stephen-like behavior with no threshold, and viscosity $\eta_\perp >> \eta_\parallel$, as corresponds to the initial slopes observed in R/R_n vs. **H** (inset) for parallel and perpendicular orientations. For comparison, shown in Fig. 2.9 is a typical I-V result measured at 77 K and 0.1 T. Here a linear I-V characteristic is still evident for angles smaller than 60^o, even at low fields and at temperatures far from T_c. However, for field orientations near the a-b plane we see a change from linear to threshold behavior. We therefore directly observe a trend towards

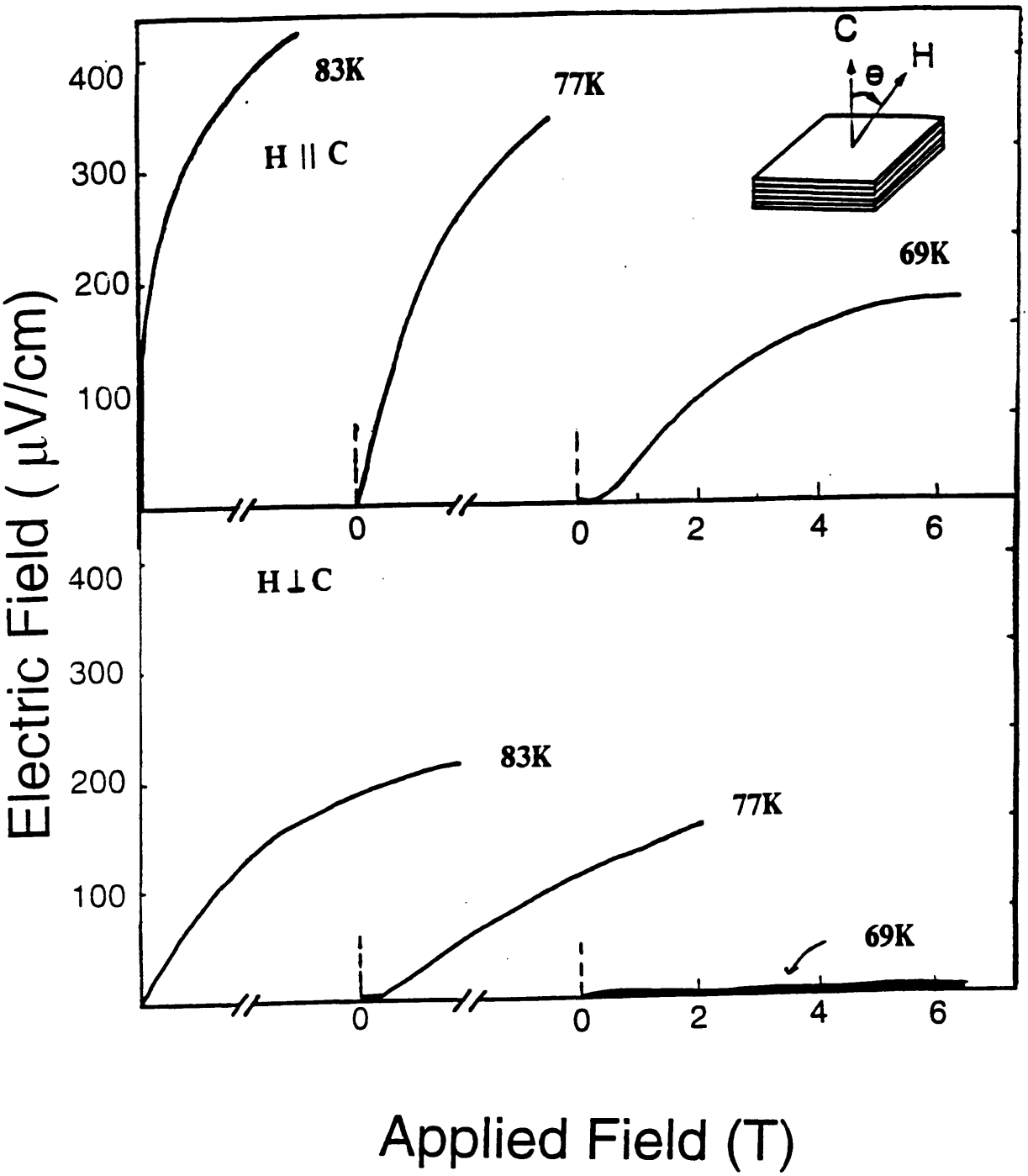

Figure 2-7: Effect of lowering the temperature upon the resistive transition as a function of applied field. Field direction is parallel to (upper) and perpendicular to (lower) the c-axis of the crystal. The voltage evolves more gradually with field at lower temperatures and perpendicular magnetic field orientation.

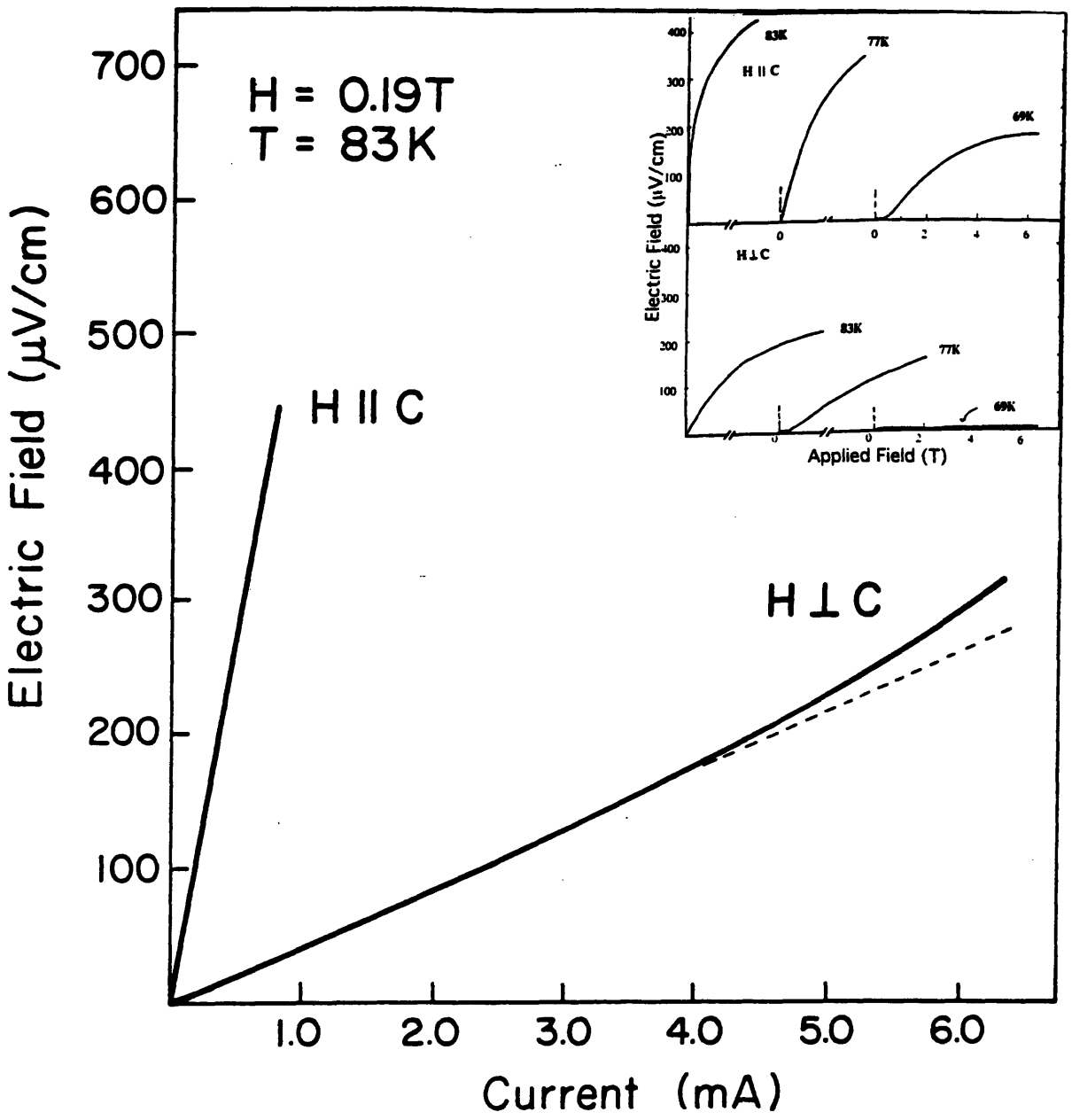

Figure 2-8: Electric field vs. current at **H**=0.19 T for parallel and perpendicular field orientations. At 83 K Bardeen-Stephen-like behavior with no threshold is observed, and viscosity $\eta_\perp >> \eta_\parallel$, as corresponds to the initial slopes observed in R/R_n vs. **H** (inset). $J \approx I/10^{-5}$ cm^2 and $V \approx E \cdot 0.1$ cm.

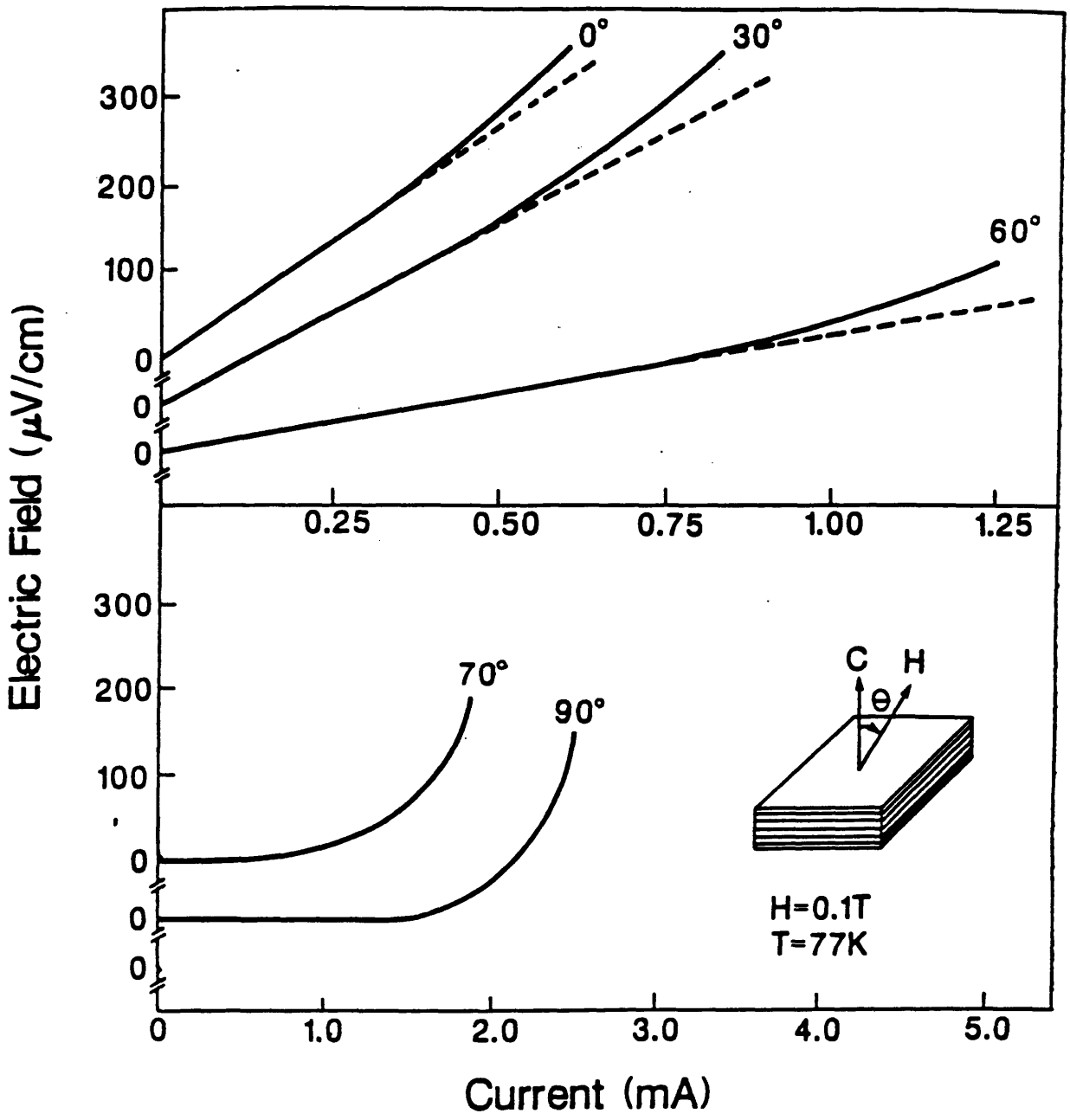

Figure 2-9: Typical characteristics of electric field vs. current for various field orientations at 0.1 T and 77 K. For orientations near the a-b plane we see a change from linear to threshold behavior. $J \approx I/10^{-5}$ cm^2 and $V \approx E \cdot 0.1$ cm.

the development of a real critical current with decreasing temperature and increasing angle.

The angular dependence of the critical current at 77 K is plotted in Fig. 2.10 at fields of 0.0186 T and 0.1 T for electric field criteria of 8 μV/cm and 40 μV/cm. The standard J_c criterion of 1 μV/cm is not practical here because the resistance develops so quickly that J_c cannot be read off the graph for this condition. Note for example that at 1 kOe using even 8 μV/cm the critical current disappears for $\theta > 120^o$ (when **H** is oriented more than 30^o from the a-b plane, as was directly evident from Fig. 2.9). For either criterion and both values of applied field it is apparent that all of these curve shapes, by comparison to Fig. 2.4, more closely resemble the shape of the "critical field" anisotropy for the lower transition state, $R/R_n = 0.15$ than for $R/R_n = 0.30$. This further supports our view that the critical field data are progressively more representative of flux flow effects than of the upper critical field for the lower R/R_n transition criteria. It is not clear how such an immediate dissipation develops in this material and what mechanisms other than flux flow may need to be addressed. Flux creep (see sections 3.2.2 and 3.2.6) of an unprecedented magnitude is one possibility, as suggested by the "giant flux creep" model of Yeshurun and Malozemoff (see reference # 9 of Chapter 3). Flux lattice melting (see section 3.2.3) is another alternative, proposed by Gammel et al. (see reference # 11 of Chapter 3).

The large flux-flow resistance observed in clean single crystals of $Bi_{2.2}Sr_2Ca_{0.8}Cu_2O_{8+\delta}$ led us to speculate as to whether the presence of grain boundaries would inhibit flux motion in this material. Shown in Fig. 2.11 is the angular dependence of the field-induced resistive transition of a thin film of $Bi_2Sr_2CaCu_2O_{8+\delta}$. These sputtered samples, grown by a process described elsewhere[21], are nearly single phase and consist of a "mosaic" of highly textured grains with the c-axis perpendicular to the film surface. Although this structure contains grain boundaries parallel to the c-axis which might be expected to pin flux and suppress the onset of resistance for **H** $\parallel$ **c**, these curves are remarkably similar to the single crystal result (inset) for all orientations. While the temperature of this measurement was only 4 K below the zero resistance temperature (72.5 K) of the film, and lower temperature regimes should be investigated, the striking similarity to the single crystal data indicates that grain boundary pinning does not play a significant role in this material.

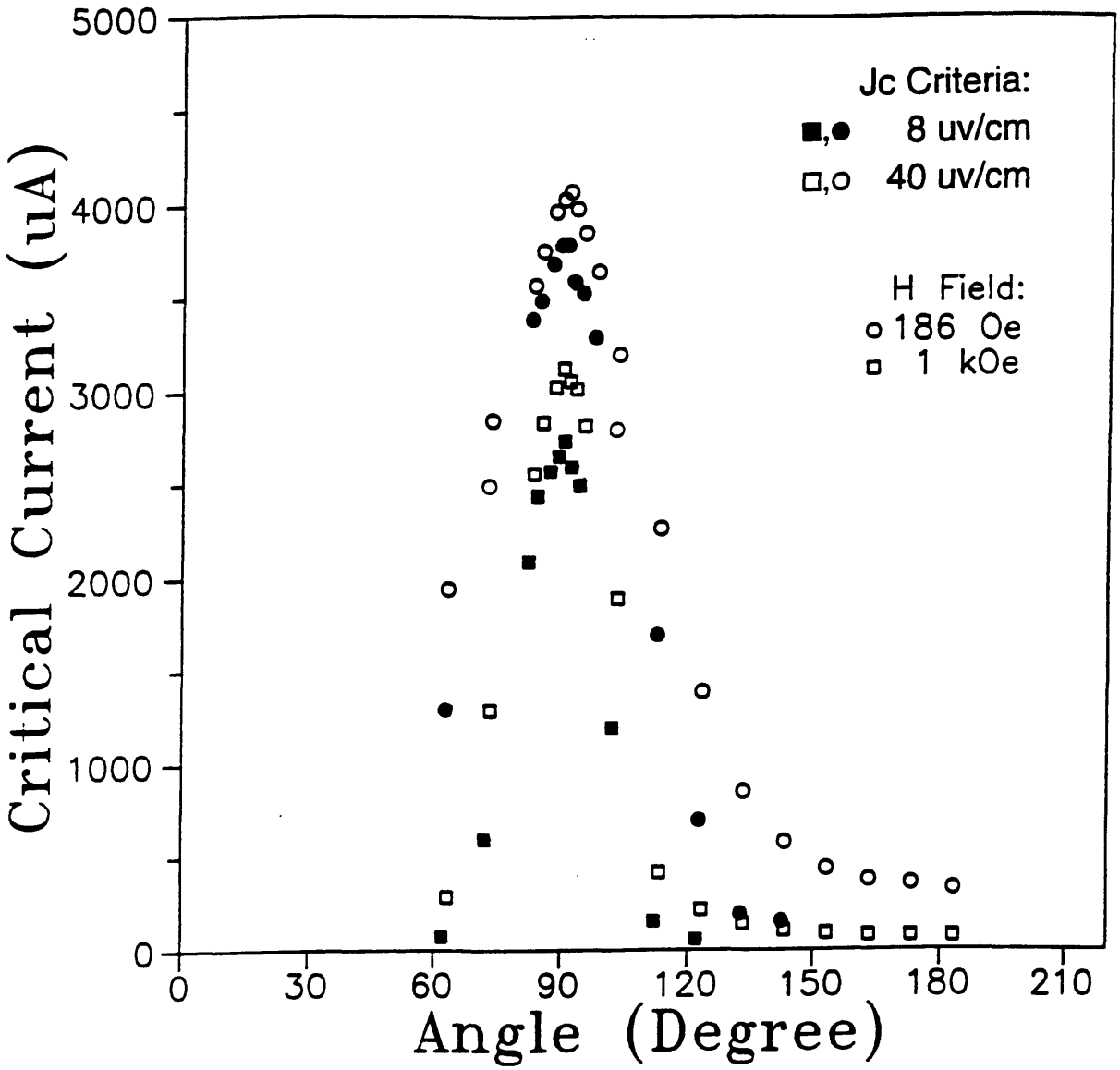

Figure 2-10: Angular dependence of the critical current at 77 K at fields of 0.0186 T and 0.1 T for electric field criteria of 8 μV/cm and 40 μV/cm.

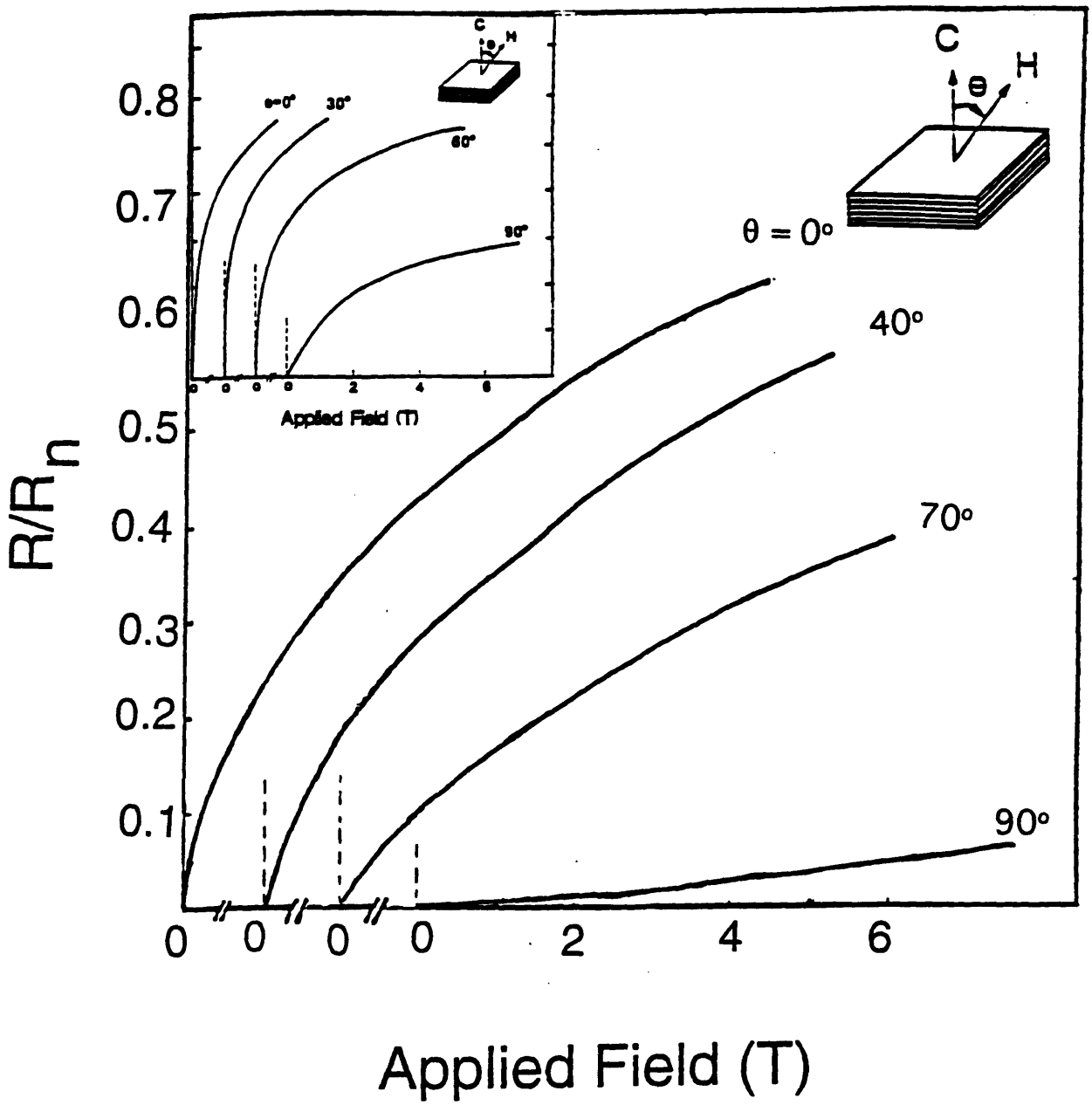

Figure 2-11: Thin film result of the resistive transition as a function of applied field for various field orientations relative to the c-axis. The measurement temperature was 72.5 K. Inset shows similarity to single crystal results implying lack of grain boundary pinning.

In summary, we have measured the detailed angular dependence of the resistive transition in a magnetic field of $Bi_{2.2}Sr_2Ca_{0.8}Cu_2O_{8+\delta}$. We find the anisotropy to be much larger than reported values for other high temperature superconductors. Unlike $YBa_2Cu_3O_7$, the angular dependence of the in-field resistive transition cannot be fit with the three dimensional effective mass model. The observed field-induced resistance in the sample is attributed to flux flow, which begins at fields as low as 100 Oe in this temperature regime. The large anisotropy is attributed to a correspondingly large difference in the viscosity for flux motion in the a-b plane relative to motion normal to the a-b plane. The flux-flow picture is further confirmed by current-voltage characteristic measurements. Preliminary measurements of thin films suggest that grain boundary pinning is not effective. Determination of the upper critical field from these data may be possible, but extreme caution should be used in interpreting the magnetic-field-induced resistivity as directly reflecting the upper critical field of the material.

2.4 References

1. V. L. Ginzburg and L. D. Landau, Zh. Eksp. i Teor. Fiz. **20**, 1064 (1950).

2. A. A. Abrikosov, L. P. Gor'kov, Zh. Eksp. i Teor. Fiz. **42**, 1088 (1962) [Sov. Phys. JETP **15**, 752 (1962)];L. P. Gor'kov, Zh. Eksp. i Teor. Fiz. **36**, 1918 (1959); **37**, 1407 (1959) [Sov. Phys. JETP **9**, 1364 (1960); **10**, 998 (1960)].

3. N. R. Werthamer, E. Helfand, and P. C. Hohenberg, Phys. Rev. **147**, 295 (1966).

4. D. R. Tilley, Proc. Phys. Soc. (London) **85**, 1177 (1965); **86**, 289 (1965); **86**, 678 (1965).

5. M. Tinkham, Phys. Lett. **9**, 217 (1964)

6. J. M. Tarascon, W. R. McKinnon, P. Barboux, D. M. Hwang, B. G. Bagley, L. H. Greene, G. W. Hull, Y. LePage, N. Stoffel, and M. Giroud, Phys. Rev. B **38**, 8885 (1988).

7. S. A. Sunshine, T. Siegrist, L. F. Schneemeyer, D. W. Murphy, R. J. Cava, B. Batlogg, R. B. van Dover, R. M. Fleming, S. H. Glarum, S. Nakahara, R. Farrow, J. J. Krajewski, S. M. Zahurak, J. V. Waszczak, J. H. Marshall, P. Marsh, L. W. Rupp, Jr., and W. F. Peck, Phys. Rev. B **38**, 893 (1988).

8. J. M. Tarascon, Y. LePage, P. Barboux, B. G. Bagley, L. H. Greene, W. R. McKinnon, G. W. Hull, M. Giroud, and D. M. Hwang, Phys. Rev. B **37**, 9382 (1988).

9. S. Martin, A. T. Fiory, R. M. Fleming, L. F. Schneemeyer, and J. V. Waszczak, Phys. Rev. Lett. **60**, 2194 (1988).

10. L. F. Schneemeyer, R. B. van Dover, S. H. Glarum, S. A. Sunshine, R. M. Fleming, B. Batlogg, T. Siegrist, J. H. Marshall, J. V. Waszczak, and L. W. Rupp, Jr., Nature **332**, 422 (1988).

11. R. B. van Dover, L. F. Schneemeyer, E. M. Gyorgy, and J. V. Waszczak, Appl. Phys. Lett. **52**, 1910 (1988).

12. Y. Iye, T. Tamegai, H. Takeya, and H. Takei, Jpn. J. Appl. Phys. Lett. **26**, L1850 (1987); T. Sakakibara, T. Goto, Y. Iye, N. Miura, H. Takeya, and H. Takei, Jpn. J. Appl. Phys. Lett. **26**, L1892 (1987).

13. D. A. Rudman, J. Y. Juang, R. B. van Dover, S. Nakahara, D. W. Capone II, and J. Talvacchio, IEEE Trans. Magn. MAG-**23** 831 (1987).

14. T. K. Worthington, W. J. Gallagher, D. L. Kaiser, F. H. Holtzberg, and T. R. Dinger, in *Proceedings of the International Conference on High-T_c Superconductors and Materials and*

Mechanisms of Superconductivity, Interlaken, Switzerland, 1988, edited by J. Muller and J. L. Olsen [Physica C **153-155**, 32 (1988)].

15. T. M. Palstra, B. Batlogg, L. F. Schneemeyer, and R. J. Cava (unpublished).

16. R. B. van Dover, L. F. Schneemeyer, J. V. Waszczak, D. A. Rudman, J. Y. Juang, and J. A. Cutro, Phys. Rev. B **39**, 2932 (1989).

17. C. R. Hu and R. S. Thompson, Phys. Rev. B **6**, 110 (1972).

18. J. Bardeen and M. J. Stephen, Phys. Rev. **140**, A1197 (1965).

19. L. P. Gor'kov and M. B. Kopnin, Zh. Eksp. i Teor. Fiz. **64**, 356 (1973) [Sov. Phys. JETP **37**, 183 (1973)]; Zh. Eksp. i Teor. Fiz. **65**, 396 (1974) [Sov. Phys. JETP **38**, 195 (1974)]; Usp. Fiz. Nauk **116**, 413 (1975) [Sov. Phys. Usp. **18**, 496 (1975)].

20. J. H. Kang, R. T. Kampwirth, and K. E. Grey (unpublished).

21. D. W. Face, M. J. Neal, M. M. Matthiesen, J. T. Kucera, J. Crain, J. M. Graybeal, T. P. Orlando, and D. A. Rudman, Appl. Phys. Lett. **53**, 246 (1988).

Chapter 3

Literature Review

The reader should note that this chapter surveys research until 1990-91, in order to place this thesis in its original timeframe. In Chapter 6 the context of this thesis is updated through the spring of 1997.

3.1 Overview

The results of the magnetic-field-induced resistive transition described in the previous chapter were difficult to interpret in terms of traditional theories of flux motion, suggesting a vortex state with virtually no pinning and/or flux creep of an unprecedented magnitude. These startling effects were in fact not limited to $Bi_{2.2}Sr_2Ca_{0.8}Cu_2O_{8+\delta}$ but were soon recognized to exist to varying degrees in all of the high T_c cuprate superconductors. In addition to reports[1–3] of the temperature and field dependences of the electrical resistivity, the early experimental evidence for this unusual vortex behavior in both single and non-single crystal materials included studies[4–9] of the time-logarithmic relaxation of the magnetization and metastability of the zero-field cooled magnetic susceptibility, anomalous results in comparisons of $H_{c2}(T)$ by different measurement techniques,[10] and the dissipation peak in the response of the vortices to forced oscillation in a magnetic field.[11] Notably, weak pinning effects were observed to become more pronounced with the degree of structural anisotropy of the material. This was consistent with the huge dissipation that we observed in our attempt to measure H_{c2} in the highly anisotropic $Bi_{2.2}Sr_2Ca_{0.8}Cu_2O_{8+\delta}$.

The precise role of anisotropy in vortex dynamics has since generated much study and controversy. There is, however, agreement that in addition to the weak interplanar couplings, these materials are distinguished from their low T_c counterparts by high critical temperatures and very short coherence lengths. Both of these diminish effective flux trapping by defects and therefore the critical current. Since any practical application depends on the ability to carry reasonable supercurrent densities, especially in magnetic fields, considerable interest has been focused since 1988 on the mechanisms of flux motion in these materials. This chapter will review some of those models.

These studies have proceeded interactively with the more applied search for an effective means of pinning flux. The extremely weak pinning in the as-grown material, especially in $Bi_2Sr_2CaCu_2O^*_{8+\delta}$, raised the issue of a possible intrinsic limitation[12] to the critical current density. In the absence of a clear theory of vortex dynamics in the high T_c materials, it was hoped that these limitations could be overcome by the introduction of extrinsic (induced) defect structures, such as grain boundaries, precipitates[13] or irradiation damage.[14,15]

The irradiation method was especially interesting, and unique for its ease in creating defects of a size comparable to the short coherence lengths in high T_c materials, thereby generating a stronger pinning force. These techniques also afford the opportunity to controllably alter the defect density by changing the incident particle fluence, and defect size or type by adjusting the incident beam energy and/or orientation, (or target temperature). Finally, nature (subject to available facilities) offers a wide variety of incident species to choose from in exploring the creation of novel defect structures in high T_c targets.

The second part of this chapter will briefly review irradiation in conventional superconductors, and then focus on the results in the high T_c oxide superconductors, available primarily on YBCO, that led up to this 1990-1991 study† of heavy-ion irradiation of single crystal

*For an explanation of the changing nomenclature regarding the stoichiometry of the Bi-2212 compound, the reader is referred to section 4.2, paragraph three.

†Over the last six years irradiation studies have evolved into a sophisticated sub-field of high T_c superconduc-

$Bi_2Sr_2CaCu_2O_{8+\delta}$. Differences between irradiation of BSCCO and the more commonly studied YBCO will be discussed, as well as the issues surrounding the use of single crystal vs. non-single crystal material.

3.2 Models of Vortices

3.2.1 Traditional Theory of Vortices

According to Abrikosov's theory[16] of the mixed state of type-II superconductors, for applied fields H such that $H_{c1} < H < H_{c2}$, the magnetic field penetrates in the form of quantized flux tubes (fluxons) which, in the absence of disorder, form a regular, rigid, triangular lattice of parallel lines. In conventional superconductors, this lattice, with spacing $a_0=(2\Phi_0/\sqrt{3}B)^{1/2}$, where Φ_0 is the flux quantum, was believed to exist at essentially all temperatures and fields up to $H_{c2}(T)$. There the normal cores of these tubes became so closely packed together as to merge, resulting in the mixed-state-to-normal (H_{c2}) phase transition.

As discussed in Chapter 2, the critical current was reached when the Lorentz force overcame the pinning force ($F_L > F_p$), causing the penetrated fluxons to move. For an ordered flux lattice, "flux flow" occurred via the motion of "grains" of flux crystal, with dimensions given by disorder-induced translational correlation lengths parallel and perpendicular to the field direction.[17] The flux-flow velocity was limited by viscous drag due to dissipation in the flux cores, giving rise to the flux flow resistivity, ρ_f (see Chapter 2). Due to the constant velocity of the vortices, for a constant applied current and magnetic field, the voltage and power dissipated are constant. Therefore the current-voltage characteristics were predicted to be linear in this regime, with the voltage first rising above zero at the critical current.

---

tivity and have now in turn shed light on the topic of vortex dynamics. This more recent work will be discussed in Chapter 6, after the presentation of my results.

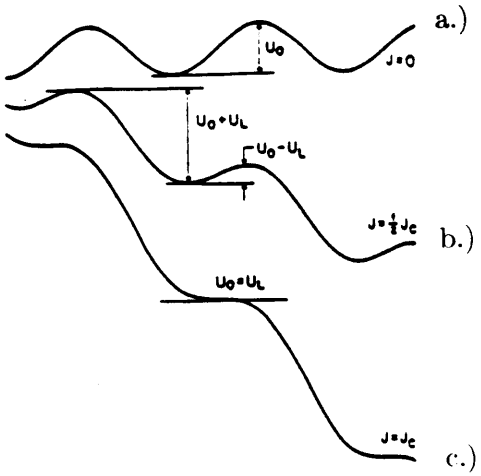

Figure 3-1: Thermally activated flux creep: pinning potential for a.) J = 0 b.) J < J_c and c.) J = J_c.

3.2.2 Thermally Activated Flux Creep

The flux creep regime is distinguished from the flux flow regime in that $F_L < F_p$. The thermally activated model was first posed by Anderson[18] to explain the time dependent relaxation of the magnetization in conventional superconductors. In this model the pinning sites are represented as a network of potential wells of depth U_0, and separation distance, d, where U_0 and d are determined by the pinning strength and pin density, respectively. The fluxon is treated as a point particle which may be trapped and then thermally activated over the pinning energy barrier thereby hopping from well to well, which can result in a net motion of flux (and therefore power dissipation) even though the Lorentz force is smaller than the pinning force.

In the absence of an applied current the wells are symmetrical, as shown in one dimension in Fig 3.1a, and the fluxon may escape in either direction with equal probability. The hopping rate over a barrier U_0 is given by

$$R = \nu_0 e^{-U_0/kT},$$

where ν_0 is the attempt frequency. The net hopping rate, for all directions is

$$R_{net} = 0.$$

However, in the presence of an applied current, the potential is tilted, as shown in Fig. 3.1b, to favor hopping in the direction of the Lorentz force ($\mathbf{F}_L$=JxB). This model assumes that the pinning sites are farther apart than the average intervortex spacing and therefore (as with flux flow), bundles or grains of flux may move (in this case, hop) together. The Lorentz force energy is given by

$$U_L = JBr_pV_c,$$

where the material-dependent microscopic quantities r_p and V_c are, respectively, the range of the pinning potential and the correlated volume of flux that moves. Now the hopping rates become, in the forward direction (the direction of the Lorentz force),

$$R_f = \nu_0 e^{-(U_0-U_L)/kT},$$

and in the reverse direction (opposite the Lorentz force),

$$R_r = \nu_0 e^{-(U_0+U_L)/kT}.$$

Then the net hopping rate is

$$R_{net} = \nu_0 e^{-U_0/kT} sinh(U_L/kT).$$

Assuming an average hopping distance, l, the average flux velocity is v_ϕ=R_{net}l, and applying Faraday's law results in a current-voltage characteristic of the form

$$V \propto e^{-U_0/kT} sinh(JBr_pV_c/kT).$$

This leads to an exponentially activated resistivity,

$$\rho = \rho_0 e^{-U_0/kT},$$

and for small current densities predicts a linear I-V curve. Importantly, in this model the resistance does not vanish for any finite temperature. (Note however that interactions between vortices have been neglected.) As the current is increased, the Lorentz force energy eventually

becomes equal to U_0, (F_L=F_p), as shown in Fig. 3.1c, and flux flow begins as the traditional critical current is reached.

In spite of its simplicity, Palstra[19] successfully used this model to describe the low resistance portion of the broadened transitions of single crystal $Bi_2Sr_2CaCu_2O_{8+\delta}$ in the range 10^{-2} - 10^{-6} R_n. The measured activation energies, U(T,H), were on the order of several hundred kelvins, about a factor of 100 smaller than in YBCO (which did not fit this Arrhenius model as well). In the language of flux creep, the insignificant critical current of BSCCO across most of the phase diagram is attributed to this low activation energy, from which, in principle, the scale of the microscopic pinning energies can be extracted.

Tinkham[20] presented a modified model which recognized that due to the large penetration depth, the vortex currents overlap as soon as $B > H_{c1}$, and therefore the thermally activated vortex velocity is limited by vortex lattice shear or phase slippage. (This is mathematically identical to the case of thermally activated phase motion in a single heavily damped current-driven Josephson junction.) He explained the HTC low pinning energies by taking the length of the flux bundle volume as the (very short) coherence length. Griessen's[21] model detailed a crossover regime to flux flow at high current density and also featured a distribution of activation energies, as did Gurevich[22] and Martin[23] et al.

3.2.3 Vortex Glass Model

Long before the discovery of the HTC oxide superconductors, Larkin[17] argued that in the presence of (even weak) pinning the long-range crystalline order of the Abrikosov lattice is destroyed, precluding freezing into a truly ordered phase. Soon after the HTC oxides were discovered, flux (Bitter) decoration experiments[24] on YBCO showed that for magnetic fields parallel to the **c**-axis, flux quanta could be observed emerging from a single crystal sample at T = 4.2 K (in fields of up to 500 G), but not at 77 K. This prompted speculation that above a certain temperature T_m, the lattice melts at a field strength smaller than H_{c2}, as occurs for example in two dimensional superconductors.

However, since decoration experiments are usually restricted to fields less than a few hundred Gauss,* claims for melting at high fields are instead based upon more indirect observations such as a peak in vibrating reed experiments, as performed on both single crystal YBCO and BSCCO.[11] [In these experiments a superconducting sample is mounted on a mechanical oscillator and placed in a magnetic field. When the oscillator is driven in a direction normal to the magnetic field at a rate that is fast compared to the relaxation time for compression of the lattice, the elastic modulus of the flux lattice will contribute to the restoring force on the oscillator assembly. If the lattice is melted, however, the flux lines will rapidly relax with respect to the sample's instantaneous orientation in the field and will not contribute to the oscillator response. The temperature at which the shift in the oscillator frequency vanishes is interpreted as the lattice melting temperature, T_m. Consistent with this interpretation is the fact that when these experiments were performed on YBCO and BSCCO, the energy dissipated in the oscillator assembly also peaked at this temperature.][25] Evidence of lattice melting has also been claimed from results of low frequency torsional oscillator experiments[26] and the observation of abrupt increases in the resistivity.[27,28]

Fisher[29] made theoretical arguments, by taking into account both pinning and collective effects of the vortex lines, that at low T in a bulk, disordered system the vortex lines should freeze into a new "vortex-glass" phase. His model takes into account that vortex lines are comprised of many adjoining segments that feel different pinning environments yet cannot move independently, and also that there are many lines. Koch[27] used this approach to show that non-linear I-V curves in thin film YBCO exhibited scaling behavior near the transition and that the critical exponents extracted were consistent with freezing into the vortex glass phase.

This approach differs sharply from the simple flux creep model in which bundles of lines are treated as single (non-interacting) point particles moving in a periodic potential of depth U (or in a more refined model a random potential of energy scale U). Also in contrast to the

*Because the magnetic field becomes almost uniform when vortex lines are much closer than the in-plane London penetration depth, λ_{ab}.

flux creep model, the vortex glass phase is predicted to be a true superconductor with zero resistance. The large dissipation regimes in BSCCO are interpreted to be above the melting transition, which occurs around 20 K - 30 K in BSCCO, as opposed to around 85 K, very close to T_c, in YBCO ($H \leq 0.1T$).[24]

3.2.4 Flux Liquid Model

Nelson used the same s-wave Ginzburg-Landau functional to describe the HTC superconductors as was used by Abrikosov for conventional materials. Striking differences arise, however, because the phenomenological coupling constants have very unusual values, and because the theory must be solved in a qualitatively different, high temperature regime. In any superconductor at any finite temperature, flux lines will wander due to thermal fluctuations, but for conventional superconductors the temperature is low and the wandering is quite small. Without the approximation of weak thermal fluctuations made in earlier studies of the Abrikosov lattice, it is found[30–33] that a melted vortex liquid replaces the conventional Abrikosov flux lattice over large regions of the phase diagram (see Fig. 3.2) due to the weak interplanar couplings, high critical temperatures and short coherence lengths characteristic of the HTC materials.

If the amplitude of flux line wandering is smaller than the spacing between the flux lines, the flux lines remain "disentangled". At higher temperatures and fields, the flux lines wander farther than the distance between them and become entangled (see Fig 3.3). Above a certain field (calculated as approximately 50 T for YBCO but only about 1 T for BSCCO), flux lines further become "superentangled", in the sense that vortices hop more than an intervortex spacing when passing from one CuO_2 plane to the next. At this point it makes little sense to draw lines connecting them and the liquid degenerates into decoupled planes of point vortices (actually, reminiscent of Clem's "pancake vortices" discussed in the next section). These unusual flux line configurations are predicted to occupy a much larger region of the phase diagram in bismuth and thallium superconductors than in YBCO.

Nelson attributes the absence of observed flux quanta[24] in Bitter decoration experiments on

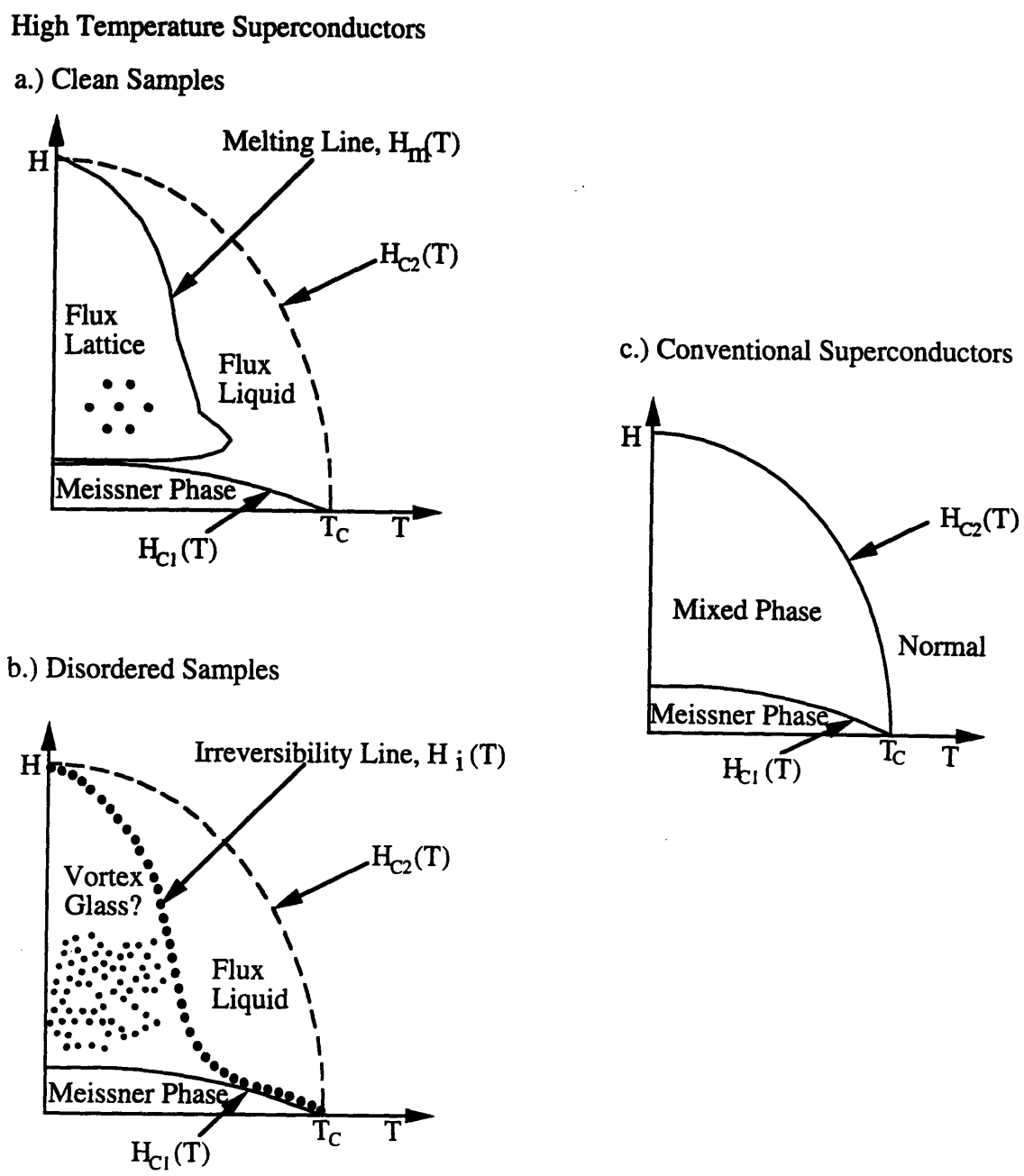

Figure 3-2: Phase diagrams for a.) clean and b.) highly disordered high temperature superconductors, as reproduced from Nelson.[31] c.) conventional superconductors.

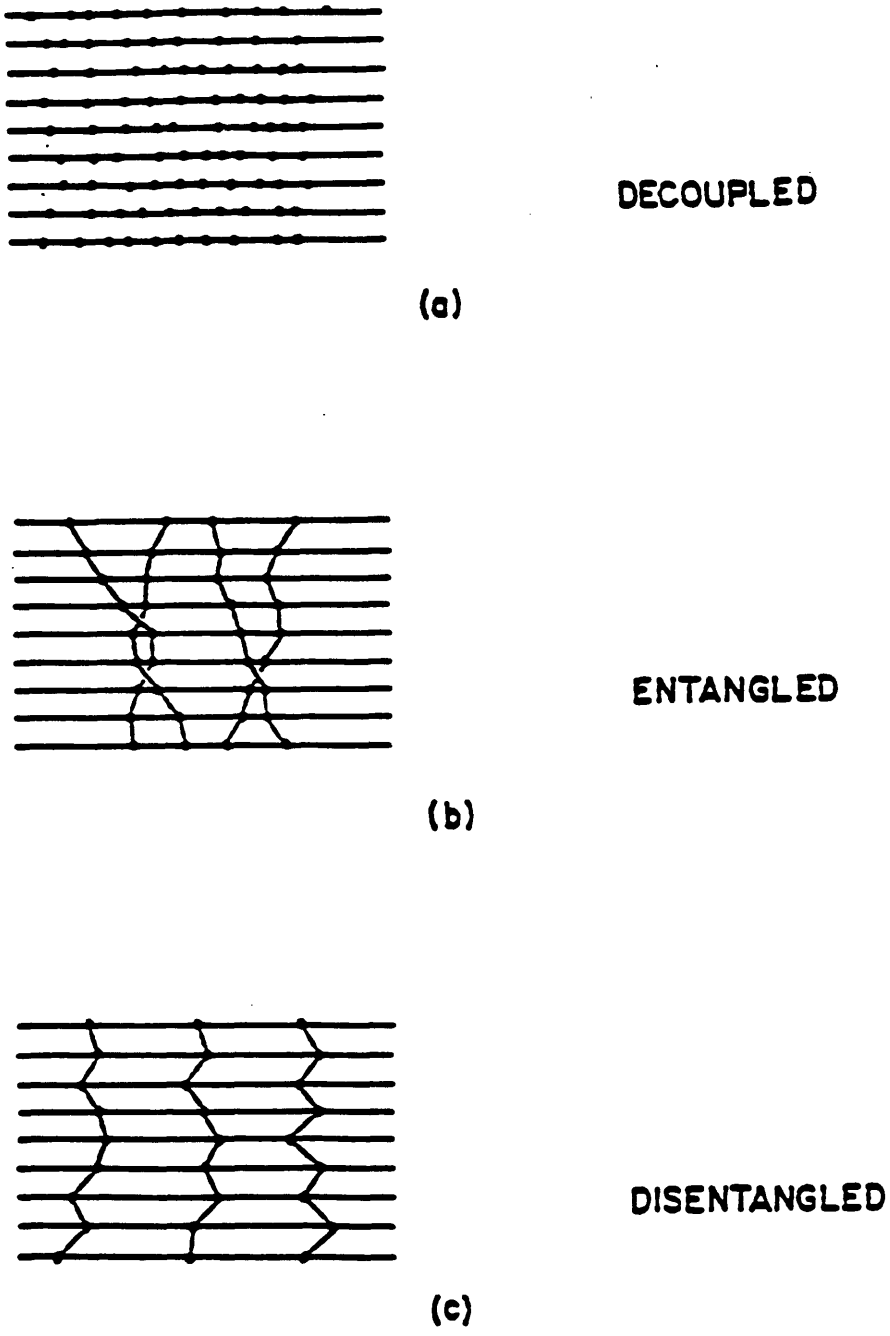

Figure 3-3: Flux lines in strongly layered high temperature superconductors relative to the CuO_2 planes, as reproduced from Nelson.[31] Three regimes are shown: a) decoupled b.) entangled and c.) disentangled.

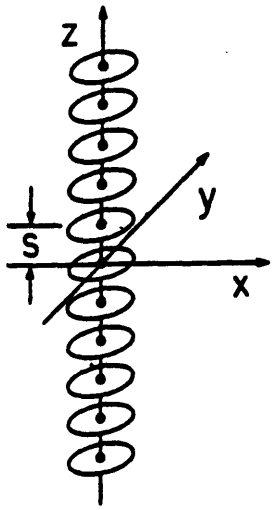

Figure 3-4: Stack of 2D pancake vortices aligned along the z axis, as reproduced from Clem.[37]

YBCO at 77 K to this time-dependent flux wandering in an equilibrated flux liquid. He points out that while regions of extensive crystallinity were subsequently observed in YBCO at low temperatures,[34] decoration studies of BSCCO revealed a transition from orderly flux arrays at low fields ($H \leq 15$ Oe) to "hexatic glass" configurations with very long range orientational order at higher fields.[35,36] He therefore suggests that melting could proceed from either the highly ordered crystalline state or the disorder dominated vortex glass state.

3.2.5 Pancake Vortices

Clem[37] proposed a model incorporating the discreteness of the CuO_2 layers. In the limit of zero Josephson coupling between planes, he asserts that the vortices in adjacent layers are independent and hence very flat (see Fig. 3.4), giving rise to the term "pancake vortices". Starting from the Lawrence-Doniach model, he calculates the field distribution for a single pancake vortex in a stack of superconducting layers which are not occupied by vortices but do have screening currents in response to the single vortex in the central layer. He is able to extend this solution by superposition to find the field from a stack of pancake vortices in such superconducting layers. When the vortices are stacked along an axis parallel to the **c**-axis, they look much like a London 3D vortex.

Interestingly, this model predicts that if the Josephson coupling is exactly zero, the condition for thermal breakup (While vortices in the same layer repel, vortices in different layers attract.) of an isolated stack of 2D vortices is precisely the same as that for the Kosterlitz-Thouless transition of an isolated superconducting thin film of screening length Λ:

$$T_b = \Phi_0^2/16\pi^2 k_B \Lambda.$$

Another very interesting consequence of Clem's analysis is that for arrays of stacks of pancake vortices, the thermal disruption of the translational order within a given layer exhibits a very different behavior than the thermal decoupling of vortices in different layers. The latter is strongly field dependent: for $B >> H_{c1}$, B suppresses alignment, which lowers the melting temperature perpendicular to the layers. The 2D melting temperature, on the other hand, is nearly independent of B over a broad range of fields. This leads to the conclusion that there will be regions of the phase diagram (relatively low T, high B) where the two dimensional pancake vortices in adjacent layers are thermally decoupled but for which the pancake vortices in each layer form 2D solids.

This model may be a good approximation in the case of extremely anisotropic materials. It would not apply very well, for example, to YBCO where vortex decoration experiments[34,38] have shown penetration depth ratios of **a:b:c** = 1.2:1:5.5, but deserves further study in BSCCO and thallium based compounds (TBCCO) because of their higher anisotropies. It may be especially relevant to multilayer structures such as PBCO/YBCO systems.

3.2.6 The Irreversibility Line

The magnetization of a high T_c superconductor at a given H and T depends, as it does in conventional superconductors, on whether the sample was cooled in the field or the field was applied after the sample was lowered below its critical temperature. The irreversibility line (IL) was first observed by Muller[4] et al. in polycrystalline La-Ba-Cu-O by mapping in the H-T plane the temperature at which the zero field cooled and field cooled measurements merge, for

a given applied H. This line is of the form

$$H = H_0(1 - T/T_c)^{3/2},$$

and divides the phase diagram into regions of reversible behavior above and hysteretic behavior below. Yeshurun and Malozemoff[9] later confirmed in a single crystal of YBCO the observations by Muller et al. in powder samples.

Once confirmed as an intragranualar phenomenon, Yeshurun and Malozemoff applied a conventional flux pinning picture, and reasoned that the superconductor behaved reversibly above this line because it was now in a state in which flux lines could move freely in the sample. It had previously been argued[4,39] that the relaxation reflected superconducting glass features resulting from Josephson weak links at grain boundaries. Yeshurun and Malozemoff modeled their single crystal result as "giant flux creep", a modification of traditional flux creep featuring very low pinning energies due to the small coherence length and an unusual degree of thermal activation.

These ideas were further developed to explain discrepancies in many different HTC measurements (particularly the temperature dependence of H_{c2}) by recognizing that the irreversibility temperature depends on the frequency of the measuring probe. If this frequency is slow compared to the frequency of thermal activation of the vortices across pinning barriers, then the vortices will have time to hop within the period of the probe frequency, and reversible behavior is expected. For example, the apparent transition temperature as measured[40] by ac susceptibility of a single crystal of YBCO decreased by several degrees as the frequency of the applied ac field (H_{dc}=0.6T) was lowered from 10^8 to 10^4 Hz. The analogous effect for a comparable fixed field (H_{dc}=0.1T) in BSCCO is much larger, with T_c dropping by more than 30K as the frequency was changed over five orders of magnitude. This is consistent with an activated net hopping rate and the smaller activation energies measured by Palstra in BSCCO (R_{net}(BSCCO)>>R_{net}(YBCO). Therefore, BSCCO should be more sensitive to frequency and its IL should (and does) lie considerable lower in temperature than that of YBCO.

The meaning of the irreversibility line has been debated and alternatively interpreted as a melting line rather than the onset of flux creep. The differing time scales of melting experiments and magnetic relaxation experiments complicate the issue. Whatever its meaning, the irreversibility line has become a helpful tool in comparing the regimes in which superconductors may be practically applied. For example, to consider the effectiveness of various irradiation treatments, a useful question to ask is, can we move the irreversibility line by these methods and if so by how much?

3.3 Irradiation in Superconductors

3.3.1 Conventional Superconductors

There was considerable interest in the effects of irradiation on conventional superconductors for more than twenty years prior to the discovery of the HTC materials.[14,15,41,42] Many of these studies were motivated by the need to quantify changes in the properties of superconducting magnets, especially of the A-15 compounds, used in radiation environments such as accelerators or fusion reactors.* Notably, some of these investigations also addressed the fundamental physics of the metallurgy and defect structure as could be controllably altered by various forms of radiation. The effects on superconductors of many forms of irradiation, including x-rays,[43] electrons,[44,45] neutrons,[15,46] protons and heavier ionic species at various energies[47,48,49] were examined.

Although the specific effects of various forms of irradiation differ, it was found in general that there are three major effects on the electrical properties of conventional superconductors. First, there is a change in the transition temperature which is usually decreased. In type-II superconductors with the A15 structure, degradation in critical temperature was attributed to a smearing of the density of states caused by irradiation disordering.[15] Secondly, there is an increase in the normal state resistivity due to the increased density of scattering centers.

*A special conference was held in 1977 to summarize knowledge and discuss future trends of research in this field, the proceedings[41] of which are an excellent reference.

Thirdly, there is a change in the critical current. Notably, some types of irradiation defects were found to pin magnetic flux lines and actually enhance the critical current density,[48] especially in superconductors with low initial defect density. Defects could be characterized according to type, size and density by electron microscopy. In many cases it was found that the more closely the size of the defect corresponded to the coherence length (or vortex core radius), the stronger was the pinning force. The J_c due to a known defect density could sometimes be related to the flux line lattice spacing ("matching effects"[50]).

3.3.2 Damage Production by Energetic Particles

The basic process of damage production in metals by energetic particles[14] is fairly well characterized and with some modification of the details can be applied to non-metallic crystals and other materials. Basically, this is a two-step process. First, the incident particle transfers, in a typical time of 10^{-17} s, recoil energy to a lattice atom referred to as the "primary knock on atom" (PKA). The distribution of energies over many such events is called the primary recoil spectrum. Secondly, slowing down of the PKA causes the creation (in $\sim 10^{-12}$ s) of a "displacement cascade". Colliding atoms distribute their energy to the neighboring lattice atoms until they are no longer energetic enough ($E \lesssim 20$ eV) to produce further atomic displacements. Then energy is dissipated from the cascade region and unstable configurations (e.g. Frenkel pairs) are eliminated.

The major factors controlling the primary recoil spectrum and in turn affecting the type of defects produced include the irradiation species type (mass, charge state), incident energy and orientation, and the specific (virgin) structure of the target. The defect density can be changed for a given species by adjusting the incident fluence ($\#/cm^2$). The temperature of the target affects the defect structure through the second, slower step of the process as the lattice relaxes. The target geometry and surface quality are also important, especially with respect to the range of a given species in the sample.

3.3.3 High T_c Superconductors

Low critical currents in HTC superconductors were an issue from the start, and attempts to improve J_c by irradiation of these materials date virtually from their discovery in 1986. Recognition in 1988 of possible intrinsic limitations to J_c focused further attention on this method in hopes of moving the irreversibility line and/or probing the associated vortex dynamics. A January, 1990 cumulative bibliography (Hitachi, internal) of irradiation effects on high temperature superconductors lists papers on irradiation by electron beam (38 papers), fast and thermal neutrons (29 papers), gamma and X-rays (21 papers) and ion beam (68 papers). Almost all of those studies were conducted on (largely non-single crystal) YBCO, with a handful performed on the La, Ga, Eu, and Tl based cuprates and thin films of BSCCO. The predominance of YBCO in these studies reflects not only its availability but also the suspicion that the highly anisotropic cuprates such as BSCCO would never be of any practical use. In fact, by the end of 1990, as the current study began, the community had all but stopped producing single crystal $Bi_2Sr_2CaCu_2O_{8+\delta}$ and it was available primarily in polycrystalline or thin film form. Therefore, review of irradiation results will center mostly around YBCO. First, a brief summary of the more general effects of irradiation on HTC superconductors will be given.

The major effects of irradiation in the high T_c superconductors are qualitatively the same as in traditional superconductors. While increases in T_c are not unheard of[51], in general, T_c degrades with exceptionally high sensitivity to fluence. This is attributed to the major role played by disorder, particularly of oxygen vacancies, in determining the value of T_c. The role of defects of oxygen sub-stoichiometry is born out by the recovery of T_c after post-anneal in oxygen,[51,52] but not in vacuum.[52] The post-annealed normal state resistance does not recover with the same efficiency, indicating, not surprisingly, that specific defects act differently on resistivity and superconductivity. As for changes in the J_c of post-irradiated samples, up until 1989 these ranged from slight improvements (mostly in just a few studies of YBCO, as will be discussed) to degradation.

It is important to note that in the early irradiation studies of HTC materials, attempts were not made to calculate the relevant primary recoil spectra in a particular superconductor

under the given irradiation conditions, although it is closely related to the defect structure induced. This is understandable, considering that in the absence of clear knowledge of pinning and vortex behavior, a prediction of the "ideal" microstructure is itself illusive. Moreover, even if the applicable primary recoil spectrum were accurately calculated and available, productive use of this information would first require that it be correlated, feature by feature, with the defect structure actually induced. This is a major task requiring exhaustive characterization, including time-consuming TEM observations, and not all the defects are even visible!

Therefore, choosing the "right" irradiation method with respect to improving the critical current becomes rather an empirical undertaking. Educated guesses can be made, based, for example, upon knowledge of the coherence length or existing microstructure in the material at hand or by analogy to defects produced in a different superconductor irradiated under similar conditions. But by and large, the "right" irradiation in a given high T_c superconductor is, by definition, the one that optimizes the J_c. Even when Kirk made his later (1991-2) calculations[53] (as compared to the time frame of my work: 10/90 - 6/91) of the primary recoil spectra for various irradiation species and conditions in YBCO, as a starting point he focused his calculational tools around techniques that empirically seemed to "work". A survey of this empirical search to improve the critical current of YBCO, which led up to the "present" irradiation study of single crystal BSCCO, follows.

3.3.4 Irradiation of YBCO

Initially, at best slight improvements were achieved in polycrystalline, bulk melt processed and thin film YBCO, as can be seen in Table 3.1, with many negative results reported. Methods of irradiation by electron beam,[54,55] and ion beam[56,57,58] were tried, but the critical current density at 77K was not significantly enhanced. Prior to 1990, proton irradiation efforts in thin films (and a few ceramics) focused largely on energy ranges either well below 1 MeV, as for example in studies[59–63] of ion implantation, which primarily investigated effects upon structure[59,60,62–64] and resistive transition,[59,62–65] or at 10's of MeV, which generally resulted in catastrophic loss of superconductivity.[66,67] These studies did not report the effects of proton irradiation upon

the critical current. Table 3.1 lists a couple of early J_c results of proton irradiation in the intermediate energy range near 1 MeV, but again showing no significant improvement in either YBCO[68] or $Tl_2Ca_2Ba_2Cu_3O_y$.[69]

Some of the results of fast neutron irradiation,[70–77] also shown in Table 3.1, were more encouraging. Kupfer[71] et al. reported a twentyfold increase in the intragranualar J_c of polycrystalline $YBa_2Cu_3O_7$ at 40 K and 1.5 T. Wisniewski[72] et al. found a twentyfold increase from 29 A/cm^2 to 520 A/cm^2 in the magnetization of ceramic at 77 K and 1 T. Using thermal neutrons, Fleischer[78] et al. achieved a similar twentyfold increase after irradiation of uranium-doped $YBa_2Cu_3O_7$, resulting in a magnetization J_c of about 10^5 A/cm^2 at 77K.

By comparison, in unirradiated thin films of YBCO, critical currents had been measured[79] ($4x10^5$ A/cm^2 at 77K and 2 T) that were two orders of magnitude higher (at similar T,H) than in either single crystal or polycrystalline (unirradiated) materials. In YBCO, apparently, different types of defects and/or higher defect densities could improve J_c above values obtained in materials which were grown under conditions expected to minimize the defect density. Ways of inducing a comparably effective defect structure in these materials by irradiation, however, had not yet been found. On the other hand, there had been no significant success in improving the (higher) J_c of thin films above the as-grown values either. Schindler[75] et al., had reported a modest (twofold) improvement to about 10^6 A/cm^2 (60 K, 8 T) in the transport J_c of a YBCO thin film after irradiation with fast neutrons. However, a result such as this, along with the any of the gains summarized in Table 3.1 (all told, ΔJ_c <20x), was difficult to interpret or improve upon due to the structural complexity of the as-grown materials. Analysis was hindered by the possibility of interactions of the pre-existing defect structure, (including for example, grain boundaries, twin boundaries) with induced defects, and the general lack of uniformity, homogeneity and reproducibility of these starting materials. More quantifiable study would require the use of high quality single crystals.

This potential was first realized in 1989 when van Dover et al. reported a factor of 100 enhancement in the J_c of single crystal YBCO after irradiation with fast neutrons[80] (E > 1

Study	Particle Fluence (cm^{-2}) Energy	J_c Before (A/cm^2)	Improve-ment Factor	J_c After (A/cm^2)	T, H, and Method of Measurement		Material
Kato[54]	Electrons	$7.5x10^2$	< x 1.5	$\sim 10^3$	77K	M*	Bulk Melt
1989	$5x10^{17}cm^{-2}$				1T		Processed
	3 MeV						
Shiraishi[55]	Electrons	74	~ x 1.5	113	77K	M	Bulk Melt
1989	$1.75x10^{18}$				1T		Processed
	3 MeV						
Roas[56]	$^{16}O^+$	$\sim 1.3x10^6$	< x 2	$2x10^6$	60K	T†	Thin Film
1989	$1x10^{14}$				3T		
	25 MeV						
Roas[57]	Xe^+	Not	"50%"	Not	60K	T	Thin Film
1990	$4x10^{11}$	Given		Given	2T		
	173 MeV						
White[58]	Ne^+	$4.2x10^5$	- x 100	$4.2x10^3$	77K	T	Thin Film
1988	$2x10^{13}$				0T		
	1 MeV						
Chrisey[68]	Protons	$2x10^6$			77K, 0T	I‡	Thin Film
1990	$4x10^{16}$	$2.5x10^7$	- x 5	$5x10^6$	4.2K, 0T		
	2 MeV						
Venturini[69]	Protons	$4x10^4$	x 5	$2x10^5$	40K	M	$Tl_2Ca_2Ba_2Cu_3O_y$
1990	$4.7x10^{15}$				50mT		
	4.5 MeV						

* Magnetization † Transport ‡ "Inductively, 1KHz"

Table 3.1: Early Irradiation Results on YBCO

Study	Particle Fluence (cm^{-2}) Energy	J_c Before (A/cm^2)	Improve-ment Factor	J_c After (A/cm^2)	T, H, and Method of Measurement		Material
Kupfer[71]	Fast		x 20		40K	M	Polycrystalline
1989	Neutrons				1.5T		
Wisniewski[72]	Fast	29	x 20	520	77K	M	Polycrystalline
	Neutrons						
	$1x10^{17}$						
Hor[73]	Fast		x 15	$2x10^5$	77K, 1T	M	Bulk Melt
1990	Neutrons			$1.8x10^7$	5K, 1T		Textured
Venkatesan[74]	Fast			$5x10^6$	77K		Epi Thin
1989	Neutrons				0.01T		Film
	$6x10^{16}$- $6x10^{17}$						
	0.1-10 MeV						
Schindler[75]	Fast	$5x10^6$			4.2K, 8T	T	Thin Film
1989	Neutrons	$6x10^5$	x 2	$\sim 10^6$	60K, 8T		
	$4.9x10^{17}$						
	E > 0.1 MeV						
Umezawa[76]	Fast	$\sim 5x10^3$	< x 2	10^4	77K	M	Single
1987	Neutrons				1T		Crystal
Fleischer[78]	Thermal		x 20	$\sim 10^5$	77K		Polycrystalline
1989	Neutrons				?		
For Comparison:							
van Dover[80]	Fast	$6.5x10^3$	x 100	$6x10^5$	77K	M	Single
1989	Neutrons				0.9T		Crystal
	$7.9x10^{16}$						
	E > 1 MeV						

Table 3.1: Early Irradiation Results on YBCO (continued)

Mev, f = 7.9 x 10^{16} cm^{-2}). The value of the magnetization critical current was improved to 6 x 10^5 A/cm^2 at 77 K and 0.9 T, for the first time comparable to values reported in thin films. Single crystal experiments clearly promised to yield cleaner information about induced defect structures, as well as how they might compare to existing defect structures (including those in non-single crystal materials), and how the type of defects induced affected the critical current.

While the above success of fast neutron irradiation of single crystal YBCO was quite promising and highlighted the analytical advantages of investigating single crystals, there were also some practical disadvantages. Nuclear reactors are relatively scarce, and may differ with respect to neutron energy spectrum, flux density, shielding of the thermal neutron component, and reliable sample temperature control. In addition, samples remain radioactive for several days. More conveniently available are monoenergetic collimated proton or ion beams of energies up to the several MeV range. The use of ion beams is also appealing because they are compatible with conventional integrated circuit technology (and pose far less significant radiation hazards). Since it was known that fission neutrons had energies of 1 Mev and above, it seemed logical next to try the simplest form of ion irradiation conveniently available, i.e. protons, in the MeV range. Fortunately, it is easy to obtain single crystals of YBCO that are thin enough so that the thickness of the sample corresponds to only a few mean free paths of an MeV proton, which then exits the sample. This simplifies analysis of the data because it creates a relatively constant damage profile by avoiding end of range damage.

3.3.5 Proton Irradiation of Single Crystal YBCO Near 1 MeV

It was quickly found that a comparable increase[81,82] in the critical current of single crystal YBCO could be produced by proton irradiation with J_c maximized at a fluence of $\sim$ 1 x 10^{16} cm^{-2} and E $\sim$ 3MeV. In the very similar experiments of van Dover[81] et al. and Civale[82] et al., the relevant pinning centers introduced by 3 MeV proton irradiation in single crystal YBCO were determined to be primarily point defects. As these results were a close precursor to the present work in $Bi_2Sr_2CaCu_2O_{8+\delta}$, it is worth reviewing the evidence for these conclusions in some detail.

At low T, van Dover et al. found that the maximum J_c of $\sim 2 \times 10^7$ A/cm^2 was arrived at for a number of induced displacements approximately equal to 10^{20} cm^{-3}, as determined from Monte Carlo calculations[83] assuming a proton fluence of 3×10^{16} cm^{-2}. (For further explanation, see section 4.7.) This corresponded to an average spacing between displacements of only 19 Å, i.e. a high density of small defects. Civale et al. relied on a calculation of Hylton and Beasley[84] done for thin films of YBCO, that showed that at low fields (dilute vortices), to account for a low temperature J_c of 3×10^7 A/cm^2, (similar to observed values in these irradiated single crystals) in three dimensions, a density of defects of 3×10^{19} cm^{-3} was required. However, Civale et al.'s TEM observations of crystals after a dose of 2×10^{16} protons/cm^2 showed only the presence of clusterlike defects of sizes 17 Å to 40 Å at an average separation of 300 Å. Therefore, the relevant source of pinning in the irradiated crystals had to be invisible, i.e. an unobservable background of point defects which cannot be resolved by TEM. This conclusion can be reconciled to some degree with the results of fast neutron irradiation in YBCO, as discussed in Appendix A.

Proton irradiation experiments on clean single crystal YBCO encouraged the critical examination of the interaction of vortices with a relatively simple induced defect structure. While van Dover et al. explained their results within the core-pinning model of flux pinning (spatial extent of a typical pinning defect about equal to the coherence length in the a-b plane), Civale et al. could not reconcile their data within any simple pinning model, including core pinning of individual vortices by individual defects. They turned instead to a model of collective pinning in the "amorphous limit" to explain the temperature and field dependence (beyond the scope of this chapter) of their data. In collective pinning, the defects are either too weak or their density is too high to individually pin a vortex. The activation volume is the Larkin domain, of transverse dimension R_c and longitudinal dimension (along the vortices), L_c. To account for the observed dependence of J_c upon fluence, they needed to choose $R_c < a_0$, hence the term, "amorphous limit". More importantly, they further found that the activation energy of their samples did not change upon irradiation, in spite of a near 100-fold enhancement of the critical current at 77 K and 1 T. They gave as the central result of their paper that the irreversibility line (IL) is largely independent of the defect density in proton-irradiated single crystals of YBCO.

The recognition that adding point defects to YBCO significantly enhanced the irreversible J_c but did not affect the irreversibility line or the related thermal activation energy raised questions of intrinsic HTC materials limitations. The simple flux creep model presented a somewhat consistent picture. If one assumes that the dominant existing (intrinsic) pins are point defects, then in unirradiated material, these will set the height and shape of the activation barrier and therefore control the value of the activation energy as well as the location of the irreversibility line. If the relevant effect of proton irradiation is simply to increase the numbers of these point defects, it is not reasonable to expect a significant shift in the irreversibility line or the activation energy. The irreversible magnetization, however, can be expected to increase, then saturate with increasing dose, as indeed it does.

In a lattice melting scenario, this lack of dependence (of the IL) on defect density is more difficult to understand. If the irreversibility line is interpreted as a melting line, its position in the H-T plane is determined by the competition between intervortex elastic energy and the thermal energy which disorders it. By assumption, defects play no role here. However, this assumption is only reasonable if the defects are much further apart than a_0. But at 1 T, for example, $a_0 \sim 450$ Å. Even the largest clusters observed by Civale et al. in TEM appear at spacings of 300 Å and both Civale et al. and van Dover et al. place the effective pinning centers (point defects) at spacings closer to 19 Å, much smaller than a_0 at 1 T. This was in part what led Civale et al. to turn to a collective pinning model.

Beyond arguments over whether collective vortex behavior or individual core pinning better explained the defect independence of the irreversibility line lay the issue of the structural dependence of this HTC superconductivity feature. In different unirradiated materials the position of the IL was known to be strongly correlated to anisotropy. This suggested that future attempts to move the IL with induced microstructures would require consideration of the role of weak interplanar couplings in vortex dynamics. $Bi_2Sr_2CaCu_2O_{8+\delta}$ is a particularly appropriate system for this type of investigation since the reversible regime covers so much more of the phase diagram. Prior to the current work, however, very few irradiation results in BSCCO were

available, and none on single crystals. A discussion of these preliminary experiments, most of which were light ion irradiations of thin ($\sim$ 0.2 μ) films, follows.

3.3.6 Irradiation of BSCCO

It is first useful to review some of the differences between BSCCO and YBCO in unirradiated form. As previously discussed, pinning in BSCCO was well known to be extremely weak. In single crystals, pinning energies were measured[2] in the range of several hundred kelvins for **H** || **c**, about a factor of 100 smaller than in YBCO. This material is also characterized by higher anisotropy (effective mass anisotropy $\gamma = (m_c/m_{ab})^{1/2}$ is around 50 in BSCCO as compared to about 5 for YBCO), absence of Cu-O chains, and lack of extended defect structures such as twins. The dominant existing pins in the as-grown material were speculated to be point defects due to extensive cross substituting, which very obviously did not act as effective pinning centers. In thin film form, as presented in Chapter 2, there was no indication that the presence of grain boundaries significantly enhanced pinning. Prior to the current study there were several attempts to investigate the effects of irradiation on thin films of BSCCO, the results of which are reviewed below.

Helium ions at 400 KeV were tried[52,85–88] at fluences between $\sim$ $10^{13}/cm^2$ - $10^{15}/cm^2$. These samples were reported to be about an order of magnitude more sensitive to structural damage[85] than films of YBCO, compared either in terms of calculated displacement density (dpa) necessary to completely destroy superconductivity or in terms of the degradation of the critical temperature, which was about 1 K/10^{-4} dpa. The normal state resistivity approximately doubled to 2 x 10^{-3} Ω-cm after irradiation by $\sim$ $10^{15}/cm^2$ He^+. The recovery of ρ_n and T_c in oxygen post-anneals but not in vacuum[52] suggested that these changes were dominated, as in YBCO, by oxygen sub-stoichiometry. Notably, the critical current[87,88] and activation energy[88] were found to decrease after irradiation.

Matsui[89] et al. irradiated thin (0.4 μ) films of BSCCO with 200 KeV Ne^+ at fluences from $10^{12}/cm^2$ - $10^{15}/cm^2$ and also reported that sensitivity to structural damage was higher relative

to YBCO. They found an increase in the **c** lattice constant which, like the degradation of the resistive transition, recovered upon post-anneal in oxygen. Unlike the helium irradiated samples discussed above, these films were subject to ion implantation (end of range damage) beyond about the middle of the film. Yoshida and Atobe[90] reported decreases in T_c and increased normal state resistivity after neutron irradiation. These results are summarized in Table 3.2.

It was suggested by Takamura[87] et al. that the degradation of the J_c in their thin films after He^+ irradiation was due to the dominating effects of weak links over pinning strength. As the current work began, T.T.M. Palstra was just obtaining the first ion irradiation result in $Bi_2Sr_2CaCu_2O_{8+\delta}$ that was not complicated by the effects of grain boundaries. Palstra[91] found that irradiation of single crystal $Bi_2Sr_2CaCu_2O_{8+\delta}$ by He^+ at 2 MeV and fluences up to 4 x $10^{14}/cm^2$ resulted in at most a 25% increase in the activation energy for $\mathbf{H} \parallel \mathbf{c}$.

Palstra interpreted his results within the framework of intrinsic structural limitations imposed by the layered crystal structure itself. He argued that the origin of lower pinning energies in $Bi_2Sr_2CaCu_2O_{8+\delta}$ is not a difference in defect structure (e.g. the absence of twin planes) but a difference in anisotropy. Like Clem, he speculated that the presence of the poorly conducting sheets of Bi-O material between the Cu-O layers leads to a very short correlation length, L_c, along the vortices, which is just the interlayer spacing (i.e. pancake vortices). This, in addition to the short coherence length, ξ_{GL}, results in a very small flux bundle volume and therefore small activation energy U_0:

$$U_0 = J_c B R_c^2 L_c \xi_{GL},$$

where R_c is the correlation length in the planes and the range of the pinning potential, for point defects, is given by ξ_{GL}. Thus, the small activation energies are not in contradiction with the large values of J_c observed at low temperature. Extremely low values of U_0, however, limit the irreversible regime to a very small area of the phase diagram.

Palstra further argued that the introduction of strong pins by irradiation should enhance J_c but would not increase L_c and would in fact decrease R_c by disordering the vortex lattice. Therefore the flux bundle volume and hence the activation energy would remain very small.

Study	Irradiating Ion Fluence (cm^{-2}) Energy	Results
Hoshiya[52] 1989	He^+ (at RT) to $2x10^{15}$ 400 KeV	Irradiation affects subsequent annealing behavior re: outdiffusion of oxygen $\Rightarrow$ irradiation may create oxygen vacancies in BSCCO films
Aruga[85] 1989	He^+ to $1.9x10^{15}$ 400 KeV	$\rho \uparrow$ with dose, $T_c \downarrow$ but onset less affected ΔT_c is more sensitive than in YBCO ΔT_c seems primarily related to dpa ΔT_c and $\Delta\rho$ are larger for low T irradiations
Takamura[86] 1989 (June)	He^+ 2-8 x 10^{14} 400 KeV	Evidence observed of flux trapping in irradiated samples not seen prior to irradiation (By comparison of J_c vs. T in zero-field and after removal of field)
Takamura[87] 1989 (July)	He^- (at RT) $7x10^{12}$, $1.2x10^{13}$ 400 KeV	$J_c \downarrow$, $\rho \uparrow$, T_c hardly changes in this regime. J_c recovers appreciably after anneal at 400°C. All changes are slight; note lower fluence and energy than in "present" study. Lack of improvement in J_c was attributed to dominating effects of weak links over pinning strength
Hoshiya[88] 1990	He^+ $2x10^{13}$ - $1x10^{14}$ 400 KeV	After irradiation activation energy, $E_A \downarrow$, $J_c \downarrow$
Matsui[89] 1988	Ne^+ 10^{12}-10^{15} 200 KeV	T_c endpoint $\downarrow$, **c** lattice constant $\uparrow$ Superconductivity destroyed above 10^{14} cm^{-2} More sensitive to structural damage than YBCO Structure and R vs. T recover upon anneal (890°, 5 Hrs.)
Yoshida & Atobe[90]	Neutrons	$T_c \downarrow$, $\rho \uparrow$

Table 3.3: Irradiation of BSCCO Thin Films

With this view of the role of anisotropy in vortex dynamics, he suggested that the irreversibility line could not be significantly altered by irradiation. The inherent assumption was that irradiation introduced primarily point defects, which is quite likely for the case of a helium ion beam.

To overcome this materials limitation, in the current work we examine the generation of defect structures other than point defects to act as pinning centers. This approach recognizes the importance of the role of anisotropy in vortex dynamics in $Bi_2Sr_2CaCu_2O_{8+\delta}$ and represents a departure from the previous strategy of simply trying to match the induced defect size to the short coherence length. We shall compare the effects of H^+, He^+, Ne^+, and Ar^+ irradiation* in the MeV energy range in the context of the developing theories of HTC vortex behavior.

*Kr^+ and heavier ions were not tried because of the additional experimental difficulties involved in obtaining complete penetration of the samples for more massive ions. Given the thickness of our crystals, very high incident energies would have been necessary, creating significant radiation hazards in the laboratory. Single crystals thinner than those used in this study ($t \sim 2\mu$) would be difficult to obtain, but irradiation by heavier ions could be explored in the low MeV energy range with complete penetration using thin film samples.

3.4 References

1. R.B. van Dover, L.F. Schneemeyer, E. M. Gyorgy, and J.V. Waszczak, Appl. Phys. Lett. **52**, 1910 (1988).

2. T.T.M. Palstra, B. Batlogg, L.F. Schneemeyer, J.V. Waszczak, Phys. Rev. Lett. **61**, 1662 (1988).

3. J.Y. Juang, J.A. Cutro, D.A. Rudman, R.B. van Dover, L.F. Schneemeyer, and J.V. Waszczak, Phys. Rev. B **38**, 7045 (1988).

4. K. A. Muller, M. Takashige, J.G. Bednorz, Phys. Rev. Lett. **58**, 408 (1987).

5. A.C. Mota, A. Pollini, P. Visani, K.A. Muller, J.G. Bednorz, Phys. Rev. B **36**, 4011 (1987).

6. C. Giovannella, G. Collin, P. Roualt, and I.A. Campbell, Europhys. Lett. **4**, 109 (1987).

7. J.F. Carolan, W.N. Hardy, R. Krahn, J.H. Brewer, R.C. Thompson, and A.C.D. Chaklader, Solid State Commun. **64**, 717 (1987).

8. M. Tuominen, A.M. Goldman, and M. L. Mecartney, Phys. Rev. B **37**, 548 (1988).

9. Y. Yeshurun and A.P. Malozemoff, Phys. Rev. Lett. **60**, 2202 (1988).

10. References 1-5 from A.P. Malozemoff, T.K. Worthington, Y. Yeshurun, F. Holtzberg, P.H. Kes, Phys. Rev. B **38**, 7203 (1988).

11. P.L. Gammel, L.F. Schneemeyer, J.V. Waszczak, and D.J. Bishop, Phys. Rev. Lett. **61**, 1666 (1988).

12. T.T.M. Palstra, private communication, 1990, and T.T.M. Palstra, B. Batlogg, L.F. Schneemeyer, and J.V. Waszczak, Phys. Rev B **43**, 3756 (1991).

13. D. Shi, M.S. Boley, U. Welp, J.G. Chen, and Youxin Liao, Phys. Rev B **40**, 5255 (1989).

14. W. Schilling, J. of Nuc. Mat., **72**, 1 (1978).

15. A.R. Sweedler, D.E. Cox, and S. Moehlecke, J. of Nuc. Mat., **72**, 50 (1978).

16. A.A. Abrikosov, Soviet Phys.-JETP **5**, 1174 (1957).

17. A.I. Larkin, Soviet Phys.-JETP **31**, 784 (1970); A.I. Larkin and Yu N. Ovchinnikov, J. Low Temp. Phys. **34**, 409 (1979).

18. P.W. Anderson, Phys. Rev. Lett. **9**, 309 (1962); P.W. Anderson, Rev. Mod. Phys. **36**, 39 (1964).

19. T.T.M. Palstra, B. Batlogg, L.F. Schneemeyer, and J.V. Waszczak, Phys. Rev. Lett. **61**, 1662 (1988).

20. M. Tinkham, Phys. Rev. Lett. **61**, 1658 (1988).

21. R. Griessen, Phys. Rev. Lett. **64**, 1674 (1990).

22. A. Gurevich, Phys. Rev. B **42**, 4857 (1990).

23. S. Martin and A.F. Hebard, Phys. Rev. B **43**, 6253 (1991).

24. P.L. Gammel, D.J. Bishop, G.J. Dolan, J.R. Kwo, C.A. Murray, L.F. Schneemeyer, and J.V. Waszczak, Phys. Rev. Lett., **59**, 2592 (1987).

25. Paraphrased from p. 20 of "High-Temperature Supercurrents May Not Be Forever", by A. Khurana, Physics Today, p. 17, March 1989.

26. D.E. Farrell, J.P. Rice, and D.M. Ginsberg, Phys. Rev. Lett. **67**, 1165 (1991).

27. R.H. Koch, V. Foglietti, W.J. Gallagher, G. Koren, A. Gupta, and M.P.A. Fisher, Phys. Rev. Lett., **63**, 1511 (1989).

28. T. K. Worthington, F.H. Holtzberg, and C.A. Feild, Cryogenics **30**, 417 (1990).

29. M. P. A. Fisher, Phys. Rev. Lett., **62**, 1415 (1989).

30. D.R. Nelson, Phys. Rev. Lett., **60**, 1973 (1988);D.R. Nelson, and S. Seung, Phys. Rev. B **39**, 9153 (1989).

31. D.R. Nelson, in *Proceedings of the Los Alamos Symposium; Phenomenology and Applications of High Temperature Superconductors*, Los Alamos, New Mexico, 1991.

32. D.R. Nelson, J. Stat. Phys., **57**, 511 (1989).

33. A. Houghton, R.A. Pelcovits, and A. Sudbo, Phys. Rev. B **40**, 6763 (1989).

34. G. J. Dolan, G.V. Chandrashekar, T.R. Dinger, C. Field, and F. Holtzberg, Phys. Rev. Lett., **62**, 827 (1989).

35. C. A. Murray, P.L. Gammel, D.J. Bishop, D.B. Mitzi, and A. Kapitulnik, Phys. Rev. Lett., **64**, 2312 (1990).

36. D.G. Grier, C.A. Murray, C.A. Bolle, P.L. Gammel, D.J. Bishop, D. B. Mitzi, and A. Kapitulnik, Phys. Rev. Lett., **66**, 2270 (1991).

37. J.R.Clem, Phys. Rev. B **43**, 7837 (1991).

38. L. Ya. Vinnikov, I.V. Grigoryeva, L.A. Gurevich, and Yu. A. Osipyan, JETP Lett. **49**, 83 (1989).

39. I. Morgenstern, K.A. Muller, and J.G. Bednorz, Z. Phys. B **69**, 33 (1987).

40. A.P. Malozemoff, T.K. Worthington, Y. Yeshurun, F. Holtzberg, P.H. Kes, Phys. Rev. B

38, 7203 (1988).

41. "Radiation Effects on Superconductors", J. Nucl. Mater., **71-72**, (1977-8).

42. F. Rullier-Albenque, Ann. Chimie **12**, 573 (1987).

43. S. Bouffard, Rapport CEA-R-5149 (1982).

44. A. K. Ghosh, H. Weismann, M. Gurvitch, H. Lutz, O.F. Kammerer, C.L. Snead, A. Goland, and M. Strongin, J. Nuc. Mat., **72**, 70 (1978).

45. F. Rullier-Albenque and Y. Quere, Phys. Lett. **81A**, 232 (1981).

46. B.S. Brown, R.C. Birtcher, R.T. Kampwirth, and T.H. Blewitt, J. of Nuc. Mat., **72**, 76 (1978).

47. S.T. Sekula, J. Nuc. Mat., **72**, 91 (1978).

48. G. Ischenko, S. Klaumunzer, H. Nuemuller, H. Adrian, and P. Muller, J. Nucl. Mater., **72**, 212 (1978).

49. I. V. Voronova, J. Nucl. Mater., **72**, 129 (1978).

50. A.M. Campbell and J.E. Evetts, Adv. Phys. **21**, 199 (1972).

51. Y. Quere, Nucl. Inst. and Meth. in Phys. Res., B **33**, 906 (1988).

52. T. Hoshiya, S. Takamura, T. Aruga, and M. Kobiyama, Jap. J. Appl. Phys., **28**, L1352 (1989).

53. Private Communication, 1991, and M. A. Kirk and H. W. Weber, in *Studies of High Temperature Superconductors* (ed. Narlikar, A. V.), Vol. **10**, 253-315, (Nova Science Publishers, New York, 1992)

54. T. Kato, K. Shiraishi, J. Kuniya, and M. Suwa, Jap. J. Appl. Phys., **28**, L766 (1989).

55. K. Shiraishi, T. Kato, and J. Kuniya, Jap. J. Appl. Phys., **28**, L807 (1989).

56. B. Roas, B. Hensel, G. Saemann-Ischenko, and L. Schultz, Appl. Phys. Lett. **54**, 1051 (1989).

57. B. Roas, B. Hensel, S. Henke, G. Saemann-Ischenko, L. Schultz, S. Klaumunzer, B. Kabius, W. Watanabe, and K. Urban, in *Proceedings of the NATO Advanced Study Institute on High Temperature Superconductivity*, Bad Windsheim, West Germany, 13-26 August 1989, edited by R. Kossowsky.

58. A.E. White, K.T. Short, R.C. Dynes, A.F.J. Levi, M. Anzlowar, K.W. Baldwin, P.A. Polakos, T.A. Fulton, and L.N. Dunkleberger, Appl. Phys. Lett. **53**, 1010 (1988).

59. G.C. Xiong, F. Weschenfelder, O. Meyer, G. Linker, H.C. Li, and J. Geerk, *Proceeds. Inter. Conf. at Interlaken*, Physica C **153-155**, 1447 (1988).

60. T. Kato, K. Aihara, J. Kuniya, T. Kamo, and S. Masuda, Jpn. J. Appl. Phys. **27**, L564 (1988).

61. T. Kato, K. Aihara, J. Kuniya, T. Doi, and S. Masuda, *MRS: Intern. Meeting on Adv. Maters.*, Tokyo, MRS Int'l Mtg. on Adv. Mats. **6**, 377 (1989).

62. T. Kato, K. Usami, J. Kuniya, and S. Masuda, Jpn. J. Appl. Phys. **27**, L1104 (1988).

63. G.H. Wang, G.Q. Pang, C.L. Luo, S.Z. Yang, Y. Li, Z.M. Ji, and Z.J. Sun, Phys. Letters A **130**, 405 (1988).

64. G.H. Wang, J. Chen, G.Q. Pang, C.L. Luo, Phys. Letters A **130**, 495 (1988).

65. G.C. Xiong, H.C. Li, G. Linker, and O. Meyer, Phys. Rev. B **38**, 240 (1988).

66. D.B. Chrisey, G.P. Summers, W. G. Maisch, E.A. Burke, W.T. Elam, H. Herman, J.P. Kirkland, and R.A. Neiser, Appl. Phys. Lett. **53**, 1001 (1988).

67. D.B. Chrisey, W. G. Maisch, G.P. Summers, A.R. Kundson, and E.A. Burke, IEEE Trans, Nucl. Sci., **35**, 1456 (1988).

68. D.B. Chrisey, J.S. Horwitz, H.S. Newman, M.E. Reeves, B.D. Weaver, K.S. Grabowski, and G.P. Summers, J. of Superconductivity, **4**, 57 (1991).

69. E.L. Venturini, J.C. Barbour, D.S. Ginley, R.J. Baughman, and B. Morosin, (unpublished results).

70. H. Kupfer, I. Apfelstedt, W. Schauer, R. Flukiger, R. Meir- Hirmer, H. Wuhl, and H. Scheurer, Z. Phys. **69**, 167 (1987).

71. H. Kupfer, C. Keller, T. Wolf, I. Apfelstedt, R. Meier-Hirmer, U. Wiech, and R. Flukiger, in *The Science of Superconductivity and New Materials*, (ed. Nakajima, S.) **172-182**, (World Scientific, Singapore, 1989).

72. A. Wisniewski, M. Baran, P. Przystupski, H. Szymczak, A. Pajaczkowska, B. Pytel, K. Pytel, Solid St. Commun. **65**, 577 (1988).

73. P.H. Hor, Z.J. Huang, L. Gao, R.L. Meng, Y.Y. Xue, C.W. Chu, Y.C. Jean, and J. Farmer, Mod. Phys. Lett. B, **4**, 703 (1990).

74. T. Venkatesan, (unpublished results).

75. W. Schindler, B. Roas, G. Saemann-Ischenko, L. Schultz, and H. Gerstenberg, Physica C

169, 117 (1989).

76. A. Umezawa, G. W. Crabtree, J.Z. Liu, H.W. Weber, W.K. Kwok, L.H. Nunez, T.J. Moran, C.H. Sowers, and H. Claus, Phys. Rev. B **36**, 7151 (1987).

77. J.R. Cost, J.O. Willis, J.D. Thompson,and D.E. Peterson, Phys. Rev. B **37**, 1563 (1988).

78. R.L. Fleischer, H.R. Hart Jr., K.W. Lay, and F.E. Luborsky, Phys. Rev. B **40**, 2163 (1989).

79. K. Watanabe, H. Yamane, H. Kurosawa, T. Hirai, N. Kobayashi, H. Iwasaki, K. Noto, and Y. Muto, Appl. Phys. Lett. **54**, 575 (1989).

80. R. B. van Dover, E. M. Gyorgy, L.F. Schneemeyer, J.W. Mitchell, K.V. Rao, R. Puzniak, and J.V. Waszczak, Nature (London) **342**, 55 (1989).

81. R. B. van Dover, E. M. Gyorgy, A.E. White, L.F. Schneemeyer, R.J. Felder, and J.V. Waszczak, Appl. Phys. Lett. **56**, 2681 (1990).

82. L. Civale, A.D. Marwick, M.W. McElfresh, T.K. Worthington, A.P.Malozemoff, and F.H. Holtzberg, Phys. Rev. Lett. **65**, 1164 (1990).

83. F.J. Ziegler and J.P. Biersack, *The Stopping and Range of Ions in Solids* (Pergamon, New York, 1985).

84. T.L. Hylton and M.R. Beasley, Phys. Rev B **41**, 11661 (1990).

85. T. Aruga, S. Takamura, T. Hoshiya, and M. Kobiyama, Jpn. J. Appl. Phys. **28**, L964 (1989).

86. S. Takamura, T. Aruga, and T. Hoshiya, Jpn. J. Appl. Phys. **28**, L1118 (1989).

87. S. Takamura, T. Hoshiya, T. Aruga, and M. Kobiyama, Jpn. J. Appl. Phys. **28**, L1395 (1989).

88. T. Hoshiya, S. Takamura, T. Aruga, and M. Kobiyama, S. Miura, Y. Kubo, N. Shohata, Jpn. J. Appl. Phys. **29**, L2026 (1990).

89. S. Matsui, H. Matsutera, T. Yoshitake, and T. Satoh, Appl. Phys. Lett. **53**, 2096 (1988).

90. H. Yoshida and K. Atobe, *MRS:Intern. Meeting on Adv. Maters.*, Tokyo, (1988). MRS Int'l Mtg. on Adv. Mats. **6**, 371 (1989).

91. T.T.M. Palstra, B. Batlogg, L.F. Schneemeyer, and J.V. Waszczak, Phys. Rev. B, **43**, 3756 (1991).

Chapter 4

Experimental Procedures

The purpose of this experiment was to make a meaningful comparison of the effects of four different types of ion irradiations on vortex behavior in the $Bi_2Sr_2CaCu_2O_{8+\delta}$ superconductor.* In this chapter we begin by giving an overview of the experimental design, which addresses the significant difficulties involved in this task. The experimental procedures are then discussed in detail.

4.1 Experimental Design

First, to minimize complications arising from sample variations, we determined that the use of high quality, well characterized, reproducible single crystals was essential. The advantages afforded by such samples in a typical experiment (for example, well determined structure and anisotropy without the complication of grain boundaries), here become a necessity, because we seek to distinguish as clearly as possible the effects of post-growth sample treatments from the effects of nonuniformity or inhomogeneity in the as-grown material. Moreover, in this experiment there is potential for any anomalous features in the unirradiated material to interact in the damage production process to create singular and possi-

*$Bi_2Sr_2CaCu_2O_{8+\delta}$ was chosen for this study rather than the three-layer compound, $Bi_2Sr_2Ca_2Cu_3O_{10+y}$, in part because its structural and electrical properties had been far more extensively characterized. This was an advantage with respect to examining the effects of modifying the material with irradiation. Also, at the time (1990), it was still relatively difficult to synthesize the three-layer compound in single phase form. It was easier to establish conditions of crystal growth to isolate the 2212 phase from the 2223 phase than vice versa.

bly irreproducible defect structures. The availability of high quality samples for this experiment was critical in addressing these difficulties. Nevertheless, even the sample variations observed in the best starting material can complicate the analysis of the results. Therefore, it was also considered imperative to compare measurements on the same single crystal sample before and after irradiation. These experimental features, as simple as they may sound, are in contrast to many studies which have attempted detailed analysis of irradiation results in thin films or polycrystalline materials and/or without sample specific comparisons.

Secondly, the breadth of characterization had to be carefully defined, as all measurements were to be repeated for four different ionic species before and after irradiation. We elected to concentrate on transport rather than magnetization techniques, which although representing a higher level of experimental difficulty, give more direct and unambiguous information about the superconducting properties. In some cases, however, critical currents were also inferred from measurements by a vibrating-sample magnetometer. A survey of the phase diagram was conducted in detail as a function of temperature and current, while magnetic fields were confined to particular values. This allowed us to compare low and high density vortex behavior at various temperatures, without attempting a detailed analysis as a function of applied field.

Specifically, before irradiation, detailed R vs. T measurements were performed from approximately 95 K to below the transition temperature (minimum of 4.2 K) at four currents (10 μA, 100 μA, 1 mA, and 10 mA), giving a rough I-V characteristic at all temperatures. Detailed I-V curves were then measured in temperature ranges of interest, where rapid changes were occurring. These measurements were performed in zero field, low field (0.05 T) and in high field (5.0 T). Samples were then irradiated, and the measurements repeated. Irradiations were usually restricted to one set of conditions per ionic species. As will be discussed in detail, an argument was constructed for choosing ion fluences to reflect a roughly equivalent level of damage for different ions, in a regime that was estimated to be the most likely to optimize the critical current. The design of the experiment is summarized by the flowchart in Fig. 4.1.

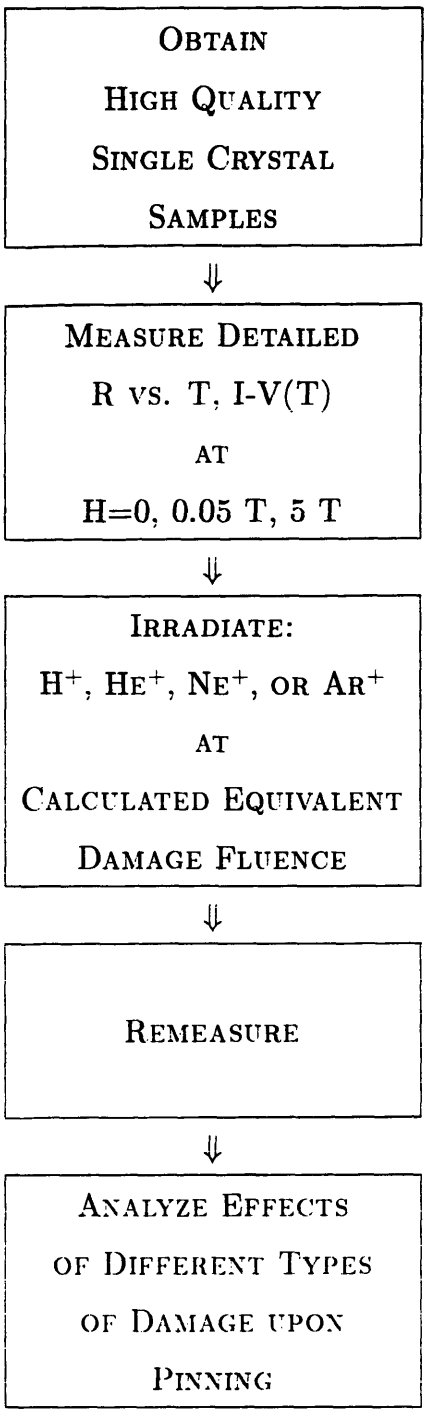

Figure 4-1: Flowchart of the experiment.

4.2 Sample Growth

Samples were grown by two methods, the flux growth method of L. F. Schneemeyer[1] and a directional solidification method originally developed by D. B. Mitzi.[2] The flux growth method requires considerable expertise and therefore these samples were prepared by L. F. Schneemeyer, whereas directional solidification samples were prepared by the author.

For a complete description of the flux growth method, the reader is referred to Chapter 2 (section 2.2.2). In the current experiment, KCl was the only salt used and crucibles were platinum or Coors Alumina. This method yielded very thin samples of approximately 2 μ in thickness. Because they are so thin, these crystals are somewhat flexible and tend to have curled shapes (like potato chips). Interestingly, occasionally this method inadvertently produced material containing some amount of 2223 phase superconductor (T_c = 110 K) as well as the desired 2212 phase, resulting in "stairstep" transitions with zero resistance temperatures as high as 93 K. Some preliminary characterization was done on these samples. However, all fully characterized samples for detailed study of irradiation had clean transitions and were selected from "batches" of single phase 2212 material.

Note that for the samples studied in Chapter 2, the stoichiometry of $Bi_{2.2}Sr_2Ca_{0.8}Cu_2O_{8+\delta}$ was precisely determined from x-ray structure refinement. By the time of the irradiation experiments, this stoichiometry had been found to be consistent with analysis of 2212 crystals grown around the world. The x-ray characterization was therefore not repeated on crystals grown by the same method for the current experiment. While a sightly different stoichiometry is evidenced by higher T_c's in the later 2212 samples (with clean transitions and no step at 110 K), this reflects the optimization of the oxygen content as controlled by post-annealing procedures. For this material, the resistance goes to zero close to 90 K rather than near 84 K as in the older samples of Chapter 2, which were among the earliest attempts to synthesize Bi-2212. For convenience, the exact stoichiometry is in general no longer quoted, in favor of less cumbersome nomenclature. Therefore, $Bi_{2.2}Sr_2Ca_{0.8}Cu_2O_{8+\delta}$ is often referred to as $Bi_2Sr_2CaCu_2O_{8+\delta}$ or $Bi_2Sr_2CaCu_2O_8$ in this thesis, particulary after the early work of Chapter 2.

Reactant	Weight (g)
Bi_2O_3	25.1056
$SrCO_3$	13.2570
$CaCO_3$	4.4939
CuO	7.1434

Table 4.1: Reactant Powders for Bi-2212 Crystal Growth

The directional solidification or Mitzi method starts from almost the same set of reactant powders as the flux growth method, except that here the source of calcium was $CaCO_3$ instead of $Ca(OH)_2$. These powders were weighed out within $\pm$ 1 mg as given in Table 4.1 to yield a (bismuth rich) atomic ratio of 2.4Bi:2Sr:1Ca:2Cu. The excess Bi_2O_3 allows for evaporation during growth and acts as a flux for the crystal growth.* The total weight of the starting material was 50 g.

The reactant powders were thoroughly mixed with a mortar and pestle, placed in a 50 ml Coors alumina crucible (CH 50 65504 13), covered with aluminum foil, and placed in a box furnace. In order to provide a temperature gradient, the crucible was pushed up against the wall of the oven within approximately 0.5 cm of the heating element. The mixture was heated in air to 900°C - 930°C, held at this temperature for 2 hours and allowed to cool at a rate of 1°C/h to a temperature of 725°C, which took about 1 week. The furnace was then turned off and the crucible was removed several hours later when cool enough to handle. This method yields a walnut-sized chunk (about 20 cm^3) of material which may be recovered from the crucible by breaking it with a hammer. From this, samples of the appropriate size may be obtained by procedures that will be described.

*It may be useful to note here that the melting point of elemental bismuth (271° C) is considerably lower than the maximum heating temperature during crystal growth, which is above 900° C. For comparison, the melting points of the other elemental components are, for Sr: 769° C, Ca: 839° C, and Cu: 1084° C. The specific behavior of mixtures of the melted oxides and carbonates of these components is, however, beyond the scope of this thesis.

4.3 Sample Handling

Bi-Sr-Ca-Cu-O materials are inherently prone to breakage as they are micaceous and very brittle. Very thin samples are especially fragile and will break if held between conventional tweezers in the usual way. For handling larger pieces of material, such tweezers are an appropriate tool, but very thin ($< 10\ \mu$) samples are best handled with a combination of vacuum tweezers and prodding instruments (such as the tips of conventional tweezers or approximately 1/16" diameter wooden sticks).

4.3.1 Sample Thinning

As previously described, the Mitzi method produces a large chunk of material, so a method of removing small samples was developed. First, pieces of about 0.5 cm^3 or smaller were gently flicked off with a sharp razor blade, and examined under a stereo microscope to identify exposed cleavage planes. These appear as extraordinarily smooth shiny black surfaces. Then a thin layer of acetone soluble adhesive was melted on a standard Corning glass slide at a hotplate temperature of about 70°C. The chunks were set down in the glue with the crystal face down, taking care not to smear glue up the sides of the samples, and allowed to cool. From this point there are several ways to obtain very thin (a few μ's) samples, finding the best of which is a matter of practice and luck. The desired result is a clean sample with crystal planes exposed on both sides.

A particularly successful method was to use ordinary scotch tape to remove layers of material while observing the sample under the stereo-microscope for the appearance of a clean crystal face. The tape was pressed down on the sample (moderate finger pressure) and then quickly pulled (not peeled) straight off. In general, more finger pressure removes more material, as can be fine-tuned with practice. Once a clean plane is obtained in this manner, the razor blade can be used to cleave from underneath, which works cleanly a reasonable percentage of the time. Resulting sample thicknesses varied widely with this method.

Alternatively, the tape process can be used until very little material is left on the slide.

Then, provided that gentle removal of the material very near the bottom successfully exposes a face, the material left stuck on the slide can be used as the sample. The glue can be dissolved by washing the slide in a series of solvents, for example trichlorethylene followed by acetone and then methanol, and recovering the sample. This method produced the thinnest samples (down to 5 μ) and thinner samples probably could have been obtained with practice. Material thin enough to see through was observed but could not be removed from the slide without destroying it. The most common failure of this method was that frequently the entire sample was inadvertently pulled off, leaving nothing on the slide.

Finally, the most serendipitous method was to simply flick off large quantities of samples using only the razor blade and search the pile for a thin one that had cleaved cleanly on both sides. This method had the obvious disadvantage of low yield but was also the least tedious.

Samples produced by the flux growth method obviously did not need to be thinned as their thicknesses as-grown were known[3] to be about 2 μ.

4.3.2 Sample Thickness by Weighing

Sample thickness could sometimes be determined fairly accurately by weighing the small flakes produced by the methods above. Areal dimensions were measured under the stereo microscope with a vernier eyepiece and the sample density was estimated at 6 g/cm^3. Very thin flakes of small area presented difficulty because they could not be accurately weighed. Therefore, the largest flakes were first weighed and then cut into smaller pieces of appropriate geometry for attaching line contacts. Note that areal determinations were approximate, (5 - 10% accuracy), as samples were not perfect rectangles, especially before they were cut down. Coupled with errors in the weighing, the total accuracy of this type of thickness measurement is estimated to be better than 15%.

This method worked well for the thinned down samples grown by the Mitzi method, which tended to be larger in area and were found to have thicknesses no smaller than 5 μ. In contrast,

the flux-growth samples had smaller areal dimensions and were significantly thinner. Because of their small size, attempts at individual thickness determinations by weight were not successful. (For example, a sample of areal dimension 1 mm x 0.5 mm and 2 μ thickness would weigh about 6 μg. The zero of the balance oscillates by about 6 μg over a period of several seconds, putting this near the limit of error of the instrument. Sample areas and therefore their weights were often smaller than this.) Because previous measurements by L. F. Schneemeyer had shown that KCl flux samples naturally form with a thickness of approximately 2 μ, more sophisticated methods of measuring individual thicknesses of these samples were not considered necessary.

4.4 Electrical Contacts

Since critical current data were to be taken, four point Ag contacts were attached in a well defined in-line geometry, as shown in Fig. 4.2a. Samples were cut with a razor blade into rectangles of approximate dimension 1 mm x 0.5 mm. The cut edges had no particular alignment with respect to a-b directions. Masking, wire attachment and mounting were accomplished under the stereomicroscope by the following procedures, utilizing the extremely helpful advice of R. B. van Dover.

4.4.1 Masking

The samples were placed on standard Corning glass slides and viewed under the microscope to estimate dimensions. Tiny pieces of aluminum foil strips were cut to the approximate sizes needed to protect the regions which would be in between the contacts from the Ag evaporation, as shown in Fig. 4.2b. For the smaller side regions in between the current and voltage contacts it was sometimes more effective to mask with a strip of flattened wire of approximately 0.002 in. diameter, or alternatively the foil strips were cut along a slivered angle to get very narrow widths. The masking strips were set aside, and then tiny pieces of 3M yellow tape were cut using scissors (not the razor blade) to about the same dimensions as the sample. These were also set aside. The masking strips were then laid across the sample to produce the typical in-line pattern

of Fig. 4.2a. The small strips of yellow tape were used to stick the mask materials to the glass slide on either side of the sample, but without actually touching the sample. The occasional accident of touching the superconductor itself with the tape invariably produced catastrophic results. The sample was quite adequately held in place by inertia and slight pressure from the strips above. By this method, several samples could be placed on a given slide and masked, and then stored in the dry box for periods ranging up to a day or so to await Ag evaporation.

Evaporations were performed in a standard thermal evaporator. A thickness of 2000 Å Ag was deposited, as measured with a standard crystal monitor. After evaporation the masks were pulled off with tweezers, and the patterned samples were annealed in a furnace at 400°C for approximately 2 hours. This procedure generally yielded contact resistances from 1 Ω - 10 Ω, with some exceptions.

4.4.2 Wire Attachment

Bare silver wires of 1 mil diameter were attached to the contact pads with conductive Ag epoxy. This was a difficult task as both the wires and the contact pads are very small. A good technique was to first dip a slightly larger diameter wire (2 mil) in the epoxy and use it to hold a small globule in which to roll the 1 mil Ag wire. Very fine mechanical tweezers (standard, available from any semiconductor supply source) were needed to grip the smaller wire for this coating procedure. The coated end was gently laid on the contact pad, taking care not to let the epoxy run in between the contacts or down the side of the sample (which would have glued it to the glass slide beneath). The slide and sample were then placed in a 150°C furnace for 5-10 minutes to set the epoxy. Sometimes it was advantageous to do this procedure one wire at a time although it is possible to attach up to all four wires at once. It required some skill to get enough epoxy on the wire to insure a strong bond but not so much that it smeared across (and ruined) the sample. In some cases, it was best to bake the sample immediately, to prevent the epoxy from spreading all over it, before proceeding to the next wire.

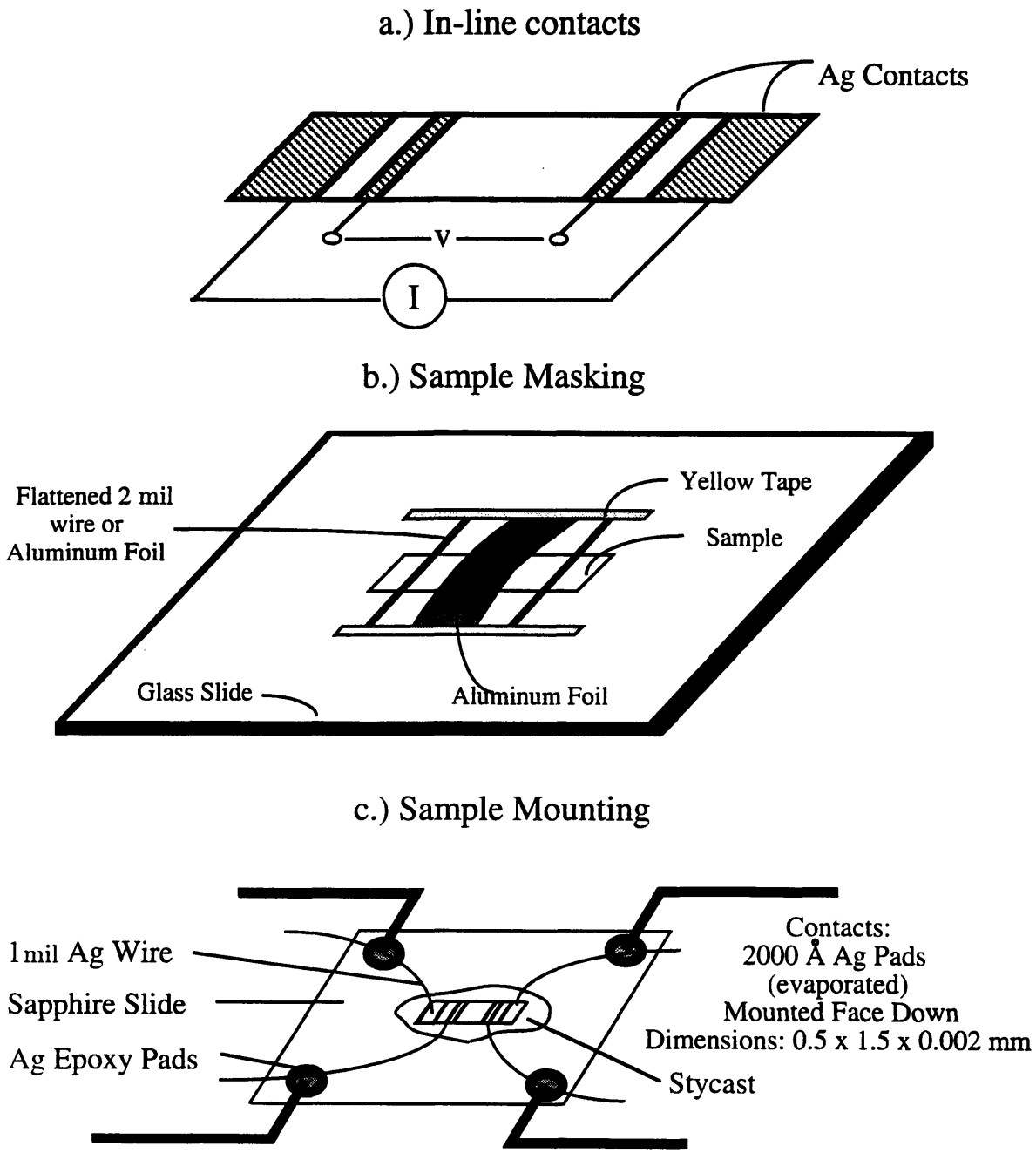

Figure 4-2: Electrical contacts: a.) in-line contacts b.) sample masking c.) sample mounting

4.4.3 Sample Mounting

The mounting method was designed to facilitate both the irradiation procedure and the electrical measurements. By mounting the sample face down it was possible to uniformly expose the entire area of the backside of the sample to the ion beam without obstruction by the electrical contacts/wire arrangement. The contacted side was instead embedded in a thermally conductive, electrically insulating adhesive ("Stycast"). This provided excellent heat-sinking during irradiation as well as a high degree of thermal, electrical and mechanical stability during measurement.

The first step of the mounting procedure was to cut a sapphire slide into a rectangle of approximate dimensions 3 mm x 5 mm. Then four silver epoxy pads were made at the corners with bare wires embedded as shown in Fig. 4.2c, and cured in the oven as previously described. The adhesive Stycast was mixed to a relatively firm consistency and applied to the center of the slide. The sample was picked up by grasping one of its attached 1 mil wires with tweezers and was gently laid face down in the viscous stycast. Important considerations at this stage were to orient the sample so that the four 1 mil wires passed relatively close to the four silver pads, and to insure that the face of the sample was in good contact with the Stycast but without letting the sample sink. This could usually be accomplished by mixing the stycast to the right viscosity and handling the sample carefully; however some samples were rendered unusable at this stage due to partial sinking. Samples were set aside to cure overnight at room temperature in a drybox. After the adhesive was set, the 1 mil silver wires were epoxied to the pads, and the sample was ready to be measured.

4.5 Transport Measurement Techniques

Simple T_c measurements from room temperature down to 4.2 K were performed in zero-field by dipping in liquid He using various typical measurement apparatus designed for this purpose. Detailed transport measurements requiring precise in-field temperature control were carried out in a standard He flow cryostat. The sample was positioned on a measurement probe that

was inserted into the temperature controlled zone of the cryostat, as shown in Figure 4.3. Fields of up to 8 tesla, directed along the vertical axis of the cryostat, could be generated in the sample region by a superconducting magnet, which was operated in these experiments in the persistent mode. Samples were mounted in the orientation H || c on the copper block at the probe tip, with thermal contact secured by a small amount of thermally conductive compound (Wakefield Grease) applied between the block and the sapphire slide. The sample temperature was measured by a carbon glass resistance thermometer fastened on the copper block. All electrical connections were made by soldering to the probe contacts. Probe wires led up and out of the cryostat as twisted pairs (voltage measurement leads) or microcoax. Temperature control was achieved with a programmable Oxford Intelligent Temperature Controller ITC 4, which could control accurately to within 0.1 K. As will be described, for measurements made at constant temperature, a secondary sample heater was sometimes used.

All measurements were under program control by various subroutines of the Basic program "Works", written by R. B. van Dover. Three basic types of in-field measurements were performed; resistance vs. temperature (R vs. T) recorded at dc currents of 10 μA, 100 μA, 1 mA, and 10 mA, current vs. voltage (I-V) measured with a standard dc technique, and current vs. voltage measured using a special pulse current technique. The pulse I-V measurements were used whenever possible to avoid sample heating, but dc measurements were included in cases where samples responded unpredictably to pulse input. Each of these measurement techniques will now be described in detail.

4.5.1 R vs. T Measurements

For R vs. T measurements the rate of change of the temperature was set by manually programming the Oxford ITC 4 in the desired temperature range and then the voltage was recorded at 30 s intervals for each of the four currents by the subroutine "Izvstime". The resulting data intervals were typically around 0.1 K for data of low structure and approximately 0.005 K for data of high structure. The current originated from a Keithley 224 Programmable Current Source and the voltage signal was filtered (50 dB, 15 KHz) and then measured by a Keithley

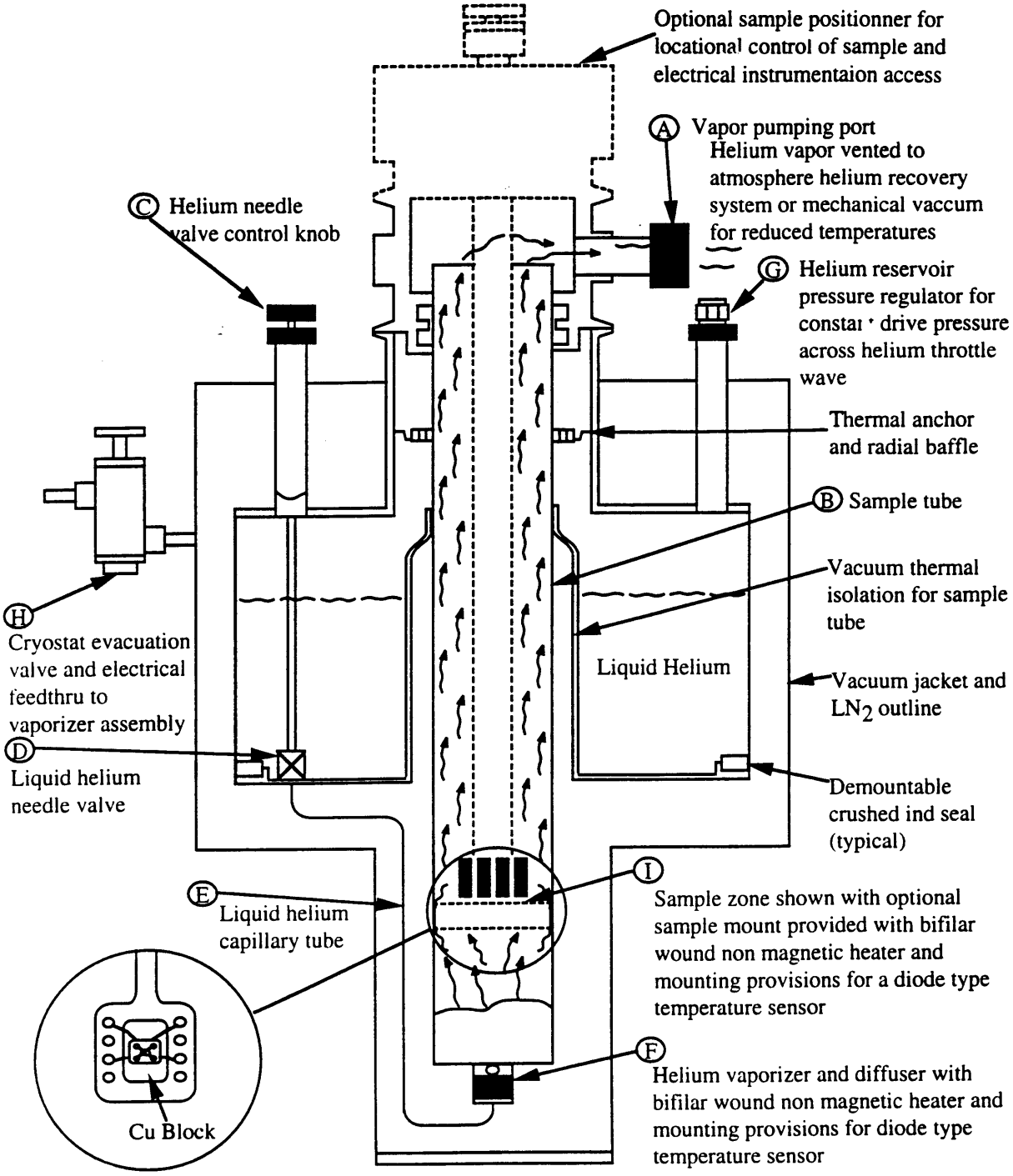

Figure 4-3: Schematic of the helium flow cryostat

181 Nanovoltmeter.

4.5.2 DC I-V Measurements

DC current-voltage measurements were controlled by the subroutine "Iv", which ramped the (Keithley 224) current in the desired increments and range. The data recorded were the current requested by the program (i.e. not independently measured) and the corresponding voltage measured by the Keithley 181. The temperature was held constant during the measurement within 0.1 K (except in cases of note as observed in the dc measurement at higher currents and higher contact resistances and designated as such in the presentation of the data). To more quickly attain the desired setpoint temperature, an additional heater was used as necessary. For this method of temperature control, employed for both dc and pulse I-V measurements, the Oxford ITC 4 was set slightly (about 2 K) below the desired temperature and the secondary heater was controlled by a PAR Cryogenic Temperature Controller through a resistance bridge and EG&G PAR Model 116 Differential Preamplifier.

4.5.3 Pulse I-V Measurements

The pulse IV measurement technique, designed by R. B. van Dover, was somewhat more complicated. The goal of the technique is to accomplish a dc-like measurement while avoiding sample heating from dissipation at the contacts. To do this, a short (100 μs flattop) current pulse with a very long period (5.6 ms) was input to the sample and then a boxcar averager was used to "look" at the voltage signal only during a 50 μs interval (aperture) delayed to fall within the flattop time of the pulse. Thus only the steady state voltage is observed after the transients have died away, making this equivalent to a dc I-V measurement. The advantage of this technique is that for such a short pulse and long period, the sample has a very short heating time compared to a very long cooling time between pulses, which minimizes the effects of sample heating upon the measurement.

A block diagram of the pulse IV measurement, which was under control of the subroutine

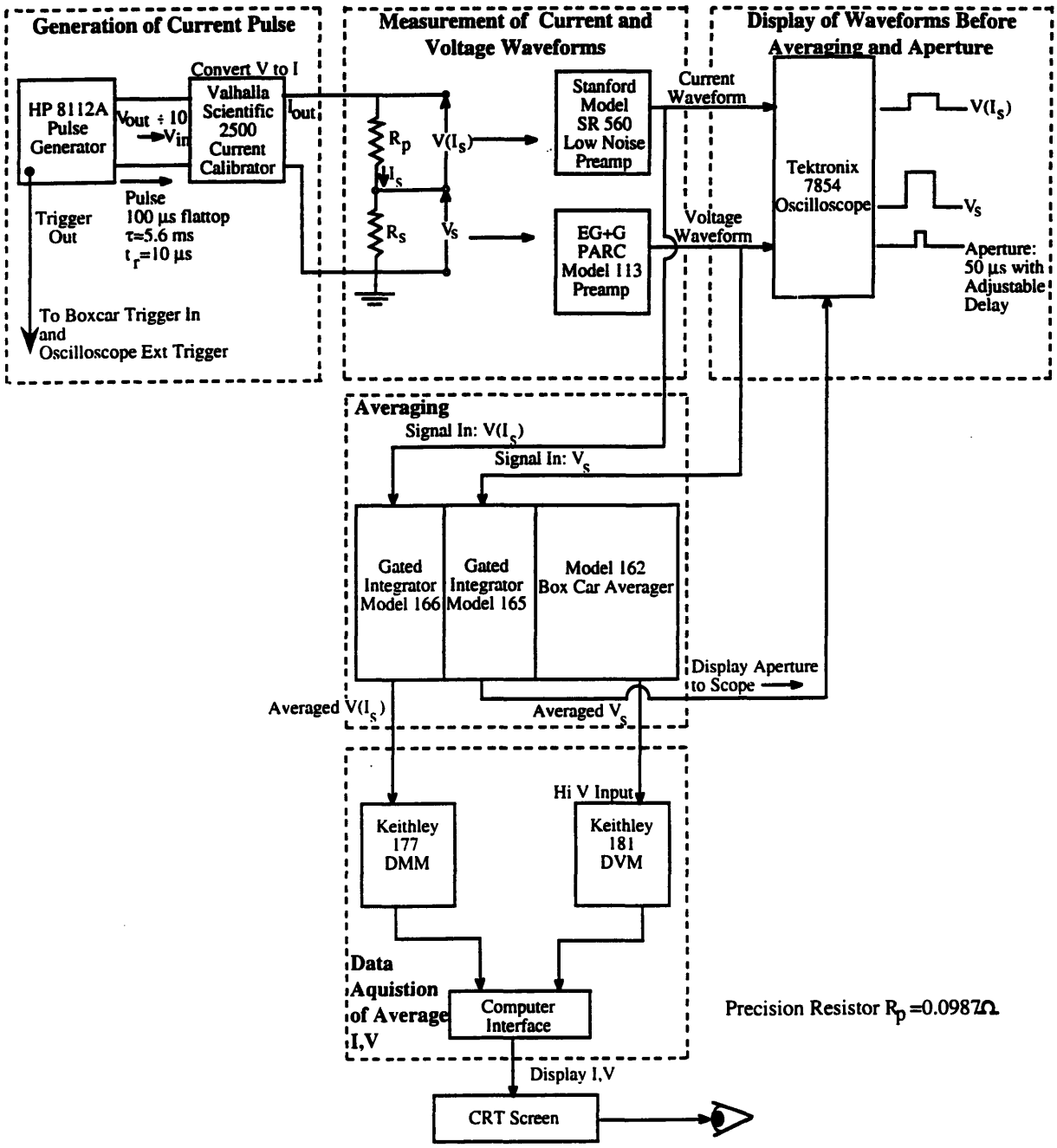

Figure 4-4: Block diagram of the pulse I-V measurement.

"Ivpulse", is given in Fig. 4.4. To generate the input current pulse, the program ramped the Hewlett Packard 8112A Pulse Generator, which output a voltage pulse (100 μs flattop, T = 5.6 ms, 10 μs risetime) to a Valhalla Scientific 2500 Current Calibrator. The Valhalla converted the voltage signal to a current signal of the desired magnitude (full scale output available between 1 μA and 1 A), and this pulse current was output to a precision measurement resistor (0.0987 Ω) in series with the sample. The measurement of the average sample current (during the time that the boxcar aperture is open) was accomplished by feeding the filtered and amplified (Stanford Model SR 560 Low Noise Preamplifier) voltage across this resistor into one of the gated integrators (Bin Model 166) of the Model 162 Boxcar Averager. The boxcar was triggered off of the pulse generator to open the 50 μs aperture with the desired delay time (adjustable). The average signal output of the gated integrator was measured by a Keithley 177 Microvolt Digital Multimeter. This was interfaced to the computer so that the average ramp current could be recorded and also displayed to the CRT screen. In order to monitor the actual waveform of the current through the sample, the pulse signal (before averaging) was routed for display to an oscilloscope (Tektronix 7854), which was also triggered off of the HP pulse generator.

The voltage across the sample was fed into a EG&G PARC Model 113 Preamplifier. The filtered and amplified signal was output to another gated integrator (Bin Model 165) of the boxcar averager and also to the oscilloscope for display. The aperture of the boxcar was displayed on the oscilloscope with the sample voltage waveform to make it possible to directly inspect whether any transient features in the waveform fell inside (or outside) the observation window. The output signal of the boxcar was measured by the Keithley 181 Nanovoltmeter and sent to the computer for onscreen display and recording of the sample voltage as a function of current.

4.6 Non-contact Magnetic Measurements

The author made use of the facilities and expertise available at AT&T Bell Laboratories to obtain additional non-transport measurements on a number of samples. The sample magnetization as a function of applied field was measured on a Vibrating Sample Magnetometer by R.

B. van Dover and E. M. Gyorgy and the data was reduced by the author. J_c's were inferred from the critical state model with appropriate geometrical corrections[4] according to the formula,

$$J_c = 20\Delta M \frac{1/d}{(1 - d/3l)}$$

where

$$\Delta M = \Delta m / V$$

and Δm is the width of the loop in emu's at a given field, V is the sample volume, and d and l are the smaller and larger lateral dimensions, respectively, of the sample.

The transition temperature of one sample was measured using low field ac susceptibility by R. B. van Dover.

4.7 Selection of Irradiation Conditions

In choosing irradiation conditions for the different ions, extensive use was made of the calculational tools available to simulate the interactions of ion beams with solids, most notably the program TRIM (TRansport of Ions in Matter) by J. F. Ziegler.[5] Since our aim was to try to compare the effects of different types of damage due to different irradiating ionic species, efforts were made to eliminate extraneous effects in order to try to isolate this variable. The main goals were to induce damage as homogeneously as possible throughout the volume of each sample, and to induce roughly the same level of damage for different ions. The first goal ideally requires that the samples be thin enough to transmit the ions through, as the ion interactions with the target increase considerably as they slow down, creating a characteristically "humped" damage profile as a function of depth in the sample. Secondly, a criterion of equivalent damage was necessary, independent of the incident ionic species. For this we selected the irradiation conditions that would approximately match the average number of vacancies induced per unit volume, as calculated (simulated) by the program TRIM for different ions. This criterion, while having certain limitations (see sections 5.2, 5.7), made it possible to draw comparisons of the

Ion	H^+	He^+	Ne^+	Ar^+
Projected Range (μ)	27.24	7.51	1.85	1.19
Energy (MeV)	2.0	3.0	3.1	2.5

Table 4.2: Projected Ranges of Ions in Bi-2212 Crystals

different types of damage induced by different ionic species.

4.7.1 The Range of Different Ionic Species

For a given incident energy, the heavier ions have a shorter range in the target due to their larger collision cross sections. To determine if the samples were thin enough to transmit the ions, the projected range of each type of ion in the target was calculated by the subprogram STOP of the program TRIM. The incident ion energies used (H^+: 2.0 MeV, He^+: 3.0 MeV, Ne^+: 3.1 MeV, Ar^+: 2.5 MeV) were the maximum compatible with laboratory safety constraints for the heavier ions, in order to attain maximum transmission. The energy of 2 MeV for H^+ was selected by analogy to the H^- irradiation conditions that had maximized the critical current in previous experiments on $YBa_2Cu_3O_7$. (For the purposes of analysis, these minor variations in incident energy are not very significant.)

Because the targets available within TRIM are limited to four element compounds, this and all subsequent TRIM calculations were performed on an averaged target. Because of the importance of the copper oxide planes, the Cu and O were preserved and the Sr and Ca, assumed to be the least important of the five, were averaged to Ge, which has the appropriate atomic weight for the weighted average of 2Sr:1Ca. Thus $Bi_2Sr_2CaCu_2O_{8+\delta}$ became $Bi_2Ge_3Cu_2O_8$ for calculational purposes. The projected ranges of the ions in this target are given in Table 4.2.

Clearly, total transmission is assured for H^- and He^- but there is some implantation for Ne^+ and especially Ar^+. As will be seen, this is also evidenced in the non-linear shape of the damage profile for the heavier ions.

4.7.2 Damage Profiles

Damage profiles were calculated by TRIM from a Kinchin-Pease model,* and the number of vacancies produced per ion per unit length (vacancies/ion/Å) were plotted as a function of depth in the sample, as shown in Figs. 4.5a - 4.5d. In these profiles, the vacancies resulting from primary knock-on atoms (PKA's) and those due to recoiling target atoms, as calculated by TRIM, have been summed. The simulation has been carried beyond the actual sample thickness (generally about 2 μ) out to a depth of 3 μ. Note that far from regions of implantation, the damage profiles are approximately linear, as seen out to 3 μ for the lighter ions, as compared to the humped portion of the profile or "end of range" damage, present at less than 2 μ depth for Ne^+ and especially Ar^+. In no case is the profile flat,† corresponding to our ideal goal of homogeneous damage. However, within the sample depth, deviations are in the worst case held to within roughly an order of magnitude, and the level of implantation is absolutely not chemically significant. To obtain yet thinner samples would be extremely difficult and time consuming, so a certain amount of end of range damage cannot be avoided.

4.7.3 Equivalent Damage

The total number of vacancies/ion/Angstrom were integrated out to a depth of 2 μ using linear regressions or approximating areas by hand as appropriate. This procedure gives the total induced vacancies per incident ion. Clearly this number is strongly dependent upon the size of the particular incident species. For example, it is around 1/2 for H^+ at 2 MeV but approximately 2500 for Ne^+ at 3.1 MeV. Therefore to make the Ne^+ irradiation produce approximately the same average number of vacancies per unit volume as the H^- irradiation, the incident fluence (ions/cm^2) has to be adjusted downward by a factor of 5000. Fluences for each species were selected accordingly, to match the number of vacancies produced by an H^+ fluence of 1 x 10^{16}

*The Kinchin-Pease model uses an analytic solution to calculate the displacement damage due to the recoil cascade initiated by a primary knock-on atom (PKA). This is a "quick" alternative to the full cascade calculation, in which each recoiling target atom is followed individually to arrive at the number of displacements ultimately produced.

†Although the profile for He^+ appears to have a very small slope, lower than that for H^+, note that the vertical scale in Fig. 4.5b is a factor of ten larger than in Fig. 4.5a. The profile for He^+ damage is actually steeper than that for H^+. Note also the large scales on the vertical axes in Figs. 4.5c and 4.5d, reflecting difference factors of several thousand in vacancy production per ion per Angstrom by the heavier ions.

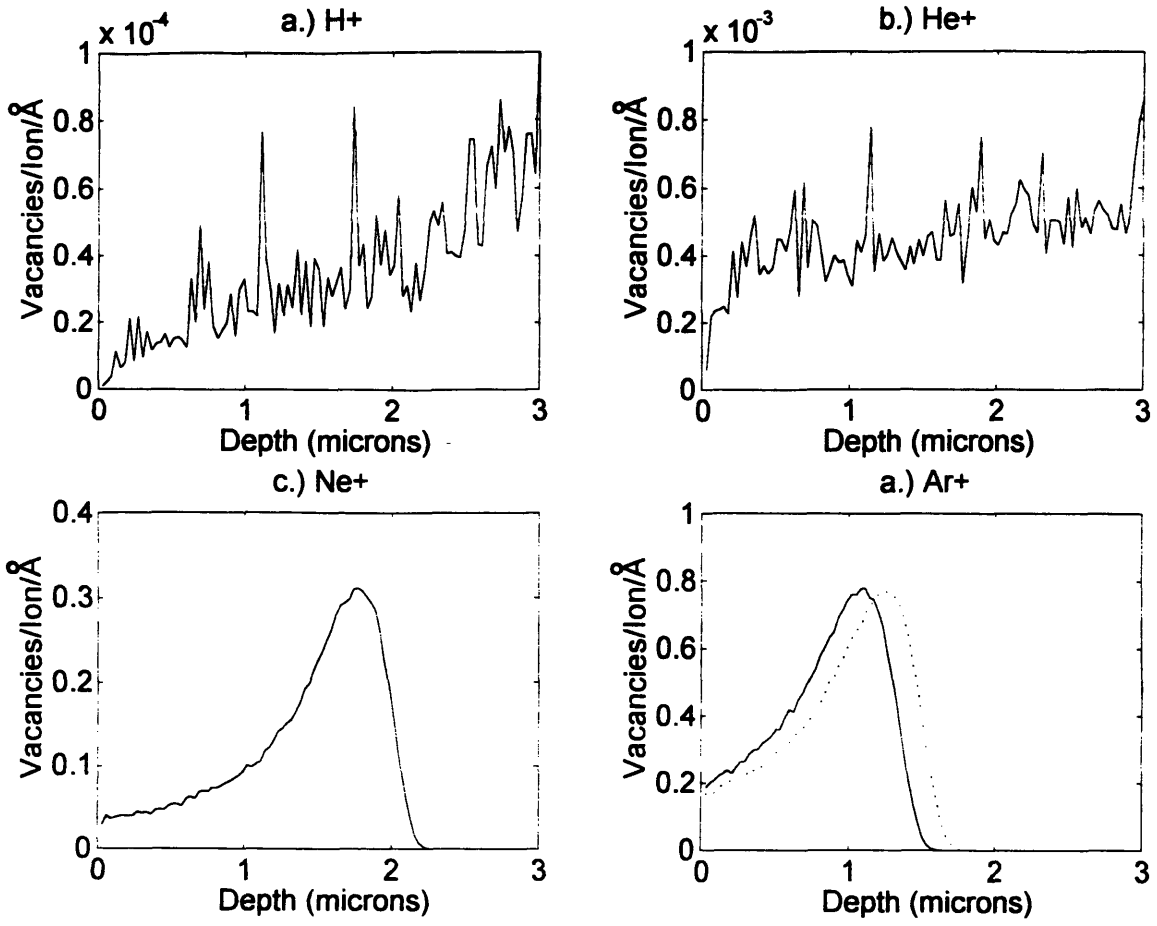

Figure 4-5: Damage profiles for all ions: a.) H^- at 2.0 MeV b.) He^+ at 3.0 MeV c.) Ne^+ at 3.1 MeV d.) Ar^+ at 2.5 MeV, solid line and 3.0 MeV, dotted line. Simulated damage has been plotted to a depth of 3 μ, to insure that the profile includes total actual sample depth. Vacancies due to PKA's and recoils have been summed.

Ion	H^+	He^+	Ne^+	Ar^+
Fluence (ions/cm^2)	1 x 10^{16}	6.4 x 10^{14}	2 x 10^{12}	6 x 10^{11}
Energy (MeV)	2.0	3.0	3.1	2.5*

Table 4.3: Equivalent Damage Fluences

cm^{-2} at 2 MeV. As previously mentioned, the conditions for H^+ were independently selected, by analogy to the H^+ irradiation conditions that had maximized the critical current in experiments on $YBa_2Cu_3O_7$. The doses thus selected are given in Table 4.3, along with the incident ion energies.*

4.7.4 Irradiation Technique

All samples were irradiated at room temperature using standard ion beam techniques (Tandem Van de Graaf accelerator) by A. E. White at AT&T Bell Laboratories.

*After the equivalent damage fluence was calculated based on an incident energy of 3 MeV, the actual irradiation was done at 2.5 MeV, based on the safety concerns of A. E. White. The error introduced by this discrepancy is minimal. In Table 4.2 the range is given for the actual incident energy of 2.5 MeV. In Figure 4.5 damage profiles for Ar^+ are shown at both energies for comparison. The difference in the integrated numbers of vacancies is negligible.

4.8 References

1. L. F. Schneemeyer, R. B. van Dover, S. H. Glarum, S. A.Sunshine, R. M. Fleming, B. Batlogg, T. Siegrist, J. H. Marshall, J. V. Waszczak, and L. W. Rupp, Jr., Nature **332**, 422 (1988).

2. D. B. Mitzi, L. W. Lombardo, and A. Kapitulnik, Phys. Rev. B **41**, 6564 (1990).

3. Private Communication, L. F. Schneemeyer.

4. E. M. Gyorgy, R. B. van Dover, K. A. Jackson, L. F. Schneemeyer, and J. V. Waszczak, Appl. Phys. Lett. **55**, 283 (1989).

5. J. Biersack and L. Haggmark, Nucl. Instrum. Methods, **174**, 257 (1980); J. F. Ziegler, J. P. Biersack, and U. Littmark, *The Stopping and Range of Ions in Solids*, (Pergamon, New York, 1985).

Chapter 5

Results and Discussion

5.1 Sample Selection

The sample growth and mounting procedures of Chapter 4 resulted in the preparation of more than forty samples from which were chosen those best suited for irradiation. These samples were cut from material grown by both the Mitzi and flux growth methods and from various different "batches", both single and non-single phase. They were evaluated for the quality of the zero field resistive transition, normal state resistance, contact resistance, thickness as compared to the transmission range of the intended irradiating ion, and general thermal, mechanical and electrical stability after mounting. Of these, the four best samples, all but one of which came from the flux growth batch designated 8-60-1, were chosen for extensive characterization before and after irradiation. The preparatory evaluations of the broader group of samples, including some preliminary irradiation results, are of some interest however, and are occasionally referred to in the text.

The samples selected for this experiment were of excellent quality as evidenced by variations of less than 1.5 K in the T_c at mid-transition and less than 2 K in the value of T_R=0, and extremely low normal state resistivity ($\approx$ 50 $\mu\Omega$-cm at 95 K). Still, as will be seen, sample variations are comparable to irradiation-induced changes, emphasizing the need to compare measurements performed on the same samples before and after irradiation. The zero-field resistive transitions of these samples before irradiation are presented in Figs. 5.1a - 5.1d. Table 5.1 sum-

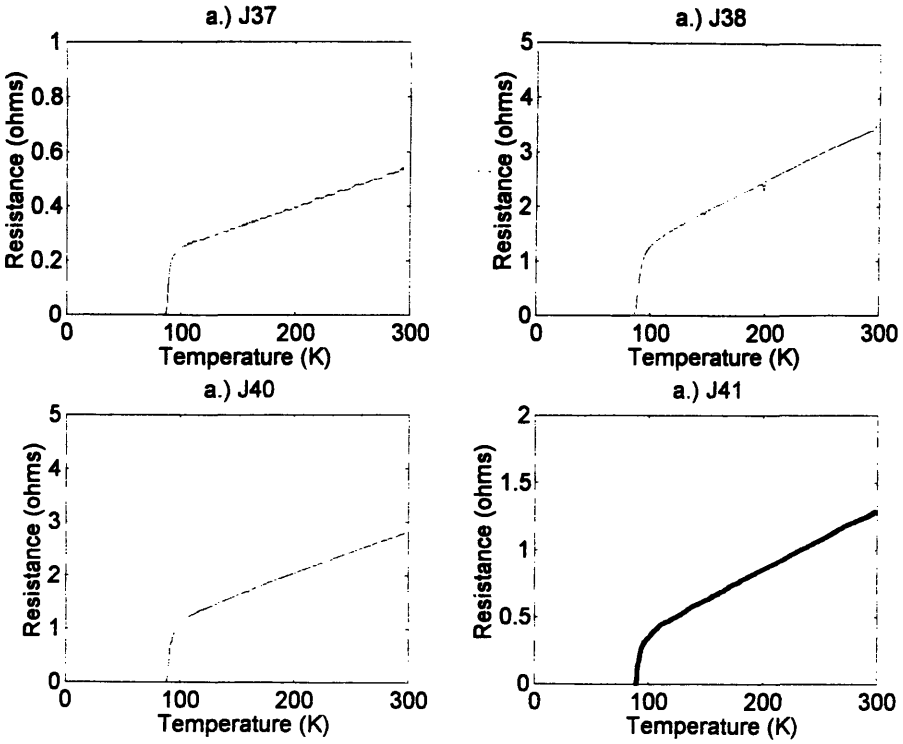

Figure 5-1: Resistive transition before irradiation

marizes the basic characteristics of these samples, and identifies their assignments for irradiation. Since all are flux growth method samples, their estimated thicknesses are no more than 2 μ.

5.2 Effects of Irradiation in Transport: Resistive Transition

The effects of irradiation common to all ions were: an increase in the normal state resistivity, degradation of the T_c with the post-irradiated resistive transition remaining approximately parallel to the unirradiated transition curve, as shown in Fig. 5.2, and increases in the pinning energy.

Figure 5.3 shows an Arrhenius plot of the resistive transition at 0.05 T before and after irradiation by H^- and Ar^-. The resistance has been normalized to R_{n0}, the resistance at 93

Sample	Ion	Fluence (cm^{-2})	Energy (MeV)	Dimensions (cm)			T_c (K)	ρ(95K) ($\mu\Omega$-cm)
				l	w	t		
J37	H^+	1 x 10^{16}	2.0	0.089	0.035	.0002	89.1	18
J38	He^+	6.4 x 10^{14}	3.0	0.126	0.048	.0002	89.6	87
J40	Ne^+	1x10^{12}/2x10^{12}	3.1	0.145	0.045	.0002	90.2	62
J41	Ar^+	6 x 10^{11}	2.5	0.0867	0.0267	.0002	90.6	22

Table 5.1: Sample Identification with Irradiation Conditions

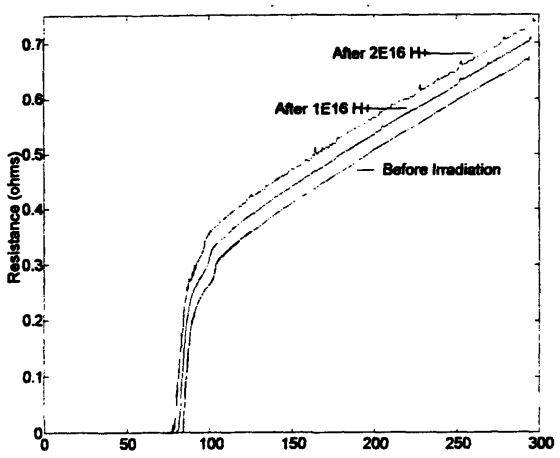

Figure 5-2: Effect of irradiation upon the resistive transition: R vs. T before irradiation, after 1 x 10^{16} H^+, and after 2 x 10^{16} H^+.

K before irradiation. The low resistance portion of the data may be interpreted within the model of thermally activated flux creep, in which $\rho = \rho_0 e^{-U_0/kT}$, as described in Chapter 3 (section 3.2.2). In the flux creep regime, the pinning potential is large compared to kT, whereas in the high temperature (high resistance) regime, thermal fluctuations overcome the pinning energy and a model of flux trapping and thermal activation no longer applies.* The calculation of activation energies, determined by drawing the best line through the linear section of the low resistance portion of the data, as shown in Fig. 5.3, provides a useful means of comparing the relative pinning energies before and after irradiation. In the as-grown crystals at 0.05 T these energies are roughly within $\pm$ 10% of 1500 K, as given in Table 5.2. After irradia-

*These regimes occupy different regions of the H-T phase diagram, which was discussed in section 3.2.4, and which is now (in 1997) significantly better understood. Further comment will be made in Chapter 6 as to what regions of the phase diagram are most likely being probed in the various experiments of this chapter.

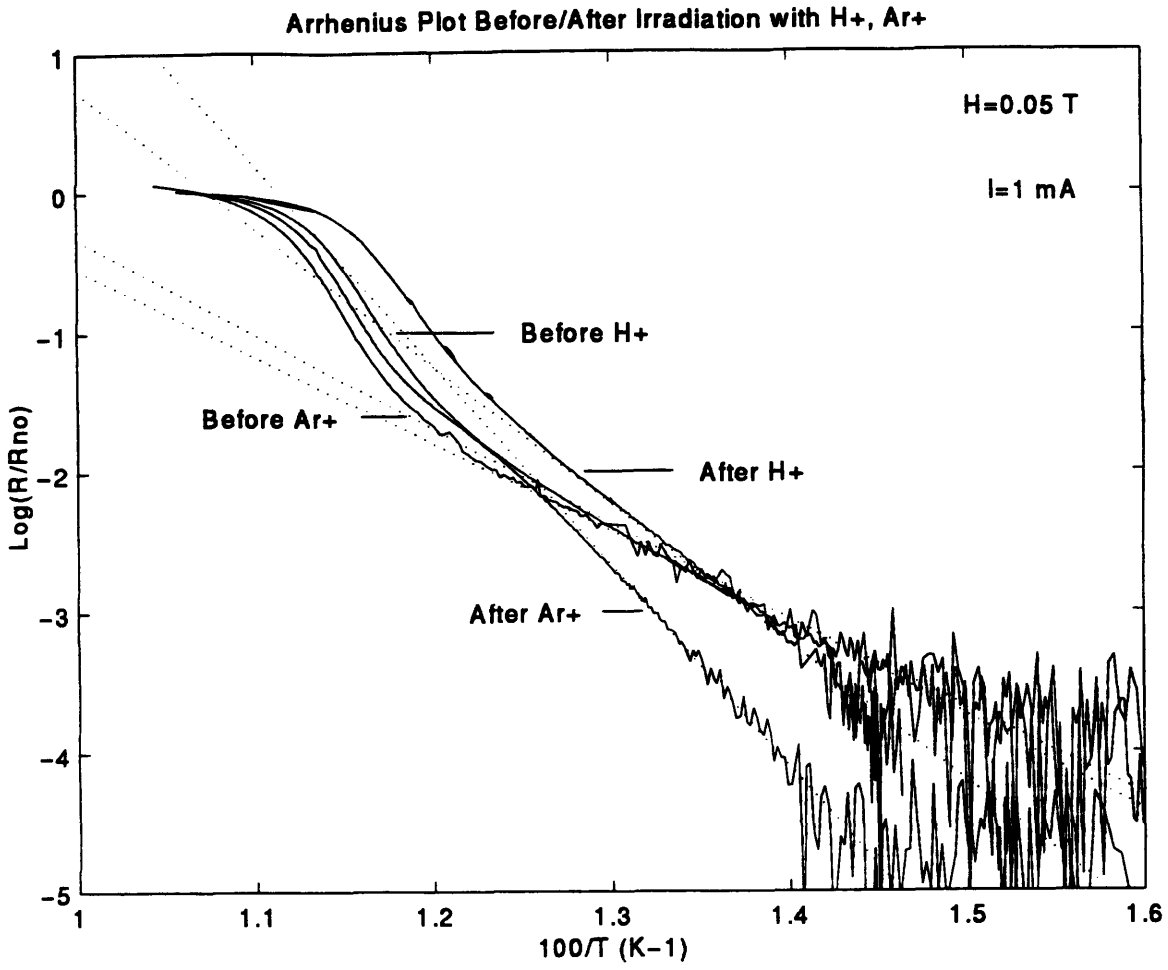

Figure 5-3: Arrhenius plot of the electrical resistivity of a $Bi_2Sr_2CaCu_2O_8$ single crystal at H=0.05 T before and after irradiation with H^+ and Ar^+ ions. Curves are normalized to R(93K). The marked suppression of the resistive tail resulting from Ar^+ irradiation is attributed to an increased pinning energy.

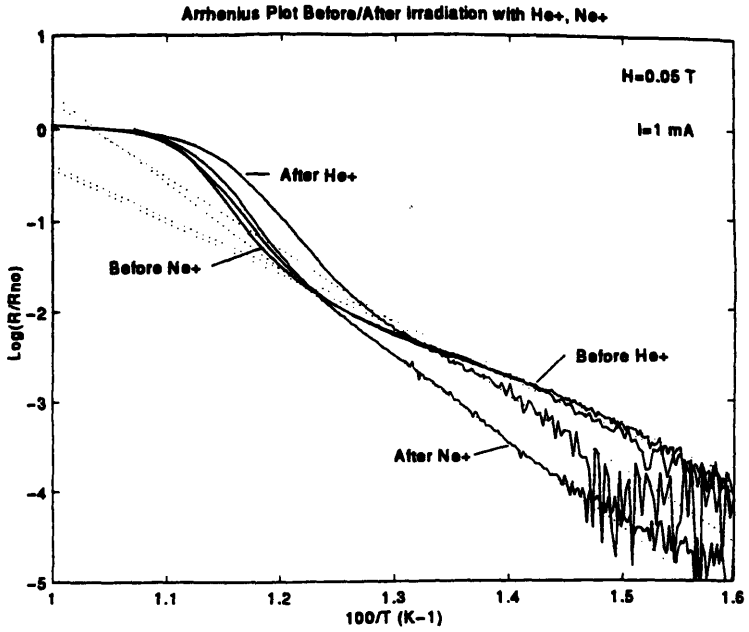

Figure 5-4: Arrhenius plot of the electrical resistivity of a $Bi_2Sr_2CaCu_2O_8$ single crystal at H=0.05 T before and after irradiation with He^+ and Ne^+ ions. Curves are normalized to R(93K).

tion with Ar^+, the activation energy increases by a factor of 2.3, as compared to only 1.4 for H^+. Thus, higher pinning energies result from the heavier ion irradiations. Results obtained for He^+ and Ne^+, shown in Fig. 5.4 and listed in Table 5.2, support this interpretation and are consistent with results reported for He^- irradiation of $Bi_2Sr_2CaCu_2O_8$ by Palstra[1] et al. Interestingly, the effects of vacancy equivalent doses of light vs. heavy ions also differ with respect to T_c degradation which is greater by a factor of four for H^+ and He^+ than for Ne^+ and Ar^+, as shown in Table 5.2. This effect is noticeable in Fig. 5.3 in that the temperature at which the post-irradiated resistance falls below that of the as-grown crystal is considerably higher for Ar^+ than for H^+. Whatever the exact nature of the induced defects, an attractive explanation for both of these trends is that heavier ions produce, in addition to small or point defects, significant numbers of large or clustered defects resulting from damage cascades of high energy recoils of primary knock-on atoms.[2] In contrast, the dominance of low energy recoils in light ion bombardment is more likely to result in a predominance of point defects, as was inferred for $YBa_2Cu_3O_7$.[3,4] Clearly, equivalent vacancy density as calculated by TRIM does not correspond to equivalent pinning energies. While this may in part reflect difficulties in

Ion	Activation Energy: E_A(K)			T_c(K)		ΔT_c
	Before	After	After/Before	Before	After	
H^+	1570	2276	1.45	89.1	86.7	-2.4
He^+	1326	1856	1.40	89.6	87.4	-2.2
Ne^+	1338	2200	1.64	90.2	89.6	-0.6
Ar^+	1445	3302	2.29	90.6	90.1	-0.5

Table 5.2: Arrhenius Results of the Resistive Transition at H=0.05T Before/After Irradiation

modeling heavy ion damage with vacancy production, it is clear for the same reasons that the character of such damage is unlike that produced by protons, and includes such possibilities as defect clusters or amorphized regions of varying size. Such spatially extended defects would interact with longer segments of the vortices, resulting in the observed higher pinning energies. In the most simplistic approximation, clusters would also be less destructive to the superconductivity than an equivalent number of point vacancies randomly distributed, thus explaining the relatively smaller reduction in T_c. This explanation would equally apply if T_c degradation were primarily a result of (distributed) oxygen lattice disordering, as has been suggested.

Results are qualitatively similar at high fields, as shown in Figs. 5.5a - 5.5d, although nonlinearity of the Arrhenius plot makes the determination of activation energies less meaningful. (These data, even before irradiation, do not show the high degree of linearity reported by Palstra at high fields.[5]) The same trends in the Arrhenius slopes are nonetheless present in that heavier ions are significantly more effective in suppressing the resistive tail.

5.3 Effects of Irradiation in Transport: Critical Current

The detailed response of the current-voltage characteristics to irradiation is not an easy subject for quantitative analysis, as even in the unirradiated material the I-V characteristics are not generally well understood at this time. Within the scope of this study we shall rather attempt to qualitatively describe the current-voltage behavior of these samples, and then discuss the changes induced by different types of irradiation. The presentation of the current-voltage results is also made difficult by the sheer volume of the data, which was taken on four samples, at many

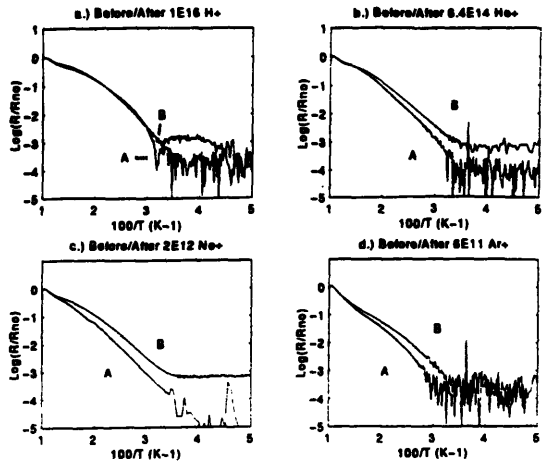

Figure 5-5: Arrhenius plot of the electrical resistivity of $Bi_2Sr_2CaCu_2O_8$ single crystals at H=5 T before and after irradiation with a.) H^+ b.) He^+ c.) Ne^+ and d.) Ar^+. Curves are normalized to R(93K). I=1 mA. The letters B and A denote measurements before and after irradiation respectively.

temperatures, before and after irradiation, at three fields, and in some cases repeated using dc instead of pulse measurement techniques. In this section we propose initially to compress the volume and complexity of the data by first presenting an overview of the effect upon the critical current of different ion irradiations as a function of temperature and field. With this result in hand we will proceed to the presentation of the detailed I-V data in the following section. For the purposes of understanding the critical current results, let it suffice for the present to say that the detailed current-voltage characteristics of these samples can be described in the most general terms as concave upward, under some conditions approaching linearity. As will be seen, the behavior of the critical current before and after irradiation is consistent with the Arrhenius results, showing a trend of improvement after irradiation by the heavier ions. Light ion irradiation, however, results either in lack of improvement or decreases in the critical current.

Critical currents were determined based upon an electric field criterion of 1 μV/mm. The temperature range of this measurement at a given magnetic field fell between a minimum temperature at which the critical current exceeded the maximum applied current and a maximum temperature where the critical current vanished. Pulse current-voltage measurements were

made out to maximum currents of 100 mA ($J \approx 1\text{-}2 \times 10^4$ A/cm^2) at intervals of approximately 0.5 mA, with more highly detailed data (approximately every 50 μA) sometimes recorded in the range 0 - 10 mA. DC measurements were in some cases made from 0 - 25 mA at intervals of 0.25 mA or less. The voltage measurement threshold was approximately 0.05 μV, corresponding to an electric field of about 0.05 μV/mm.

Figures 5.6a - 5.6d show a comparison of the temperature dependence of the critical current density before and after irradiation by H^+, He^+, Ne^+ and Ar^+, respectively. As shown in Fig. 5.6a, after hydrogen irradiation, at all fields and temperatures, all critical currents clearly lie below their pre-irradiated values. The effects of T_c degradation, as discussed in the previous section, clearly play a role in the reduction of the J_c, especially in the higher temperature range. Fig 5.6b shows similar decreases in J_c for helium at zero field, and the J_c results at 0.05 T and 5 T are about the same before and after irradiation. It should be mentioned here that transport measurements of the helium irradiated sample were hampered by the degradation of the electrical contacts, with heating at the contacts particularly problematic after irradiation, as indicated in Fig. 5.6b. These and associated experimental difficulties involved in measuring this particular sample are more fully discussed in Appendix B. However, independent results of the post-irradiated magnetization J_c of this sample, which are presented in Section 5.5, clearly show that the critical current after irradiation is not significantly different from that of a typical unirradiated sample, especially with respect to the temperature at which the J_c diminishes to zero. This indicates that the heating which occurred in the transport measurement was not masking any significant improvement in the critical current. We therefore conclude that light ion irradiation results in either lack of improvement or decreases in the critical current.

By comparison, the results of the Ne^+ and Ar^+ irradiated samples, shown in Fig. 5.6c and 5.6d respectively, show improvements in the critical current for all fields and temperatures. At low field (H=0.05 T) after Ne^+ irradiation, the critical current improves by up to a factor of four and approximately doubles or triples at high field (H=5 T). After Ar^+ irradiation, two to five-fold improvements can be seen at low field and the J_c approximately triples at high field. Finally, in contrast to the zero-field results for light-ion irradiation, after heavier ion irradiation,

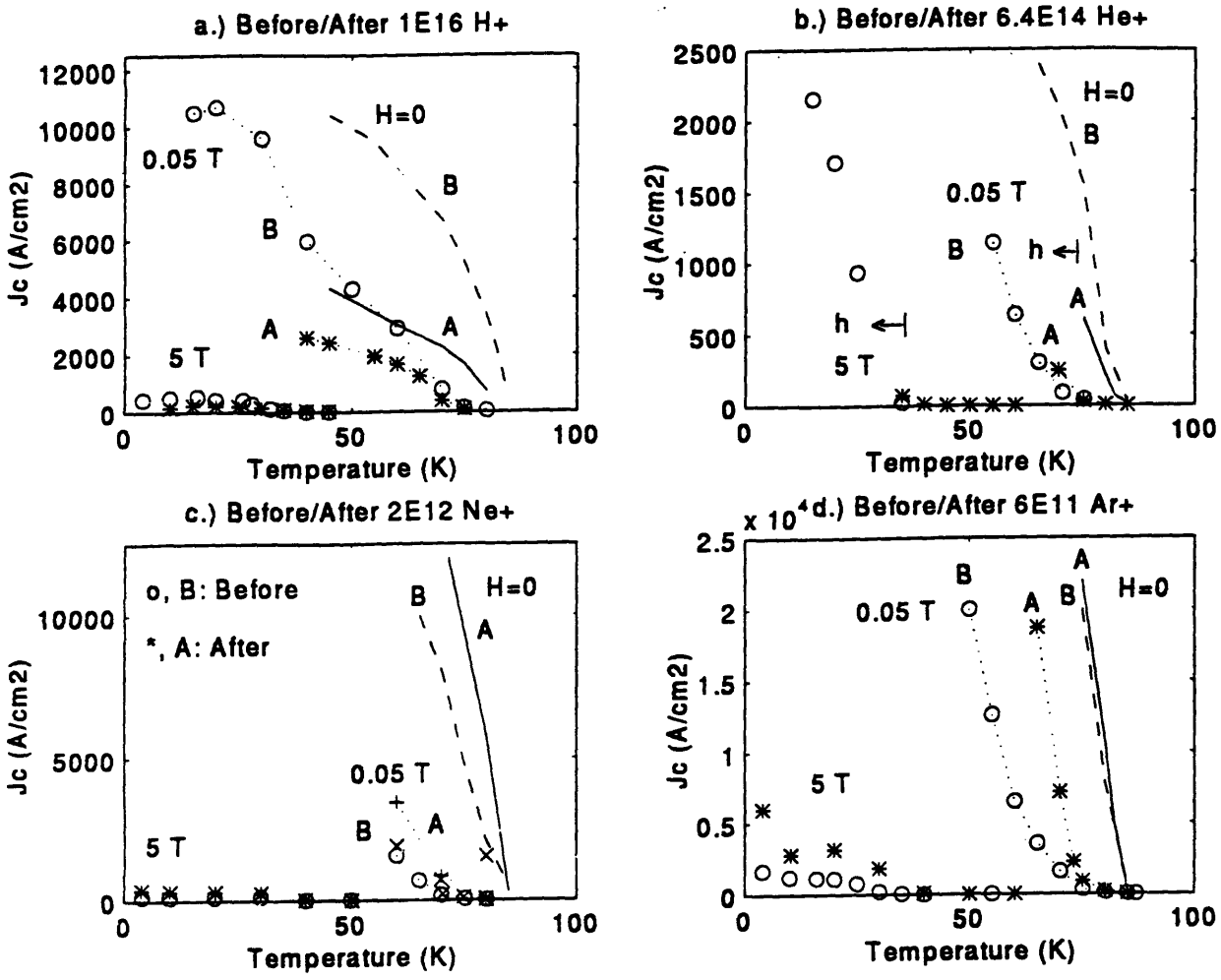

Figure 5-6: Transport critical current vs. temperature before and after irradiation by a.) H^- b.) He^- c.) Ne^- and d.) Ar^-. J_c increases after irradiation by the heavier ions, Ne^- and Ar^-. Critical currents were determined based upon an electric field criterion of 1 μV/mm. The letter B and open symbols indicate measurements before irradiation while the letter A and star symbols denote measurements after irradiation. An "h" indicates sample heating.

at H=0 the critical current significantly improves. Much of this difference is attributable to the lack of the dominating effects of T_c degradation observed for H^+ and He^+, which was associated with the predominance of damage of the distributed or point defect type in those samples. Note finally in the critical current results of Figs. 5.6a - 5.6d the obvious sample to sample variations, which can be much larger than the irradiation-induced changes, confirming the need for same sample comparisons.

To summarize, consistent with the Arrhenius results, significant improvements in the critical current are observed after Ne^- and Ar^- irradiation but irradiation by H^- or He^- results in either lack of improvement or degradation of the critical current. This is consistent with the presence of a different character of damage (spatially extended and unlike intrinsic defects) induced by the heavier ions, such as large defect clusters or amorphized regions, that serve to pin flux more effectively and account for the observed increases in both the critical currents and the pinning energies.

5.4 Effects of Irradiation in Transport: I-V Characteristics

Because of the large volume of the current-voltage data, first a general description will be given of the results, which will be followed by the presentation of various selected examples. As previously mentioned, in the most general terms the current-voltage curves can be described as "concave upward", under some conditions approaching linearity. This was already seen in the preliminary results of Chapter 2, where the angular dependence of the I-V was probed, but results of the temperature dependence were then limited to temperatures above 77K, where the existence of a threshold had only just become apparent. The earlier presentation in this chapter of the Arrhenius results, (together with previous work[5]), revealed that there is a lower temperature domain, where, for low enough fields and currents, the voltage falls below detectable limits. The I-V measured in this region is flat. Then as the current is increased, the voltage rises above detectable limits smoothly. As a function of increasing temperature and applied field, the value of the current at which the voltage is first detectable gradually goes to

zero current, and the I-V curve resembles a parabola (although it is not*). A combination of further raising the temperature and field tends to drive the I-V characteristics toward a limiting behavior with very little curvature that will be termed "linear". This transition is not sharp and is admittedly scale dependent, and sample dependent as well, but remains well behaved and consistently reproducible for a given sample at a given set of temperatures and fields. This is in contrast to the only other notable behavior observed, which was the appearance of a sharp upward kink in the dc I-V, only occurring at very low temperature (below 20 K) and high field. The most abrupt version of this feature was never observed using pulse techniques.† In most cases this kink resembled a true threshold only when plotted on large voltage scales; however on smaller scales it was evident that the onset of voltage occurred at currents well below the kink.** This feature (kink) was not well behaved and did not appear in every sample. If present before irradiation, it was accentuated after irradiation, which may have been precipitated by local increases in heating, which will be discussed. Otherwise, for a given sample, essentially all behaviors that are seen before irradiation are present after irradiation, but the conditions of temperature and field at which these behaviors occur can be shifted. Heavier ion irradiation results in suppression of the voltage developed at a given current, temperature and field, and retards the transition to linear behavior induced by higher temperatures and fields. In the "linear" regime of the I-V plot, lower slopes are observed after irradiation by the heavier ions. Light ion irradiation, however, as was seen in the presentation of the critical current, either degrades or at best does not improve the current-voltage characteristics. After light ion irradiation, for a given temperature, field and current, the voltage is generally higher than in the unirradiated sample. Also, features in the curves such as bends or kinks tend to move to lower currents and become sharper. Some comparisons of I-V data taken before and after both light and heavier ion irradiation follow.

Figs. 5.7a, b, and c show the I-V results at zero-field, 0.05 T and 5 T respectively before

*Neither can it be fit by a sinh or simple power law dependence.

†In general, pulse and dc results are almost the same except for some slightly higher dc voltages observed, as one might expect from heating.

**With the exception of one example of true abrupt threshold behavior observed at currents below 2mA ($\approx$ 250 A/cm^2) in sample J40 after Ne^+ irradiation (0<T<20K. H=5T). In this case barely detectable voltages were observed only just below the kink. These data were just above the noise level and there was no definitive trend observed with temperature, so local heating may have been a factor here as well.

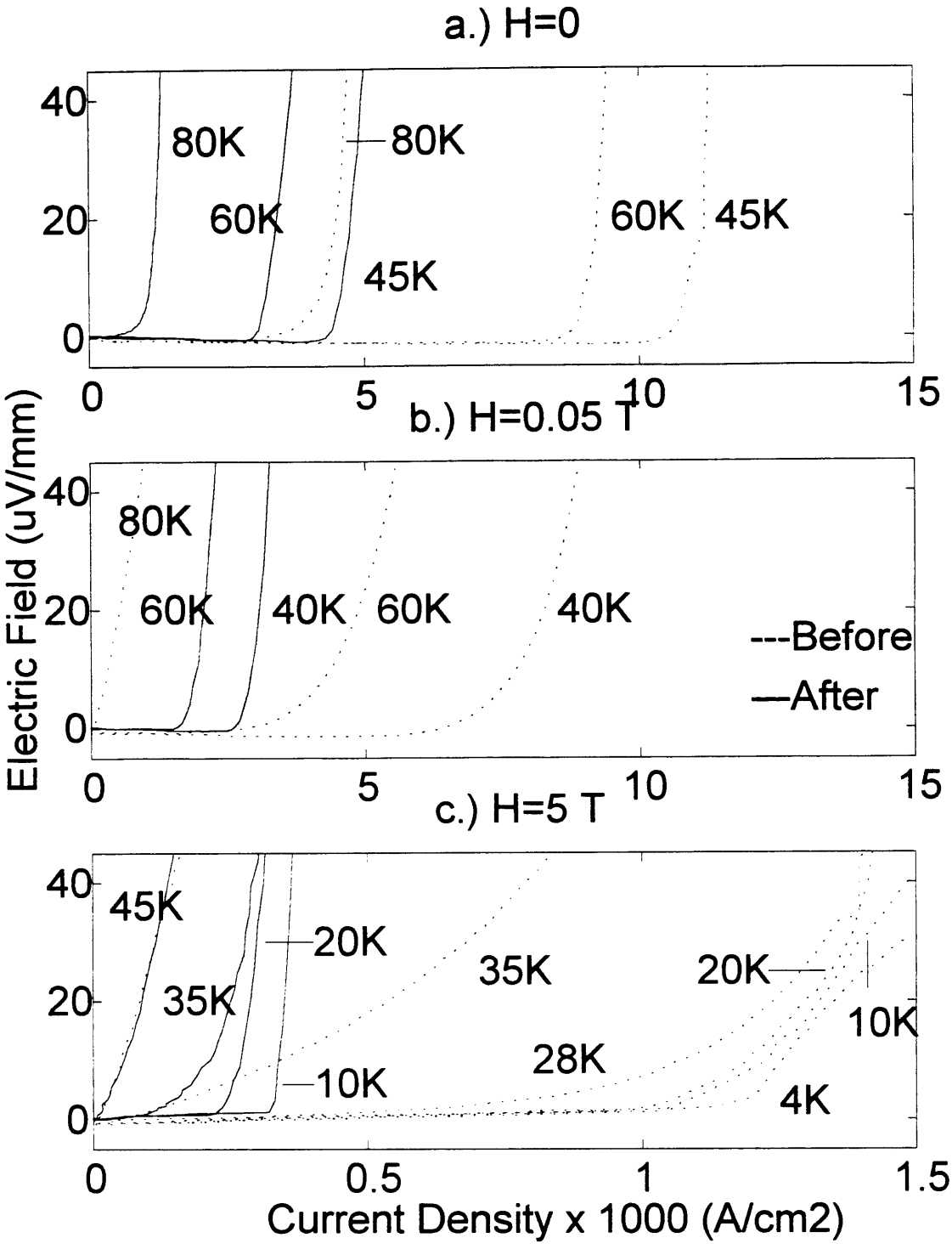

Figure 5-7: Electric field vs. current density (pulse method) before and after irradiation with H^+ at a.) H=0 b.) H=0.05 T and c.) H=5 T. $V \approx E \cdot 1$ mm and $I \approx J \cdot 10^{-5}$ cm^2.

(dashed lines) and after hydrogen irradiation (solid lines) of sample J37. Shown in Fig. 5.7a are some typical zero-field I-V curves at 45 K, 60 K and 80 K. Both before and after irradiation these curves are concave upward, but before irradiation at both 45 K and 60 K there is a long flat region before the onset of detectable voltage around 1 x 10^4 A/cm^2 and 9 x 10^3 A/cm^2, respectively. The curve shapes are similar and we see the expected decrease in the critical current with temperature. At a temperature of 80 K, however, the "flat" region preceding the onset has shrunk considerably and examination on small scales reveals a slight positive slope. After irradiation the major change is the shift of all of the curves to significantly lower currents (as was reflected by the degradation of the critical current after H^+ irradiation reported in section 5.3), but the flat regions preceding onset at 45 K and 60 K have not disappeared. At 80 K, in contrast, after irradiation the immediate onset of voltage is obvious even on this scale.

The results in Fig. 5.7b at 0.05 T show that at lower temperatures, for example at 40 K and 60 K, the I-V characteristics of the unirradiated sample have broadened slightly in-field and, predictably, have shifted to lower currents relative to the zero-field unirradiated result. At 60 K the in-field curve has an initial positive slope. As the temperature is raised further, the bend in the pre-irradiated data becomes progressively less sharp (not all transitional curves are shown) until at 80 K the in-field I-V, unlike the zero-field data, has become almost linear. The effect of irradiation on the low temperature in-field curves is similar to the change at zero-field in that the curves shift to lower currents, but here, the curve-shapes have also noticeably sharpened. Still, at higher temperatures the post-irradiated in-field I-V follows the trend towards linearity. At 75 K the post-irradiated result lies essentially on top of the 80 K pre-irradiated result (omitted from the graph as they are difficult to distinguish), behaving after irradiation in effect as though the temperature were higher. This would be easy to misinterpret as an indication of a decrease in the activation energy, which has obviously not occurred here (see Table 5.2). Instead we look to the explanation of a combination of significant T_c degradation and increased normal state resistance, both of which are clearly evident from Fig. 5.3. It is interesting to recall from Chapter 2 that reducing the angle between the field direction and the **c** axis also had an effect on the current-voltage characteristics similar to increasing the temperature. (This was attributed at the time to directional differences

in flux flow viscosity.) In the thermally activated flux creep model, these angle-dependent observations can be well accounted for with an angle-dependent activation energy, U(H,θ). Both U(H,θ) and J_c(H,θ) increase monotonically with θ as θ is increased from 0 to $\pi/2$. The changes in the post-irradiated I-V curves of Fig. 5.7b are of a different nature, as the activation energy has actually increased slightly, but the critical current has decreased dramatically.

Shown in Fig 5.7c are the results at a field of H = 5 T. All curves now have initial positive slopes, as was confirmed by examination on smaller scales. Before irradiation the I-V is relatively insensitive to temperature below 28 K. Above this temperature the critical current rapidly decreases and there is a change from the kinked or threshold-like behavior observed at 4 K (and to a lesser extent at 10 K and 20 K) to a more gradual concave upward shape which, with increasing temperature, evolves towards the nearly linear result seen at 45 K. After hydrogen irradiation, as with the zero-field and low field results, the low temperature I-V curves shift to much lower currents and assume a more threshold-like form, (although all initial slopes are still positive). Also, the low temperature kink observed at 4 K before irradiation has sharpened dramatically, and at 10 K we see an extremely abrupt increase in voltage. At high temperature there is the same trend towards linearity as in the unirradiated material. Interestingly, the effect of hydrogen irradiation upon this sample at 5 T and 45 K appears to be negligible at low currents (I $\leq$ 1 mA), as these curves lie virtually on top of one another in this range. However the four-current R vs. T data show that at a current of 10 mA ($\approx$ 1400 A/cm^2), the voltage is much higher after irradiation.

It is worth noting that the low temperature/high field kink described above was not consistently observed at 10 K after irradiation and did not occur at the exact same current reproducibly. It was not seen at all at 4 K (not shown in Fig. 5.7c), where the data was essentially a "kinkless" version of the 10 K curve shown. This leads to the speculation that the very sharp features observed in the I-V data only at low temperature are associated with (or at least accentuated by) the low heat capacity and a resulting process of thermal runaway. As the applied current is increased, a local increase in the electric field at a given place in the (inhomogeneous) sample produces heat. At low temperature, since the heat ca-

pacity of both the sample and the helium gas environment are extremely small, the temperature rises rapidly and with it the local resistance which in turn produces more heat, and a "hotspot"/high resistance domain could form and rapidly grow in size and resistivity under these circumstances. This process would not necessarily occur reproducibly each time, leading to the lack of consistent macroscopic observations of the low temperature I-V characteristics noted. While this speculation is based upon relatively casual repetition of measurements of the irradiated sample only, it is reasonable to assume that such an effect would be emphasized after irradiation due to increases in the normal state resistivity and possibly an increased degree of spatial inhomogeneity within the sample as well. There was no obvious lack of reproducibility in measurements of the unirradiated sample. However, in both the pre- and post-irradiated sample, for measurements conducted below 20 K, macroscopic heating on the order of 0.1 K (over a duration of several seconds during the measurement), was directly observed on the carbon-glass thermometer. This indicates that the effects of heating must be considered in the interpretation of these current-voltage characteristics. It is possible that the relatively sharp feature already existing in the unirradiated sample at 10 K (Fig. 5.7c) was in part attributable to the heating effects discussed above and became sharper and less well behaved after irradiation due to the increased resistivity and inhomogeneity caused by ion damage.

Because of the essential similarity to the results just presented above, only a brief description of the current-voltage data for the He^- sample (J38) will be given here in the context of this section. The detailed data are presented in Appendix B, where measurement difficulties associated with heating in this sample are discussed. These data before irradiation differed from that described above for the H^+ sample mainly in that there were no kinks observed in the data and the critical currents were at least an order of magnitude lower on the average. (The normal state resistance of this sample was about five times higher.) The zero-field result after He^- irradiation was similar to that produced by H^+ irradiation, in that the I-V curves shifted to lower currents with no other major changes. (Again T_c has decreased and ρ_n has increased.) In-field, after irradiation, a combination of lower measurement temperatures and continued degradation of the contact resistance made sample heating a significant enough problem to prohibit investigation of the high current portion of the curves. At low currents,

however, there was little change, as already suggested by the critical current results. Light ion irradiation, therefore did not result in improvement of the current-voltage characteristics.

Fig. 5.8a shows the I-V results at 0.05 T from 60 K - 80 K before and after Ne^+ irradiation of sample J40. The sample to sample variation can be seen here in that the transitions in the as-grown material are somewhat broader in-field than those observed in the unirradiated H^+ sample, J37. Otherwise the I-V curves before irradiation have the same basic character, evolving with increased temperature towards linear behavior around 80 K. After Ne^+ irradiation, however, there is an obvious decrease in the voltage at all currents for all temperatures. At 60 K the voltage at a current density of 10^4 A/cm^2 has decreased after irradiation by half. At 70 K before irradiation the transition towards linear behavior is well underway, but after irradiation at 70 K the curve shape is quite concave, similar to the 60 K result prior to irradiation. In other words, the linear behavior has been restricted to a higher temperature range than before irradiation and therefore the voltages observed at 70 K have everywhere decreased to a small fraction of their prior values. The curves now behave as though the temperature were lower, the opposite of the light ion result. However, in this case the change is attributable to the improved pinning associated with the increase in the activation energy after irradiation. Improvements are minimal at 80 K, however, above which temperature the effects of T_c degradation dominate.

More dramatic improvements are observed at 5 T, as shown in Fig. 5.8b, the I-V results from 4 K - 50 K before and after Ne^+ irradiation. At 4 K, this sample does exhibit the sharp kink behavior previously described at low temperature and high field for sample J37. However, after irradiation, the threshold current at which this occurs has approximately tripled.* In the as-grown sample there is a feature, namely an anomalous crossing of the 20 K and 30 K current-voltage curves which persists after irradiation but again, now occurs at about triple the current. For both curves the voltages are markedly below the pre-irradiated values over the entire range of measurement. At 40 K the curves are relatively linear both before and after irradiation. The effect of irradiation on the curve shape at this tempera-

*This is the previously mentioned only true example of abrupt threshold behavior, occurring after irradiation only.

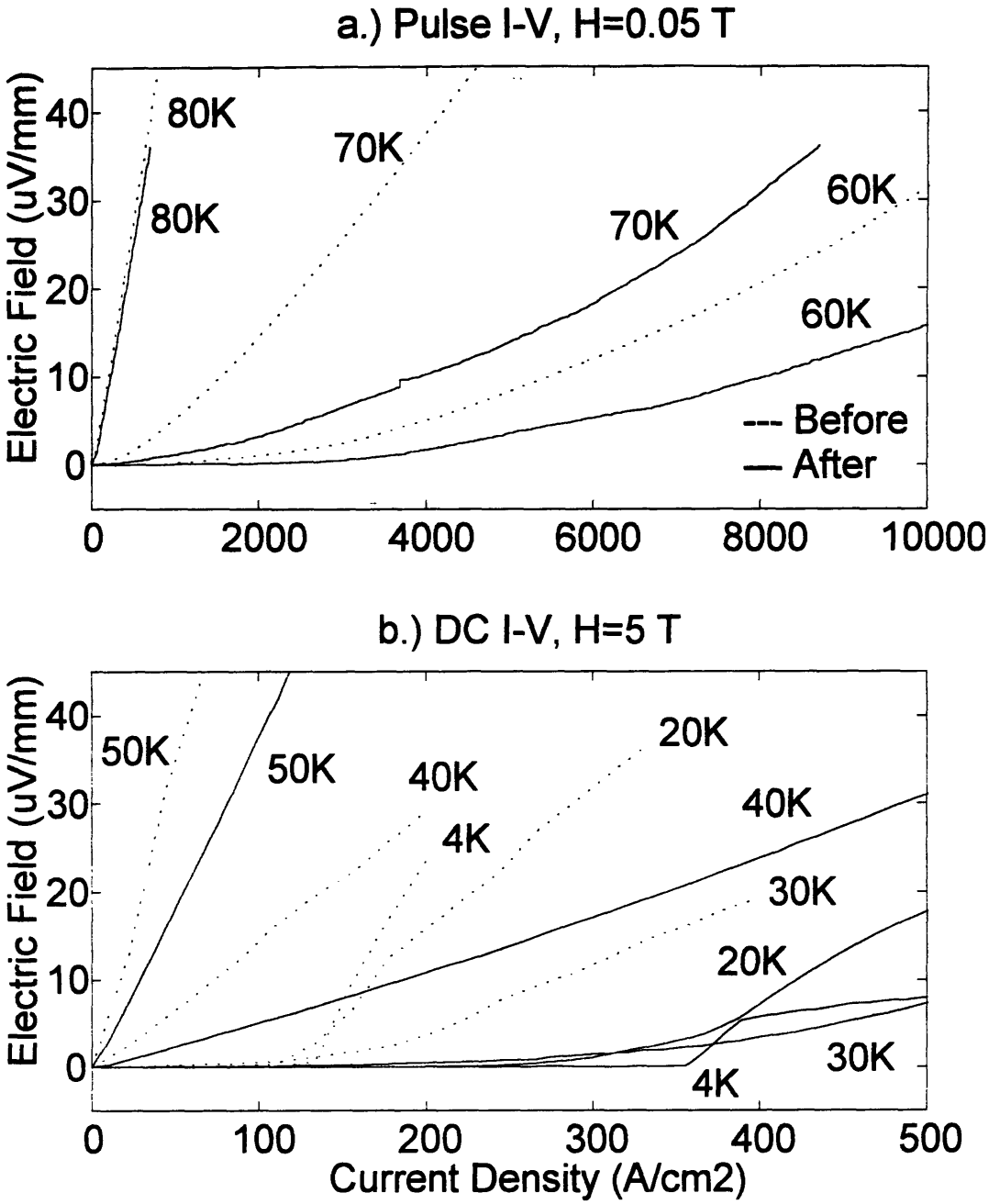

Figure 5-8: Electric field vs. current density before and after irradiation with Ne^+ at a.) H=0.05 T and b.) H=5 T. V $\approx$ E $\cdot$ 1 mm and I $\approx$ J $\cdot$ 10^{-5} cm^2.

ture is therefore fairly minimal in high field, but the slope has decreased by at least a factor of two. A similar effect is observed at 50 K, and the voltages are significantly reduced.

Fig. 5.9a shows the I-V results at 0.05 T from 50 K - 80 K before and after Ar^+ irradiation of sample J41. In the high temperature range improvements are similar to those observed for the Ne^+ irradiated sample. It is particularly striking, however, that in this sample after Ar^+ irradiation it was possible at 65 K to almost completely suppress the voltage out to a current density of 2 x 10^4 A/cm^2, even though before irradiation the voltage was above 5 μV/mm at 1 x 10^4 A/cm^2. Note also that prior to irradiation the voltage was detectable until down to 50 K, which indicates a significant upward shift in the position of the irreversibility line after irradiation. Ar^+ irradiation clearly produced the best improvement in the I-V result at low field.

Fig. 5.9b shows the I-V results at 5 T from 30 K - 60 K before and after Ar^+ irradiation. Relative improvements do not at first appear to be quite as good as those seen after Ne^- irradiation in this temperature range at high field. It is important to note, however, that the high-field response of this sample, unirradiated, was already far superior to the as-grown sample J40, (the horizontal scale of Fig. 5.9b is a factor of ten greater than that of Fig. 5.8b), indicating a higher initial density of pinning centers, and that the final result is by far the best seen for any sample under these measurement conditions. Below 30 K (not shown), this sample did not exhibit the abrupt kink behavior observed in the Ne^+ (and H^+) irradiated samples but retained the smooth concave upward shape seen at 30 K (voltage of course decreasing with temperature). Improvements in the critical current below 30 K after Ar^- irradiation were nonetheless on the same order as those seen after Ne^+ irradiation, and the shape of the low temperature I-V curve did not change significantly after Ar^+ irradiation.

To summarize, for a given sample, essentially all behaviors that are seen before irradiation are present after irradiation, but the conditions of temperature and field at which these behaviors occur can be shifted. Heavier ion irradiation results in suppression of the voltage developed at a given current, temperature and field, and retards the transition to linear behavior induced by higher temperatures and fields. In the "linear" regime of the I-V, lower slopes are observed

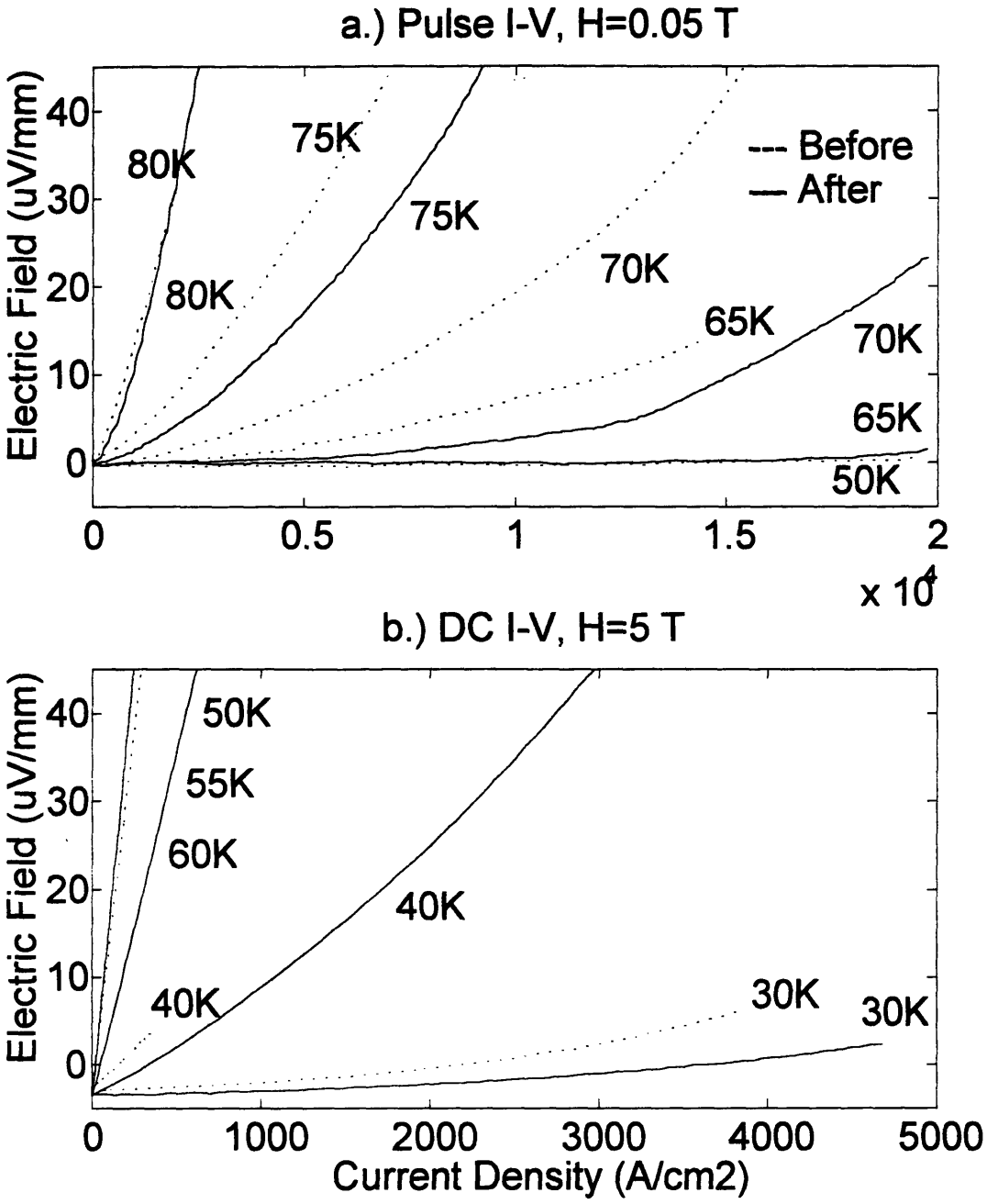

Figure 5-9: Electric field vs. current density before and after irradiation with Ar^+ at a.) H=0.05 T and b.) H=5 T. V $\approx$ E $\cdot$ 1 mm and I $\approx$ J $\cdot$ 10^{-5} cm^2.

after irradiation by the heavier ions. Light ion irradiation however, either degrades or at best does not improve the current-voltage characteristics. After light ion irradiation, for a given temperature, field and current, the voltage is generally higher than in the unirradiated sample. Also, features in the curves such as bends or kinks tend to move to lower currents and become sharper.

5.5 Temperature Dependence of the Magnetization J_c

Figure 5.10 shows the temperature dependence of J_c, inferred from magnetization, before and after irradiation by Ne^+ and Ar^+ at a field of 1 T. There is marked improvement in both samples with generally better results occurring for Ar^+. Similar results were obtained at an applied field of 0.05 T, despite the presence of a comparable self field (which would tend to mask improvements in the J_c.) At low temperature and field the apparent improvements in J_c are on the order of factors of two, but more impressive is the decreased sensitivity of J_c to elevated temperature and field. Before irradiation, J_c of a typical sample is immeasurably small at 1 T ($< 10^4$ A/cm^2) above roughly 15 K, but after Ar^+ irradiation, the critical current at 20 K is nearly 10^6 A/cm^2 and only approaches zero near 30 K. Similarly the J_c of the Ne^- irradiated sample is above 10^4 A/cm^2 at 30 K after irradiation. These results are consistent with the observation of increased pinning energies in the Arrhenius plots of activated resistivity, and (equivalently) represent an upward shift of the "irreversibility line" (IL). Pre- and post-irradiated measurements of the transport J_c's indicated that improvements resulting from Ne^- and Ar^- irradiation are of the same order of magnitude as for the magnetization critical currents. For example, at 5 T and 10 K the critical current (based on a field criterion of 1 μV/mm) increased from 1.23 x 10^3 A/cm^2 to 2.82 x 10^3 A/cm^2 after irradiation with Ar^+.

Results on H^+ and He^+ irradiated samples are shown in Fig. 5.11a and 5.11b at 0.05 T and 1.0 T respectively. The magnetization J_c's of the unirradiated samples were not measured. Results before Ar^+ and after Ne^- and Ar^- irradiation are included on the graph for reference. Although at 0.05 T the H^+ irradiated sample appears to show relatively high critical current

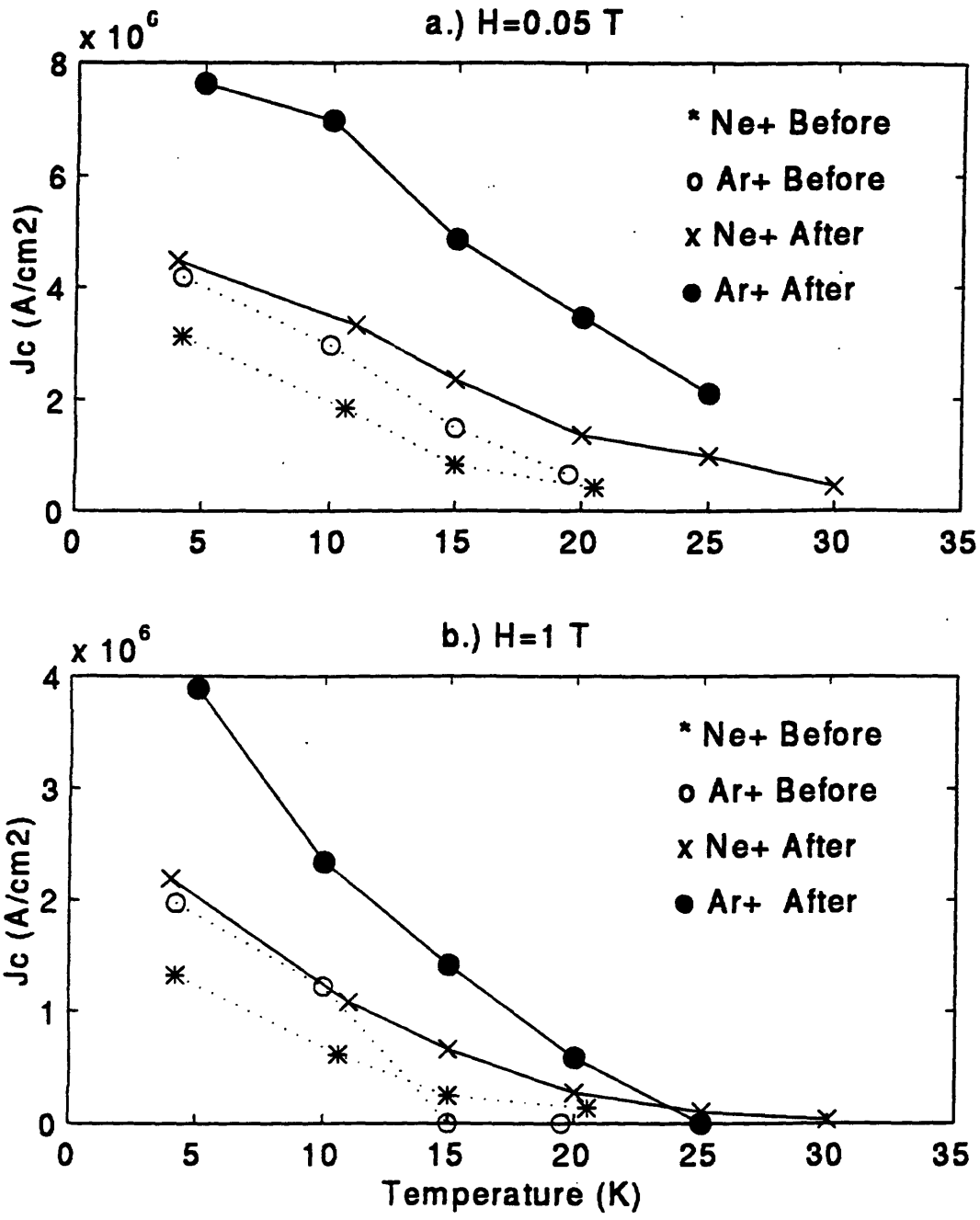

Figure 5-10: Temperature dependence of the magnetization J_c at a.) H=0.05 T and b.) H=1 T before and after irradiation with Ne^- and Ar^- ions. The characteristic temperature at which the critical current diminishes to zero is strongly increased by heavy-ion irradiation.

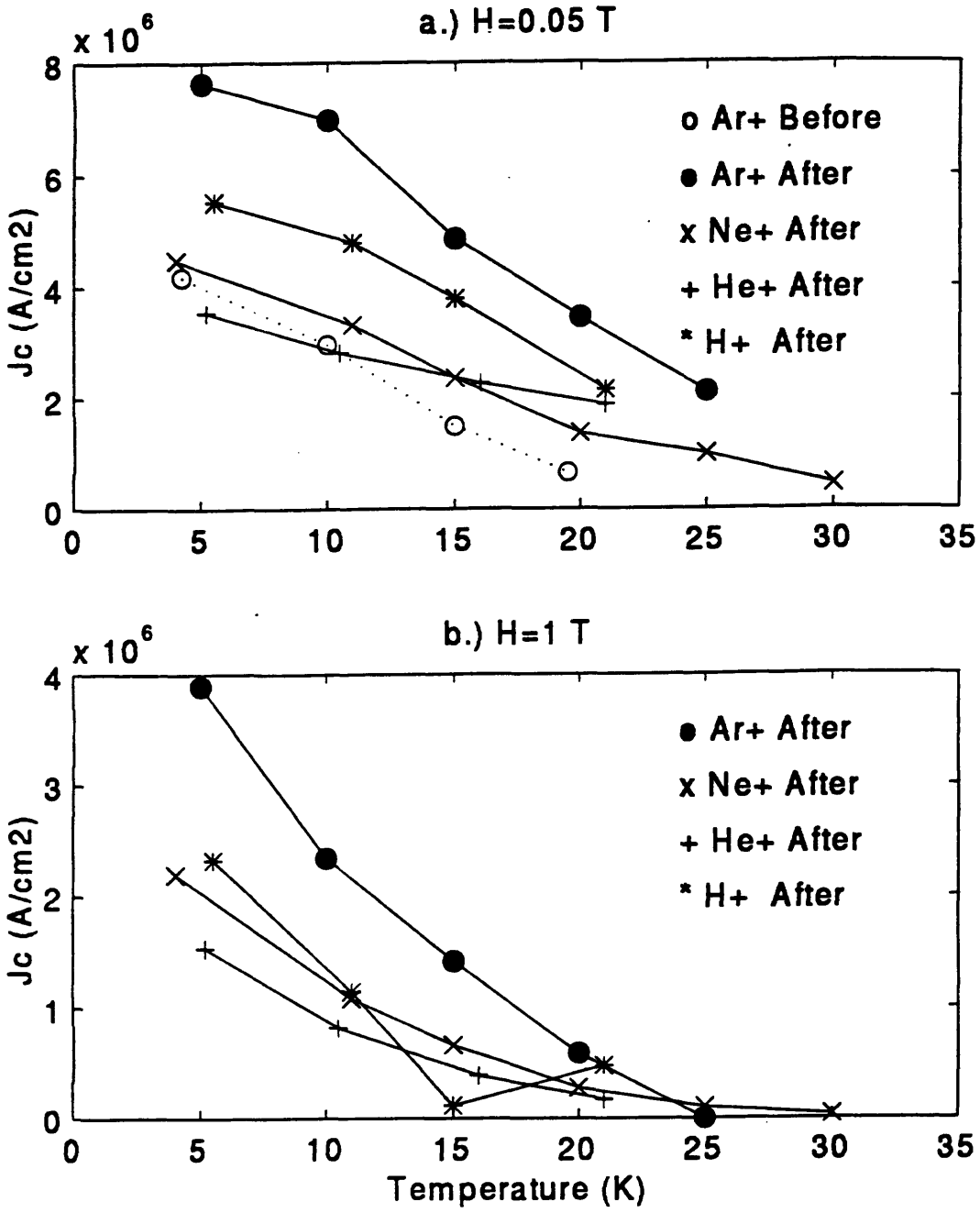

Figure 5-11: Temperature dependence of the magnetization J_c at a.) H=0.05 T and b.) H=1 T after irradiation by H^-, He^-, Ne^-, and Ar^-. The result prior to Ar^+ irradiation is shown for reference. In contrast with the heavy-ion results, the temperature dependence after light ion irradiation is similar to that observed before irradiation.

values* in the temperature range 5 K - 20 K, more important is the fact that in both the H^+ and He^+ samples at low and high field there is essentially no change in the temperature at which J_c diminishes to zero, as can be seen by comparison to the results of the unirradiated Ar^+ sample. This is an indication that the pinning energy (and the IL) have not been significantly affected after H^+ or He^+ irradiation, in contrast to the post-irradiated results for Ne^+ and Ar^+, which no longer vanish above 20 K, in both low and high field. This is again consistent with the behavior of the activated resistivity seen in Figs. 5.3 and 5.4. Furthermore, transport measurements that were performed on the H^+ sample before and after irradiation clearly showed a degradation of the critical current. While post-irradiated transport results on the He^+ sample were complicated by heating effects, both the similarity in the behavior of the magnetization J_c after He^+ irradiation to that of an unirradiated sample, and the excellent tracking between the magnetization and transport results for Ne^+ and Ar^+ cited above, strongly point to the conclusion that light ion irradiation does not improve the critical current. While it has been suggested[1] that the addition of point defects can raise the J_c at low temperatures but that the limitation of the low pinning energy (attributed to anisotropy) dominates at high temperatures, we were unable to effect such improvements by light ion irradiation, at low temperature or otherwise in this material.

Further comments will be made upon the results of the irreversible magnetization in Chapter 6, where these measurements are discussed with respect to the relevant regions of the H-T phase diagram.

5.6 Dose Dependence of the Magnetization J_c

In the improvements noted thus far there is no indication that the J_c of the heavy ion-irradiated samples had yet been optimized with dose. Figures 5.12a - 5.12c show the raw VSM data of the same sample before irradiation, after 1 x 10^{12} Ne^+/cm^2 and after 2 x 10^{12} Ne^+/cm^2 at

*Note that caution must be exercised in comparing different samples as errors in geometric factors (sample dimensions) can significantly shift the relative J_c's. which is not a problem when comparing the same sample before and after irradiation. If a sample were thicker than it's estimated value, for example, systematically higher critical current values would result.

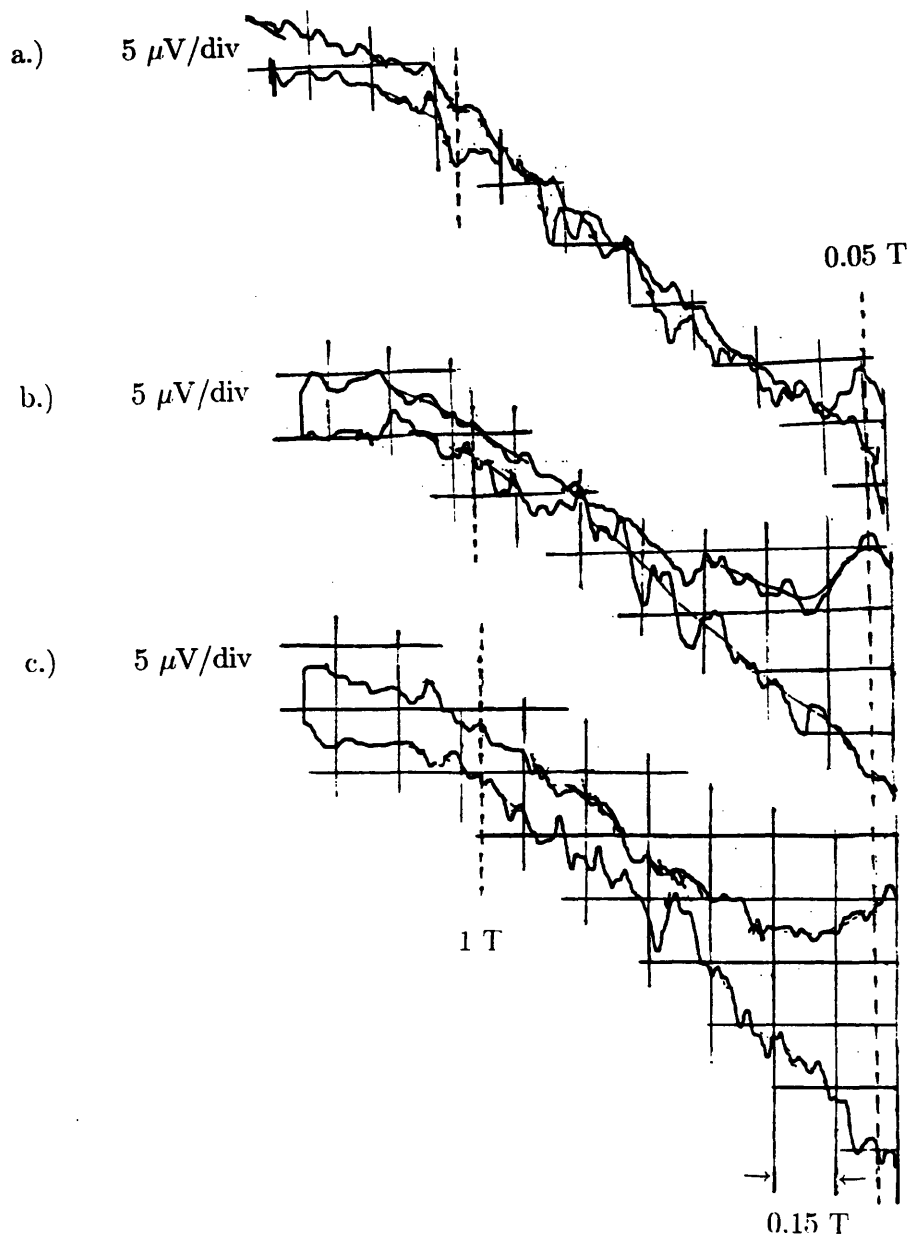

Figure 5-12: VSM data of sample J40: a.) before irradiation b.) after 1 x 10^{12} Ne^{+} and c.) after 2 x 10^{12} Ne^{+}. Magnetization loops were traced at a temperature of 20 K. For the unirradiated sample the loop is nearly closed above approximately 0.1 T but has markedly increased in size after irradiation by 1 x 10^{12} Ne^{+} and is still larger after 2 x 10^{12} Ne^{+}. These data correspond to increases in J_c from less than 1.4 x 10^5 A/cm^2 to 1.71 x 10^5 A/cm^2 to 2.74 x 10^5 A/cm^2.

a temperature of 20 K. (Recall that the "equivalent damage" dose is 2 x 10^{12} Ne^+/cm^2.) Note that for the unirradiated sample the loop is nearly closed above approximately 0.1 T but has markedly increased in size after irradiation by 1 x 10^{12} Ne^+/cm^2 and is still larger after 2 x 10^{12} Ne^+/cm^2. Here the loop has approximately doubled in width at higher fields out to the maximum of the measurement, nearly 1.5 T. These data at 1.0 T correspond to increases in J_c from less than 1.4 x 10^5 A/cm^2 to 1.71 x 10^5 A/cm^2 to 2.74 x 10^5 A/cm^2.

To further explore the dose dependence of the magnetization J_c, a more extensive series of irradiations was performed using Ar^+, which of the various ions had produced the highest increases in both the pinning energy and the critical current. This series of measurements was performed on samples BAr3 and BAr4 specifically for this purpose, rather than the previously Ar^+ irradiated sample, J41. Since measurements of the Ne^+ irradiated sample had suggested that the optimum dose would be found above the "equivalent damage" dose (EDD), we started the series with this Ar^+ fluence (6 x 10^{11} cm^{-2}) and proceeded upwards.

The dose dependence of the magnetization J_c for Ar^- in the temperature range 6 K - 28 K at fields of 0.05 T and 1.0 T is shown in Figs. 5.13a and 5.13b for sample BAr3. For all temperatures, the maximum J_c at low field is obtained at a dose of 1.2 x 10^{12} Ar^+/cm^2, while the maximum at the higher field is clearly obtained at twice that fluence at all temperatures (the anomalous peak at 17 K is attributed to experimental difficulties). A similar effect was observed in sample BAr4, shown in Figs. 5.14a and 5.14b. While these measurements were taken at larger fluence intervals, making it more difficult to specify the location of the peak, it is clear that the peak moves outward as the field is increased from 0.05 T to 1 T. (again, the anomalous peak at 17 K is attributed to experimental difficulties). It should be noted that despite the larger intervals between fluences, these data are absolutely consistent with the peaks observed for sample BAr3 at 1.2 x 10^{12} Ar^+/cm^2 and 2.4 x 10^{12} Ar^+/cm^{-2} at fields of 0.05 T and 1 T respectively.

The fact that J_c (or equivalently the pinning force density $F_p = J_cB$) peaks at a field dependent but temperature independent fluence is a strong indication that this is associated with a classical "matching effect"[6] where the highest J_c is obtained at the field for which the

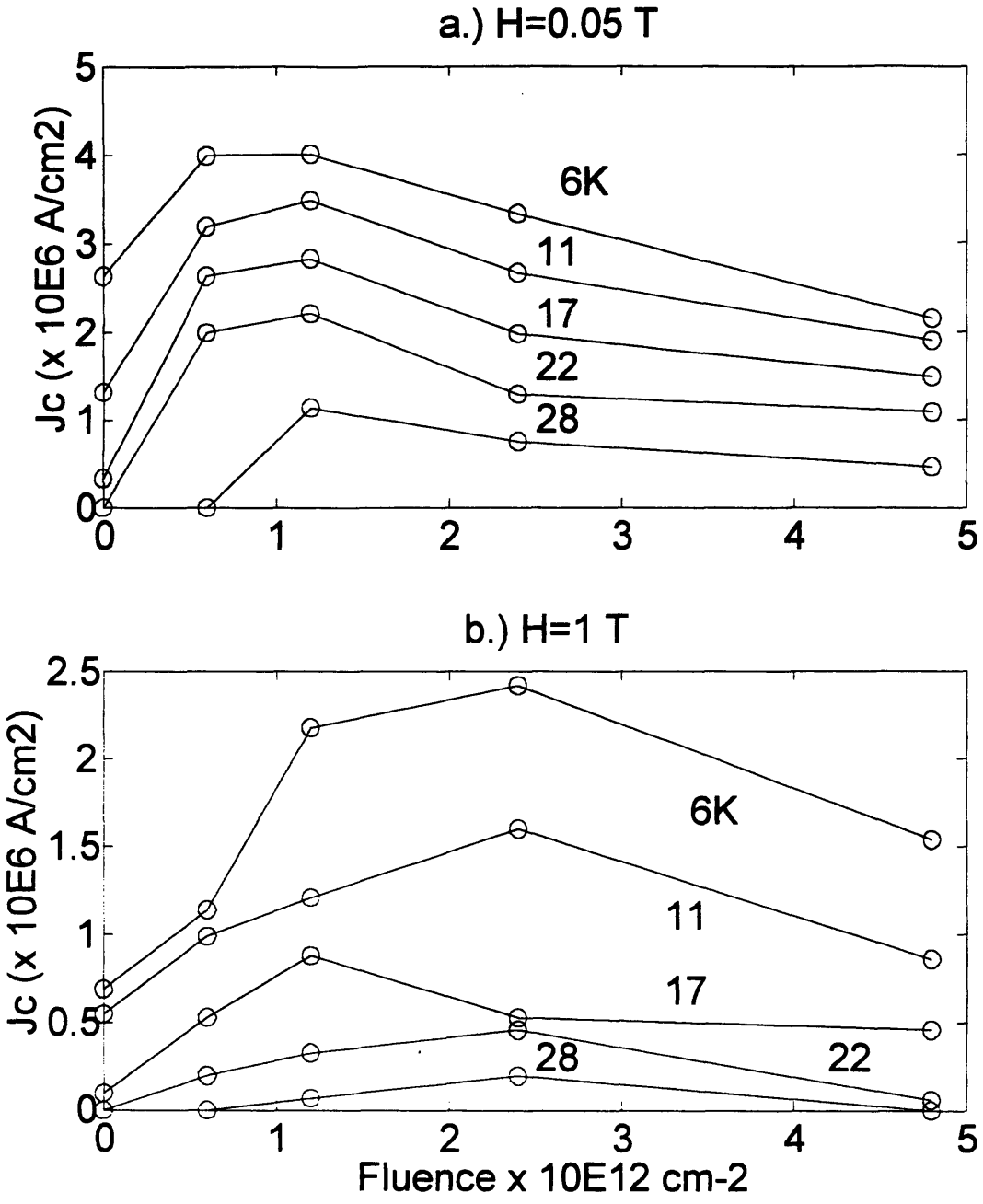

Figure 5-13: a.) Ar^+ dose dependence of the magnetization J_c at H=0.05 T for temperatures between 6 K and 28 K showing matching effect at fluence of 1.2 x 10^{12} cm^{-2}. b.) The peak in $J_c(\Phi)$ moves to higher fluence at H=1 T.

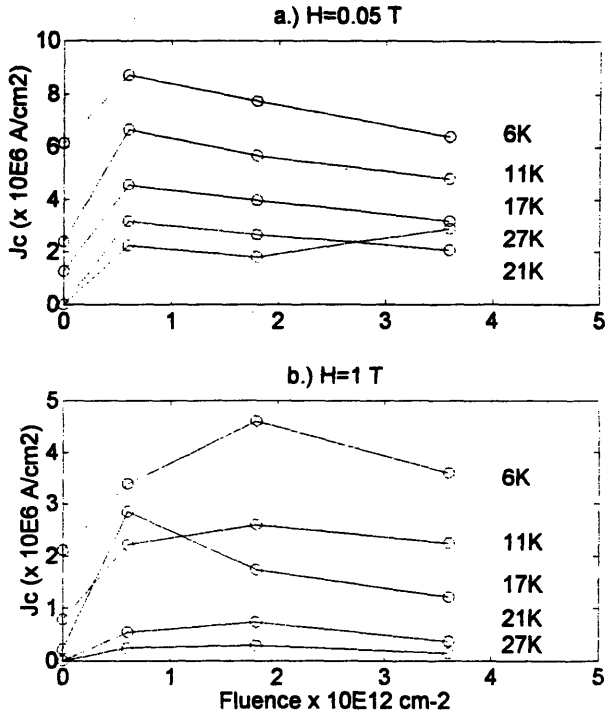

Figure 5-14: a.) Ar^- dose dependence of the magnetization J_c at H=0.05 T for temperatures between 6 K and 27 K consistent with matching effect at fluence of 1.2 x 10^{12} cm^{-2} (between 6 x 10^{11} cm^{-2} and 1.8 x 10^{12} cm^{-2}). b.) The peak in J_c (Φ) moves to higher fluence at H=1 T.

average defect spacing is equal to the vortex spacing. This may be explained with a simple model in the single-vortex, strong pinning (thin sample) limit. If we assume that the density of defects that act as effective pinning centers (a particular type of defects) is less than the vortex density at a given field, each defect pins a vortex core, and unpinned vortices are held in place only by electromagnetic intervortex forces. If the defect density is then increased, the pinning force density will increase until all of the vortices are pinned, at which point the critical current would theoretically saturate, as any additional pinning centers would fall in between the vortex cores. In this model, at higher fields, the defect density at which saturation occurs would be correspondingly higher, independent of temperature*, which is exactly what is implied in our data by the observed dose dependence of the J_c. In the samples which

*In studies of critical currents in proton-irradiated single crystals Civale[4] et al., instead found the peak in the dose dependence of J_c to be temperature dependent and field independent, leading them to consider a collective pinning model, which is clearly not suggested by our results.

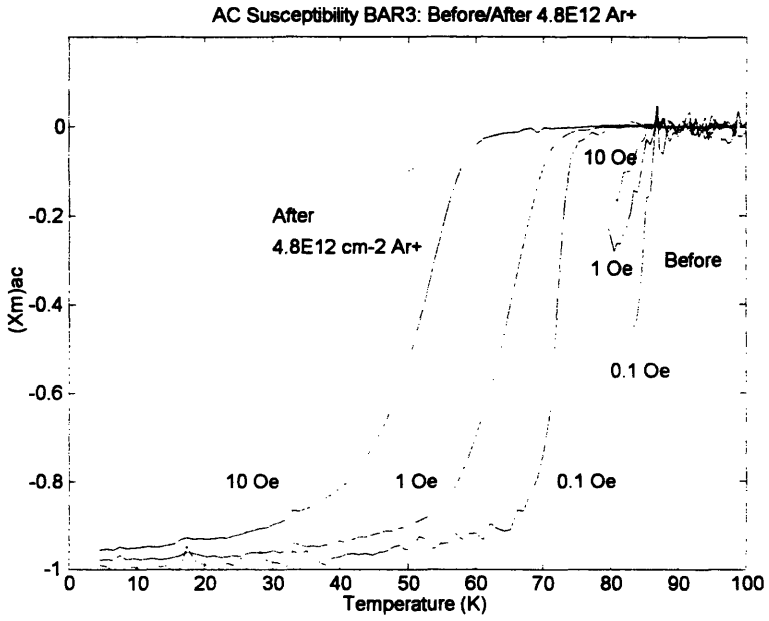

Figure 5-15: T_c degradation after 4.8 x 10^{12} Ar^+ as measured by ac susceptibility.

experienced the highest fluences, however, the critical current inevitably must decrease due to the fact that the superconducting order parameter in the region between defects will begin to diminish as the defect spacing approaches $\xi_{ab}(T)$. The overall transition temperature is found to be essentially unaffected below the peak in J_c, but at 4.8 x 10^{12} Ar^+/cm^2, for example, T_c drops from 90 K to 72 K as measured by low-field ac susceptibility, shown in Fig. 5.15.

A simple interpretation of the vacancy density produced by Ar^+ is not consistent with the observed peak effect. The intervortex spacing is a = $1.075(\phi_0/B)^{1/2}$ which is $\approx$ 48 nm at 1 T. TRIM calculations give a total vacancy density of 2 x 10^{20} cm^{-3} for a fluence of 2.4 x 10^{12} cm^{-2} (i.e. a factor of four times the equivalent vacancy density, 5 x 10^{19} cm^{-3}) or, if a random distribution is assumed, a defect separation of $(2 \times 10^{20})^{-1/3} = 1.7$ nm is obtained. We can hypothesize that it is mainly clustered or extended defects resulting from a relatively small fraction of recoil events occurring at high energies, that contribute to the increase in the pinning, and that these pinning centers are considerably further apart than the calculated vacancy spacing. This hypothesis will be further explored through calculations based on the recoil energy distributions[2,7]

for different ions, as relevant to defect density and size, which are the subject of section 5.7.

5.7 Recoil Energy Distributions of Different Ions in $Bi_2Sr_2CaCu_2O_8$

To account for the results obtained after irradiation by different ions we turned to a theoretical examination of the defect structures likely to be produced by these ions for the given experimental conditions. As discussed in Chapter 4, in order to determine the "Equivalent Damage Dose" (EDD), damage profiles had been calculated by the simulation program TRIM, using a Kinchin-Pease model, which gave the number of vacancies produced per unit length (vacancies/ion/Å as a function of depth in the averaged target, $Bi_2Ge_3Cu_2O_8$. (Recall that TRIM has a maximum capability of four element target composition.) As previously noted, the Kinchin-Pease method uses an analytic solution to calculate target damage rather than follow each collision separately. An alternative way to run TRIM is with the full cascade calculation option under which the results of every ion/atom collision can be stored in a file called COLLISION.TXT. In this file are contained tables showing each incident ion colliding with various atoms in the target, and the detailed results of any collision cascades. Both the Kinchin-Pease and the full cascade calculation, however, ultimately characterize target damage in terms of numbers of simple displacements, which, as we have already seen, is problematic with respect to modeling heavy ion damage. This method of calculating damage profiles was nonetheless useful in selecting the EDD fluence for different ions. We now refine this approach by considering the different recoil energy distributions of different mass ions.

In the full cascade calculation of the TRIM simulation, when a target atom is hit and starts a recoil cascade, the file COLLISION.TXT also stores the recoil energy of that target atom. A tabulation of calculated recoil energies such as is accumulated in the file COLLISION.TXT is of great interest in comparing the nature of simulated target damage induced by different ions to experimental results (observed or implied) of defect structure. This was first recognized by Kirk,[2] who constructed a plot of the "Integral Recoil Fraction vs. Energy" for various incident particles in a number of targets including $YBa_2Cu_3O_7$. In this construction the recoil events

are separated into a large number of discrete energy ranges or "bins" and the total number of recoil events occurring in a given energy range are accumulated in these bins. Then the total number of events occurring below a given energy, E, are added up and plotted as a fraction of the total number of recoil events vs. E. For any energy we can then read off the plot the fraction of recoil events occurring in the target below this energy, for a given incident species.

As this plot had never been constructed for a $Bi_2Sr_2CaCu_2O_8$ target, use was made by the author of the program TRIM to do so for the incident ions studied in our experiment. The result is shown in Fig. 5.16, which plots the Integral Recoil Fraction vs. Energy for H^-, He^-, Ne^+, and Ar^+ respectively, incident upon the averaged target $Bi_2Ge_3Cu_2O_8$. It is immediately evident from this plot that there is almost no difference between the recoil energy distributions of H^+ and He^+, which are clustered together in the lower energy range, showing a "soft" primary knock-on (PKA) spectrum.

Proton irradiation is experimentally known to produce damage primarily of the point defect type (and some small clusters) in high temperature superconductors. The similarity of the recoil energy distributions for the light ions suggests that for our target the defect structure due to He^- damage is not likely to be significantly different from that of protons, due to the same predominance of low energy recoils. This explains the lack of significant improvement in the activation energy of our light-ion irradiated samples. While in $YBa_2Cu_3O_7$ the pinning centers relevant to controlling J_c were found to be the point defects,[3,4] whether present as-grown or extrinsically introduced, the simple vacancies present intrinsically in $Bi_2Sr_2CaCu_2O_8$ have experimentally not been found to be nearly as effective in pinning flux in this material. This may be due to the more anisotropic nature of this material (pancake vortex effects). In this case, when more of these small defects are introduced, for example by H^+ or He^+ irradiation, the primary effect is just to disorder the material in a distributed fashion, leading to significant T_c degradation and increases in the normal state resistance. These dominate the minor improvement in the activation energy and the net effect is to decrease the critical current. These results are consistent with results reported by Palstra[1] et al., that is, fluences up to 4 x 10^{14} cm^{-2} He^- at 2 MeV on single crystals produced only modest improvements in the pinning energy.

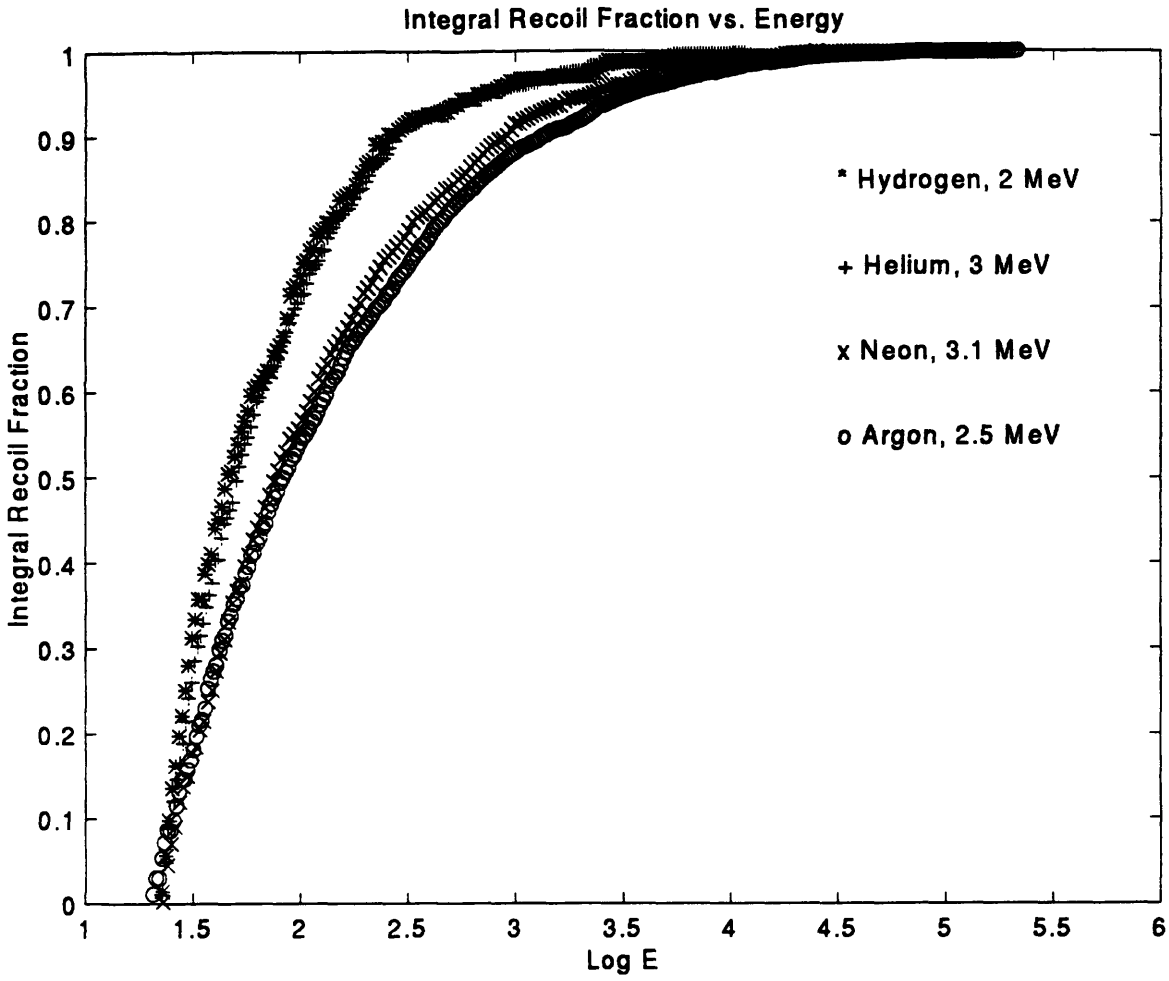

Figure 5-16: Recoil energy distributions of H^-, He^-, Ne^- and Ar^- in averaged $Bi_2Sr_2CaCu_2O_8$ target ($Bi_2Ge_3Cu_2O_8$).

Fig. 5.16 shows that the heavier ions Ne^+ and Ar^+, on the other hand, have a relatively "hard" PKA spectrum, producing a substantially larger proportion of high energy recoil events. While the relationship of the PKA spectrum to the detailed microstructure actually observed is currently a topic of active study in HTC superconductors, it has already been determined by HRTEM that the high energy recoil events (above tens of KeV), although very improbable, do induce recoil cascades that lead to "blob-like" damage.[2,8] The results of Fig. 5.16 clearly show that these events are significantly more likely for the heavier ions. It is interesting that the PKA spectra for Ne^+ and Ar^+ are distinguishable from each other on this plot, with Ar^+ having a somewhat harder spectrum in the high energy ranges, as our experimental results were noted to be generally better for Ar^+.

This calculation quantitatively supports our speculation of the existence of spatially extended damage in the heavier ion irradiated samples, which were hypothesized to act as more effective pinning centers. HRTEM might resolve questions concerning the precise defect structure in our crystals; in any case we have shown that heavy ion irradiation does result in a significantly increased pinning energy and a peak effect which is qualitatively consistent with the existence of clusters.

5.8 Summary and Conclusions

We have investigated and compared results of the in-field resistive transition, transport current-voltage characteristics and magnetization J_c as a function of temperature, before and after irradiation by H^+, He^+, Ne^+, and Ar^+ of single crystal $Bi_2Sr_2CaCu_2O_8$. Doses for the different ions were chosen to approximate the same level of damage in each sample according to a simple model of vacancy production, with the vacancy density chosen by analogy to the dose which maximizes the critical current in proton irradiated crystals of $YB_2Cu_3O_7$. We have further examined the Ar^+ dose dependence in our crystals of the magnetization J_c at different temperatures.

The effects we see for light ion irradiation are consistent with results reported by Palstra[1] et al., that is, fluences up to 4 x 10^{14} cm^{-2} He^+ at 2 MeV on single crystals produced only modest improvements in the pinning energy. After irradiation by the heavier (Ne^+ and Ar^+) ions, however, we observe significant increases in the pinning energies and critical currents, which we attribute to the introduction of spatially extended defects. Our data imply that heavier ion irradiation, unlike light ion damage, results in an upward shift of the irreversibility line. The results leading to these conclusions will now be summarized in more detail.

The relative changes in the pinning energy before and after irradiation were determined from the slopes of Arrhenius plots of the resistive transitions at low field (H = 0.05 T). The activation energy changes by a factor of 2.3 for Ar^+ as opposed to only 1.45 for H^+. Results of the resistive transition were qualitatively similar at high field (H = 5 T), in that the resistive tail was more effectively suppressed by heavier ion irradiation. We propose that the significant increase in the activation energy in heavy ion irradiated samples is due to the presence of large or clustered defects resulting from damage cascades of high energy recoils of primary knock-on atoms. The dominance of low energy recoils in light ion bombardment, on the other hand, most probably results in a predominance of point defects, as was inferred for results of proton irradiation in $YB_2Cu_3O_7$.[3,4] Point defects are thought to dominate the defect structure of unirradiated $Bi_2Sr_2CaCu_2O_8$ crystals, in which the pinning is obviously weak. We suggest that light ion irradiation does not introduce appreciably different types of defects, which accounts for the lack of significant improvement of the activation energy in those samples. (Degradation of the critical temperature and normal state resistance do however indicate an increased defect density.) Due to the short correlation length along the vortices in $Bi_2Sr_2CaCu_2O_8$, the spatial extent of pinning centers is particularly important in effecting stronger defect-vortex interactions which lead to higher pinning energies. This is in contrast to results in the more three dimensional $YB_2Cu_3O_7$ system, where point defects were found to be effective pinning centers.

Measurements of both the transport and magnetization critical currents are consistent with the Arrhenius results. Transport J_c's show two to five-fold improvements after Ne^+ and Ar^+ irradiation but after irradiation by H^+ or He^+ the critical current either fails to improve or

degrades. The functional dependence of the current–voltage characteristics is not precisely understood at this time but I-V curves are concave upward, approaching linearity at higher temperatures and fields. Heavier ion irradiation suppresses the voltage for all measurement conditions and retards the transition to linear behavior. After light ion irradiation, however, the voltage developed at a given temperature, field and current is generally higher than in the unirradiated sample. It is therefore apparent that the minor improvements in the pinning energy in these samples are overcome by the effects of T_c degradation and increases in the normal state resistance, as is consistent with a defect structure of distributed point defects.

The magnetization J_c shows significant improvement after heavier ion irradiation as well. At low temperature the increases in J_c after irradiation by Ne^+ and Ar^+ are on the order of factors of two, roughly consistent with the improvements observed in transport. More impressively, a markedly decreased sensitivity to elevated temperature and field is evident after Ne^+ and Ar^+ irradiation, which is not observed after irradiation by H^+ and He^+. As in unirradiated crystals, for a field of 1 T critical currents in light ion irradiated samples become immeasurably small ($< 10^4$ A/cm^2) above roughly 15 K - 20 K, whereas finite critical currents are measurable at temperatures as high as 30 K after heavy ion irradiation. This is consistent with the observed increases in the pinning energies and indicates that an upward shift in the irreversibility line occurs only for the case of the heavier ion damage.

The Ar^+ dose dependence of the magnetization J_c shows that the equivalent damage dose chosen in these experiments was reasonably close to the optimal dose, as was hoped. More importantly, the dose dependence exhibits a temperature independent peak which is indicative of a classical matching effect, for which the average defect spacing is equal to the vortex spacing. A simple estimate of the defect spacing based upon a model of damage by vacancy production is far too low to account for the field dependence of the observed peaks. This is suggestive of the presence of a lower density of relevant defects which act as effective pinning centers, such as would result from a small fraction of high energy recoil events producing larger defects, rather than simple vacancies.

Calculations of recoil energy spectra quantitatively support the above supposition of cluster-type defects in heavier ion irradiated samples. The PKA spectra for H^+ and He^+ are practically identical, showing a predominance of low energy recoils, whereas both Ne^+ and Ar^+ show relatively hard PKA spectra, with a small but significant fraction of events occurring above 10 KeV. These higher energy events are known to induce recoil cascades and produce cluster-type damage in HTC layered superconductors, as compared to the low energy recoils which are more likely to produce point defects.[2,8]

While this model is appealing and accounts for the general trends we observe, quantitative agreement would require incorporating complications such as the range of cluster sizes produced and details of vortex interactions, vortex correlation lengths and possible cooperative phenomena. Nonetheless, we have demonstrated the potential to improve pinning in $Bi_2Sr_2CaCu_2O_8$ with spatially extended defects in order to overcome two-dimensional pancake vortex effects. Civale et al. have produced long columnar defects in $YBa_2Cu_3O_7$ by GeV Sn^+ irradiation which illustrate this effect.[9] It is most likely that our $\approx$ 3 MeV Ne^+ or Ar^+ irradiation of $Bi_2Sr_2CaCu_2O_8$ would produce cluster-type defects rather than columnar defects (which require ionization energy loss rates exceeding 2 KeV/Å, i.e. incident energies at fractions of GeV). Increases in pinning have also been achieved using fast neutron irradiation,[10–12] a process which features a high proportion of high energy recoil events, i.e. a hard PKA spectrum.[2] Effective pinning centers need not be radiation induced; other promising structures include grain boundaries and precipitates.[13] We are optimistic that novel microstructures in $Bi_2Sr_2CaCu_2O_8$ can lead to increased vortex-defect interaction energies and thus higher critical currents at high temperatures and fields.

5.9 References

1. T. T. M. Palstra, B. Batlogg, L. F. Schneemeyer and J. V. Waszczak, Phys. Rev. B 43, 3756 (1991).

2. M. A. Kirk and H. W. Weber, in *Studies of High Temperature Superconductors* (ed. Narlikar, A. V.), Vol. **10**, 253-315, (Nova Science Publishers, New York, 1992).

3. R. B. van Dover, E. M. Gyorgy, A. E. White, L. F. Schneemeyer, R. M. Fleming, R. J. Felder, and J. V. Waszczak, *Advances in Superconductivity III, (Proceeding of 3rd International Symp. on Superconductivity-ISTEC)*, edited by K. Kajimura and H. Hayakawa, (Springer-Verlag, Berlin, 1991), p. 467.

4. L. Civale, M. W. McElfresh, A. D. Marwick, T. K. Worthington, A. P. Malozemoff, F. Holtzberg, C. Feild, J. R. Thompson, D. K. Christen, and M. A. Kirk, *Proc. XII Winter Meeting on Low Temperature Physics*, Guernavaca, Mexico, 1991.

5. T. T. M. Palstra, B. Batlogg, L. F. Schneemeyer, and J. V. Waszczak, Phys. Rev. Lett. **61**, 1662 (1988).

6. A. M. Campbell and J. E. Evetts, Adv. Phys. **21**, 199 (1972).

7. J. Biersack and L. Haggmark, Nucl. Instrum. Methods, **174**, 257 (1980); J. F. Ziegler, J. P. Biersack and U. Littmark, *The The Stopping and Range of Ions in Solids* (Pergamon Press, New York, 1985).

8. A. D. Marwick, private communication.

9. L. Civale, A. D. Marwick, T. K. Worthington, M. A. Kirk, J. R. Thompson, L. Krusin-Elbaum, Y. Sun, J. R. Klem, and F. Holtzberg, Phys. Rev. Lett. **67**, 648 (1991).

10. W. Kritscha, F.M. Sauerzopf, H.W. Weber, G.W. Crabtree, Y.C. Chang, and P.Z. Jiang, Europhys. Lett. **12**, 179 (1990).

11. W.Gerhauser, H.W. Neumuller, W. Schmidt, G. Ries, G. Saemann-Ischenko, H. Gerstenberg, and F.M. Sauerzopf, Physica (Amsterdam) C **185-189**, 2273 (1991).

12. H.W. Weber and G.W. Crabtree, in *Studies of High Temperature Superconductors*, edited by A.V. Narlikar (Nova Science, New York, June 1991), Vol. **9** and references therein.

13. D. Shi, M. S. Boley, U. Welp and J. G. Chen, Phys. Rev. B **40** 5255 (1989).

Chapter 6

Recent Progress and Present Day Context

The experimental work of this thesis was performed in two (non-contiguous) parts, both occurring between the spring of 1988 and the summer of 1991. In this chapter we attempt to place the main results of this work in a present day context, that is, the Spring of 1997. To this end we shall first briefly review recent advances in the field and then discuss the relevance of these developments to the work at hand.

6.1 Vortex Systems: A Brief Review

6.1.1 Overview

The period just after the discovery in 1986 of the HTC superconductors was a time of rapid germination and synthesis of new ideas in vortex physics, as well as immense technological initiative to develop novel and more effective means of pinning flux in these materials. A number of new theoretical concepts were put forward at that time to explain the highly dissipative properties of the HTC cuprates, as discussed in Chapter 3. These included the (sub-H_{c2}) melting of the vortex lattice, the existence of new vortex-liquid phases, decoupling of line vortices into pancake vortices, as well as adaptations of conventional theories of flux creep and vortex

glass models to the new regime of high critical temperatures, short coherence lengths, and weak interplanar couplings. Notably, today the language of HTC vortex behavior is still expressed in much the same terms. Over the last several years, however, the exploration and refinement of these ideas has led to a more integrated and detailed picture of vortex behavior in both conventional and HTC superconductors.

While it is interesting that this fundamental reexamination of vortices has also led to the emergence of the study of "vortex matter" as a discipline unto itself, the details of these theoretical investigations,* are largely beyond the scope of this discussion. A comprehensive theoretical review may be found in the 1994 article by Blatter et al.[1] Of direct relevance, however, are the implications for the HTC magnetic phase diagram, and the related consideration of the dynamic response of vortices in the presence of external forces. These developments will be focused upon in the next section.

As in earlier years, technological advances have continued to proceed interactively with theoretical developments. It is now widely recognized that novel structure in the H-T phase diagram (e.g. melting and/or 3D→2D transitions) often supersedes single vortex pinning ideas, and that therefore pinning in HTSC materials must be discussed both in terms of the underlying defect structure and the equilibrium phase diagram. This has motivated the proliferation of experiments designed to enhance flux pinning with extended and/or linear defects. Most interesting are the high energy heavy-ion irradiation efforts which produce long columnar defects, as described in the previous chapter. This approach has now been tried on a number of HTSC materials[6–12] including $Bi_2Sr_2CaCu_2O_8$, and will be discussed in comparison to my results of improved critical currents. Other methods of introducing effective pinning centers will also be surveyed.

In the last section we discuss the results of this thesis in the context of the above progress

*These studies,[1] which span diverse areas of physics, consider the statistical mechanics of large systems of interacting strings in the presence of external forces, of which vortices in superconductors are one example. Extensive use is made of the two-dimensional boson analogy. Another topic of recent interest is the application of self-organized criticality theory[2] to describe flux bundle motion.[3–5]

which has occurred in the past six years since these experiments were conducted. Because the more recent experimental work is not specifically comparable to the work at hand, these discussions are necessarily of a very general nature and are intended in the spirit of interesting speculation. Finally, we shall attempt to point out areas which still remain to be explored.

Helpful reviews on recent progress in this field include, in addition to the theoretical treatment of Blatter et al.[1] (1994) mentioned above, a broader review by McHenry and Sutton[12] (1994), an unusually accessible article by Crabtree and Nelson[13] (April, 1997), and an examination of magnetic relaxation experiments by Yeshurun, Malozemoff and Shaulov[14] (1996).

6.1.2 Vortex Phases in HTC and Conventional Superconductors

The equilibrium behavior of vortex systems in different regimes is mainly governed by the relative strengths of various types of disorder. In the absence of disorder, vortex interaction energy would favor a perfect vortex lattice. This lattice may however be disrupted by the presence either of quenched disorder (defects), or dynamic disorder in the form of thermal fluctuations, which dominate as the temperature is raised, or quantum fluctuations,[15,16] which lead to the tunneling or "quantum creep" of vortices observable in HTC magnetic relaxation experiments at very low temperatures.* As quantum fluctuations are inconsequential at temperatures above 1 K, their role in determining the phase diagram is minimal and they will henceforth be neglected in this discussion.

Expressed in terms of disorder, the most striking differences between the phase diagram of the HTC and conventional superconductors are easily summarized. In conventional materials, the pinning potential (quenched disorder) can be quite strong, whereas thermal fluctuations are weak. On the other hand, in HTC materials it is the pinning potential which is weak (as has

*Quantum fluctuations have not been previously mentioned because technologically, the impact of thermal fluctuations is of far greater significance. While quantum fluctuations are larger in HTC than in conventional superconductors, (and therefore observable) they continue to be of interest more from a theoretical then practical point of view. The tunneling rates of quantum creep are determined in part by the value of the quantum resistance, Q_u, ($Q_u \propto \rho_{n/\epsilon\xi}$, where ϵ is the anisotropy parameter, $\sqrt{m/M}$) which is at least two orders of magnitude larger in HTC materials then in conventional superconductors.

been discussed) relative to thermal fluctuations which are strong. As pointed out by Nelson, across much of the HTC vortex phase diagram thermal energy (i.e. fluctuations) favors a vortex liquid whereas in conventional materials, in which thermal fluctuations are weak, a vortex lattice of rigid lines characterizes virtually the entire mixed state. In both classes of materials, if quenched disorder is strong enough, the solid state will tend toward a glassy or amorphous phase rather than an ordered vortex lattice. Quite notably, an additional feature is introduced in the HTC materials by the strong anisotropy, which leads to a layer decoupling transition, as described in Chapter 3.

Nelson further points out that in the HTC regime, the energies which compete to determine the phase diagram, i.e., thermal energy, pinning energy, vortex interaction energy, and coupling energy between layers, can all be of the same order of magnitude. This gives rise to the complexity of the phase diagram not found for conventional superconductors. The determination of the precise structure of the phase diagrams in the HTC layered superconductors is a topic of ongoing theoretical and experimental investigation. In the next section we shall simplify this picture somewhat, and look at a phenomenological static equilibrium phase diagram for a strongly anisotropic (BSCCO-type) superconductor in the absence of pinning. Subsequently the effects of pinning will be considered, which leads naturally into a discussion of vortex dynamics.

6.1.3 Static Equilibrium Phases in the Absence of Pinning

Shown in Fig. 6.1a is a phenomenological phase diagram[1] for a highly anisotropic superconductor (such as BSCCO) in static equilibrium without pinning, for a field oriented along the c-axis. Shown for comparison in Fig. 6.1b is the analogous diagram for a YBCO - like superconductor. The presence of the various novel vortex liquid phases (disentangled, entangled, and decoupled) covering much of the phase diagram is familiar from Chapter 3 (3.2.4), as is the lower-lying melting line in the more anisotropic material. Note, however, the addition in both diagrams of a reentrant liquid phase close to H_{c1}. In this region the vortex separation grows beyond the penetration depth and vortex interactions are extremely small. Interestingly, this is proposed

to result in a vanishing shear modulus and therefore low-field melting.

At high fields, the H_{c2} line is still expected to mark the onset of enhanced diamagnetism, and possibly approximately coincide with a jump in the specific heat,[1] but is no longer expected to be a sharp thermodynamic phase transition. As in conventional superconductors this region is characterized by large fluctuations in the order parameter. However, unlike conventional type II materials, the onset of superconductivity is not rapidly accompanied by the appearance of the vortex lattice, with its well-defined compression, shear and tilt properties. Instead, in the HTC materials the vortex liquid phase forms, characterized by a linear ohmic resistivity, which at zero frequency looks much like that of a normal metal. However the different phases within the vortex liquid regime are experimentally distinguishable[13,17] and lead to interesting behaviors, for example with respect to measurements at finite frequency or interactions between vortices and pinning centers.

It is the melting line rather than H_{c2} which defines a thermodynamic phase transition. In clean systems, freezing to a perfect lattice is expected to be a first order transition. In systems with a significant degree of quenched disorder, (as discussed in the next section) freezing to a glassy solid would be a more gradual process, perhaps accompanied by a sharp second order transition.[13] Recently a first order transition was directly observed in BSCCO[18] as a jump in the magnetic induction (i.e. vortex density) upon vortex melting. Another recent experiment directly measured the latent heat at the melting transition in YBCO.[19]

The decoupling transition is here represented, according to the analysis of Blatter[1] et al., as occurring above a single, temperature independent field, $B_{2D} \approx (\pi\Phi_0/\Lambda^2)\ln(\Lambda/\xi)$, where Φ_0 is the flux quantum, ξ is the coherence length, $\Lambda = d/\varepsilon$ is the Josephson screening length in the layered system, d is the layer separation, and the anisotropy parameter, $\varepsilon = \sqrt{m/M}$. Nelson, however, defines a temperature dependent decoupling curve.[13] Nevertheless, both treatments suggest the existence of both decoupled two dimensional liquid and solid (supersolid) phases. The two dimensional melting line, (which represents the Berezinskii-Kosterlitz-Thouless dislocation mediated melting temperature, $T_m^{2D} = (\Phi_0/4\pi\lambda)^2 d/4\sqrt{3}\pi$), where λ is the penetration

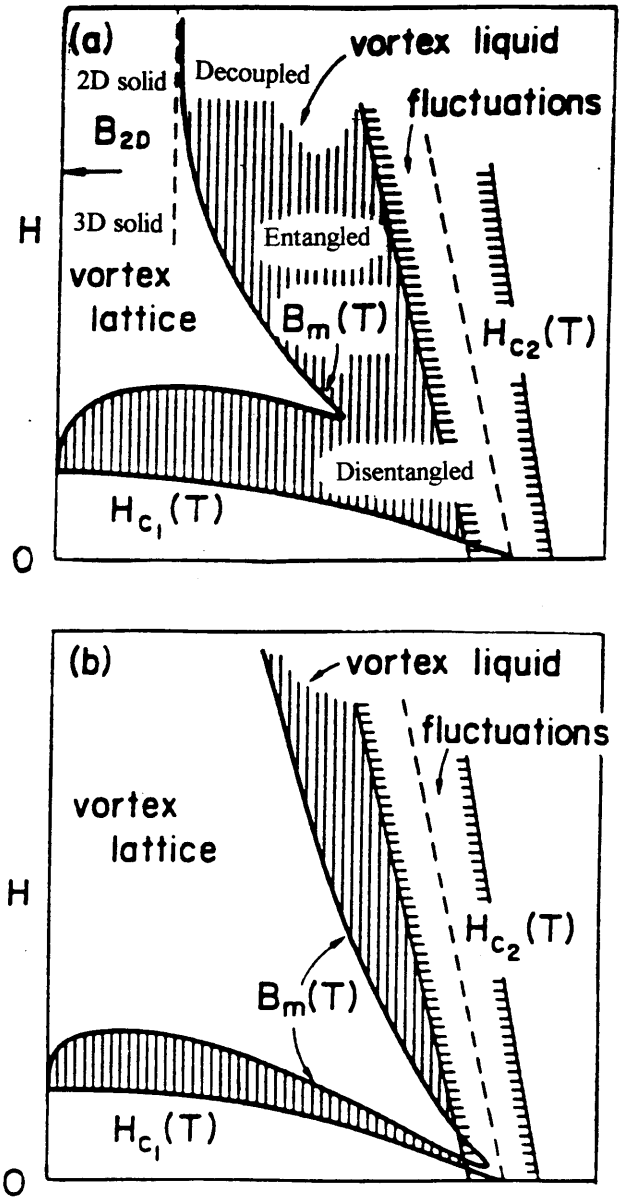

Figure 6-1: Static equilibrium vortex phase diagrams in the absence of pinning for a.) BSCCO-like superconductor and b.) YBCO-like superconductor, as reproduced from Blatter.[1]

depth, is asymptotic to the 3D melting curve and is independent of field. By comparison, in YBCO (see Fig 6.1b), these decoupling transitions are of less relevance as this material may under most circumstances be described by the three dimensional continuous anisotropic Ginzburg-Landau model. The effect of this difference upon pinning will be addressed in the next section.

6.1.4 The Effects of Disorder and Pinning

With the addition of quenched disorder, the vortex lattice phase in Fig. 6.1 is replaced by a vortex glass. If the disorder potential is weak enough (compared to the thermal disorder) then it may be treated perturbatively and the discussion of this section may essentially be mapped onto Fig. 6.1a. (However for the case of the extrinsic introduction of strong pins, this is no longer true.) The application of the concept of weak collective pinning transforms the vortex lattice into a vortex glass. An analogous transformation does not occur for the liquid, which although in lower temperature regimes may be pinned, remains a liquid. Depinning is distinguished from melting, as will be further discussed.

The phenomenon of depinning introduces vortex dynamics into the discussion. For example, thermal fluctuations present in the absence of external forces, play an important role when a current is applied. Thermal excursions of individual vortex lines over a spatial displacement $\langle r^2 \rangle^{1/2}$ result in a dynamical sampling or averaging of the disorder potential, thereby reducing the critical current.* This phenomenon is referred to as "thermal depinning" and is, not surprisingly, very significant in the HTC cuprates. Thermal fluctuations not only effect the pinning potential, but are responsible for thermally activated flux creep, as discussed in section 3.2.2. A number of the observations reported in Chapter 3 can now be more consistently related.

Returning to the phase diagram, at high temperatures near the H_{c2} boundary, thermal fluctuations overcome the pinning energy and the liquid is unpinned. This implies that under

*These excursions need to grow to a fraction of the vortex spacing in order to initiate melting of the solid phase.

the influence of external forces (applied current), the system can develop a free flow where quenched disorder then only contributes to the flux-flow viscosity. As we move to lower temperatures and approach the melting (freezing) line, we enter a regime where the pinning energy is large relative to kT. Here the resistivity becomes exponentially small and shows the activated behavior characteristic of thermally activated flux creep. Here we may associate a relaxation time, τ_r, with the vortices that is large compared to the pinning time, τ_p. (The flux-flow regime is entered when $\tau_r \approx \tau_p$.) Note that this represents a pinned liquid phase,* above the melting line. As the temperature is lowered, the viscosity of this phase increases until, upon freezing, the elastic properties of the vortex lattice are established.

More recent definitions of what constitutes a vortex glass phase have involved dynamic rather than static criteria such as long range order. It has been shown that the pinning barriers diverge[20] in the limit of vanishing current density. According to a collective pinning model, the current-voltage characteristic develops an essential singularity in the limit j→0, with the electric field vanishing as $E \propto e^{-(Uc/kT)(j_c/j)^{\mu}}$, where U_c is the collective pinning barrier. Since $\rho(j \rightarrow 0) \rightarrow 0$, the vortex glass is considered to be a truly superconducting phase in the thermodynamic sense. However, for finite currents a finite resistivity may be observed. This could make it difficult to distinguish a glass from an extremely viscous liquid using transport measurements, as opposed to for example more direct measurements of the elastic properties of the vortex lattice.[21] Koch[22] was able to distinguish a very clear crossover in YBCO from a linear I-V (liquid phase) to power law (glass phase) behavior but in BSCCO the resistivity as a function of temperature is well described by the thermally activated flux creep model down to vanishingly small voltages with no abrupt decreases in the resistivity observed. These dissimilarities may be due to differences between YBCO and BSCCO with respect to the relative positions of the melting line and the magnitude of the activation energies, as influenced by anisotropy.

These anisotropy differences have further implications with respect to depinning mechanisms. In BSCCO it is not clear for different temperatures and fields whether we are observing the depinning of line vortices, pancakes, or some intermediate step-wise mechanism which ex-

*The reentrant phase at low field is also considered to be pinned except near T_c.

ploits the low tilt modulus. In YBCO, on the other hand, while the pinning correlation length and rigidity of vortices (line tension) is at issue, especially at high temperatures, it is generally assumed that layer coupling is strong enough to insure that a vortex system of lines exists under most conditions. Clearly, the unification of the phase diagrams for all the layered superconductors (and including the effects of pinning), is a major challenge for the future. Nevertheless, the advances of the past several years have at least placed the various phenomena of flux flow, flux creep and vortex melting in perspective on the phase diagram, as well as opening new areas of exploration of novel phases. We shall shortly turn to the recent applied progress in pinning vortices which makes use of the developing picture of the HTC phase diagram in strategizing new defect structures. First, it is worth noting one further theoretical advance.

The consideration of depinning in vortex systems as discussed above has led to closer examination of the dynamical properties of the vortex lattice. In fact, the dynamic response of vortices in driven systems is currently emerging as an independent subject of investigation. While it may be too early for these studies to shed light on the work at hand, they promise to be of direct relevance and so some early results are briefly described below.

6.1.5 Vortex Dynamics

Dynamical vortex phases have been considered in the steady state* of driven motion as a function of force and temperature using numerical simulations.[23] A "rest phase" is designated for low temperatures and small forces. Above a critical depinning force is a moving phase characterized in systems with random pinning by plastic motion. Here vortices move at different velocities in different parts of the system. While in the liquid phase vortices can slide more easily past one another (particularly if they are disentangled), below the melting temperature this leads to shearing along planes where the velocity changes discontinuously. In the solid state at sufficiently high driving forces (large compared to the the pinning force) there is another transition to elastic motion, which is temperature dependent, where the vortices all move with the same average velocity.[24] Intervortex energy stabilizes this state, which tends to be

*The steady state develops naturally as vortices are created and destroyed at the sample boundaries.

suppressed at higher temperatures by thermal fluctuations.

6.2 Advances in Pinning by Induced Damage

6.2.1 Columnar Defects in YBCO

The introduction of columnar defects had remarkable effects on the flux pinning in YBCO single crystals. In these experiments long linear tracks of damage are induced in crystals by fast heavy ions, with ionization energy loss rates exceeding 2 KeV/Å. This condition is met over distances of 10's of microns, i.e. approaching sample thicknesses. The first results of this type were reported by Civale et al.[6] for samples irradiated with 580 MeV Sn^{+} ions. At a dose of 2.1 x 10^{11} cm^{-2}, corresponding to the vortex density at a field $B_\Phi = 5$ T,* critical currents of 2.5 x 10^5 A/cm^2 at 77K and 3 T were achieved. By comparison, Civale's earlier results of very similar crystals irradiated with (MeV) protons had $J_c \approx 0$ in this range. Critical currents at 5 K, however, were comparable to those measured after proton irradiation. These results were explained in terms of increased pinning energies (which had not been observed after proton irradiation) due to the confinement of the vortex core along lengths approaching the thickness of the sample. Clear evidence that the strong pinning was due to the alignment of the vortices with the damage tracks was demonstrated by the comparison of hysteresis loops measured with the applied field at an angle of $\pm 30°$ with respect to the **c**-axis but parallel to the tracks in only one of these orientations. The magnetization at 70 K was more than doubled for **H** applied along the tracks for a fluence of $B_\Phi = 1$ T. When **H** is parallel to the defects, higher critical currents can be sustained at higher fields as a function of increasing column density, indicating a matching of vortices to the columnar pinning sites.

This 1991 experiment, paralleling the approach of this thesis, marked the widespread acceptance that the pinning energy could be significantly raised by the introduction of extended defects. Because of the directional nature of these defects, it was particularly easy to asso-

*For columnar damage, dosages are typically given in terms of the equivalent field, $B_\Phi = 2\Phi_0/\sqrt{3}a^2$, where a is the average spacing between the columns. Note also that at these high incident ion energies nearly complete penetration occurs.

ciate the improvement with a longer correlation length along the vortices, in this case vastly increasing above the coherence length, if not perhaps to sample dimensions. In response to these extraordinary developments, efforts were quickly underway to see whether a similar result could be achieved in the more anisotropic Bi and Tl-based superconductors.[7–10] These results are discussed in the next section.

Soon after the success of columnar defects in YBCO, Nelson and Vinokur[25] predicted that for $B < B_\Phi$ such a system would condense into a "Bose-glass" phase at low temperatures, with vortex lines localized on columnar pins, an infinite tilt modulus and zero linear resistivity. This occurs as a result of the correlated disorder introduced by the columns, as opposed to the usual case of random quenched disorder, for which a vortex glass is predicted. At higher fields and temperatures the system undergoes a Bose glass transition to an entangled flux liquid phase. In 1994, Krusin-Elbaum et al.[26] reported a sharp melting of the Bose glass in YBCO crystals irradiated with 1 GeV Au ions. Their results were in quantitative agreement with the theory of melting in the presence of correlated disorder.

6.2.2 Columnar Defects in BSCCO

Results of irradiation of BSCCO crystals by 0.5 GeV I^+ ions at dose equivalent field values between $B_\Phi = 0.4$ T and 5.2 T were reported by Gerhauser et al.[7] in 1992. In contrast to the results of YBCO, it was found that even with the flux lines aligned parallel to the tracks, the measured activation energies did not exceed 70 meV* ($\approx$ 800 K) even at low temperatures and small fields. This represented an approximate doubling of the activation energy before irradia-

*Caution must be exercised in the interpretation of activation energies measured by magnetic relaxation, and they should not be directly compared to those measured in transport. In a recent review, Yeshurun et al.[14] explained that a number of anomalies in early magnetic measurements of U_0 are due to the use of the linear approximation for U(J) from the original Anderson-Kim model of flux creep. Because of the large relaxation rates in the HTC superconductors, the persistent current may fall far below the critical current, thereby greatly exaggerating the error resulting from this approximation. Care must be also taken in comparison of values of U_0 measured at different temperatures or, for example, before and after irradiation. Whenever measurements are not performed at the same current, the operating point on the non-linear U(J) curve changes and linear extrapolations to U(J=0) are problematic. Several non-linear models of U(J) have been proposed but in general U decreases monotonically (and sub-linearly) as a function of J. Therefore, if pinning is improved after irradiation, the resulting increase in the current may mask increases in U_0 to varying degrees if the linear approximation is assumed, as by Gerhauser et al.

tion, far less than the factor of L/ξ expected from the linear confinement of line vortices, where L is the sample thickness. These results were interpreted to be consistent with interactions between single pancake vortices and the columnar defects. To explain the low pinning energies it was necessary to assume a correlation length along the vortices equal to the separation between CuO_2 planes.

In contrast, later efforts by Thompson et al.[8] using 0.580 GeV Sn^+ ions, showed large enhancements of critical currents at high temperatures by columnar defects. At low temperatures improvements range between factors of 5 and 10, but more importantly, Thompson et al., were able to significantly extend the irreversibility regime, measuring a magnetization J_c of about 5 x 10^3 A/cm2 at 50 K and 1 T. The critical current had previously dininished to zero above 20 K, which is typical in clean single crystal $Bi_2Sr_2CaCu_2O_8$. Thompson et al., however, found very little directional enhancement of pinning, which was, not surprisingly, attributed to the much stronger two dimensional character of $Bi_2Sr_2CaCu_2O_8$.

Klein et al.[9] found similar enhancements of the critical current after irradiation by 5.8 GeV Pb^+. They, however, also presented evidence for coupled line vortices based upon observations of unidirectional pinning, particularly above 50 K. They pointed out that Thompson et al. had studied the orientational dependence of the magnetization only below 50 K. It was suggested that at lower temperatures the CuO_2 layers were not coupled by Josephson interactions and therefore that the vortices were aligned only by magnetic interactions. Their data implied a more significant Josephson coupling above 50 K so that the line vortices could then be tilted off of the defects. The transition with increasing temperature to unidirectional behavior was not abrupt, suggesting that as coupling increases the depinning mechanism gradually shifts from excitation of individual pancakes to kink formation mediated by off-axis excitation of coupled pancake vortex sections. The Josephson coupling between layers[27] and the longitudinal correlation length along the vortices[28] continue to be active topics of investigation. Both are likely to be enhanced by the presence of columnar defects.

The zipper-like depinning mechanism of flexible line vortices described above would cer-

tainly be complicated and actually inhibited by entanglement as described by Nelson,[29] due to barriers to cutting and reconnecting vortex lines in the entangled state. The presence of the columnar defects, however, likely suppresses entanglement. There is evidence in YBCO that the presence of twin boundaries can "comb the hair" of an entangled flux liquid just above the vortex glass melting temperature for finite sample thicknesses.[17] In the presence of twin boundaries, a Bose glass phase is predicted[1] at low temperatures in which the vortices are disentangled, similar to that found in YBCO samples with columnar defects. Alternatively, entanglement could be frozen in by a different type of defect configuration, as described below.

6.2.3 Splayed Columnar Defects

Hwa et al.[30] proposed that a splay, i.e. a dispersion in the orientation of columnar defects, would address the problem in HTC vortex systems (especially with higher anisotropy) of low angle, low energy off-axis excitations. A splayed pattern of defects may be produced by rocking crystals during irradiation. Transport properties are predicted to be enhanced, especially at low currents by the misorientation of columns, which would inhibit large scale tilting of vortices. This arrangement has the additional advantage of promoting entanglement which arises from pinned arrangements between adjacent tilted vortices. A frozen entangled ground state (splay glass) was found to have only a slightly reduced melting temperature with respect to a disentangled Bose glass of parallel columns, while exhibiting diverging activation barriers to low lying excitations. The behavior of such systems in real materials is a current topic of investigation.[31]

6.2.4 Effective Pinning by Other Methods

A lower energy irradiation technique that has been successful in improving the critical current is the novel method of fission fragments. Superconducting materials are doped with elements having large neutron scattering cross-sections and then bombarded with low doses of neutrons. It has been demonstrated[32] that similar increases in the critical current can be achieved in Gd doped $YBa_2Cu_3O_7$ by thermal or fast neutrons, raising the possibility of inducing significant radiation damage at lower fluences and energies. In $Bi_2Sr_2CaCu_2O_8$, use has been made of a

resonant proton absorption event on Bi atoms, whereby the fission of Bi induces damage during proton irradiation. The damage left in the wake of these fission fragments is characterized by many crossings, such as might provide stabilization of an entangled ground state, similar to the case of splayed columnar defects. This type of damage has been shown to raise the irreversibility line in $Bi_2Sr_2CaCu_2O_8$.[33] Precipitate pinning has proven more effective in YBCO (such as by a fine distribution of 211[34,35] or CuO[36] inclusions) than in BSCCO,[37,38] where increases in the critical current have been achieved in lower temperature regimes only. Surface or interfacial barriers have been shown[39] to contribute to the irreversible magnetization in YBCO at high temperatures where defect pinning is no longer effective. This mechanism has been suggested to account for high critical currents in YBCO thin films.[40]

6.3 Present Day Context of This Thesis

6.3.1 New Directions in Irradiation Efforts

Because of the success in significantly raising critical currents with the introduction of columnar defects, irradiation experiments were refocused on this method, and efforts in neutron and ion irradiations in the MeV range, such as presented in this thesis, were significantly curtailed. In addition to the impressive increases in the critical current obtained, it was also recognized that the greatly simplified character of the defect structure lent itself to more tractable analysis of experimental results. The Bose glass predictions are one such example of the analytical opportunities. In addition, the linear nature of the defects offered advantages in relation to probing anisotropy with respect to both field direction and crystal structure. By comparison, the types of damage induced by lower energy methods were of a far more complex variety, which would require exhaustive characterization, as detailed in a 1992 review by Kirk and Weber,[41] in order to quantitatively interpret data of irradiation induced changes. Therefore, the present day context of this thesis is presented not in terms of subsequent work in similar types of irradiation, but rather with respect to the very fast heavy ion irradiations and what has been deduced from them about vortex behavior in BSCCO. Although these defect structures are very different from those expected from MeV ion irradiation, it is nonetheless instructive and interesting to

compare our results of increased critical currents to later results of the measured J_c's in BSCCO crystals with columnar defects.

6.3.2 Improvements to the Critical Current: MeV vs. GeV

Shown in Figure 6.2 are results of the temperature dependence of the magnetization critical current before and after the introduction of columnar defects into single crystal $Bi_2Sr_2CaCu_2O_8$. Fig. 6.2a is the low field (0.1 T) result of Klein et al.[9] (5.8 GeV Pb^+, B_Φ=2 T) and Fig. 6.2b is the result at 1 T from Thompson et al.[8] (0.58 GeV Sn^+, B_Φ=5 T). Plotted on the same graphs for comparison are our results before and after irradiation by 2 x 10^{12} Ne^+/cm^2 at 3.1 MeV and 6 x 10^{11} Ar^+/cm^2 at 2.5 MeV. All fields are applied parallel to the c-axis and, in the columnar case, also parallel to the columns. Note that our low field results were obtained at 0.05 T rather than 0.1 T, and that critical currents below 10^4 A/cm^2 were not measurable by our VSM. Taking these differences into account, it is immediately evident not only that the as-grown samples are comparable but that at low temperatures the improvements resulting from these very different irradiations are quite similar. However, at 30 K and 1 T our highest J_c is 3.4 x 10^4 A/cm^2 as opposed to approximately 10^6 A/cm^2 in the columnar samples. Clearly, at higher temperatures vastly superior increases in critical currents result from columnar defects (notably so above 25 K - 30 K at low field and above 20 K at 1 T). This can be explained in a number of ways. In terms of activation energies, if columnar defects pin longer vortex segments than the defects in our samples, then the activation volume and therefore the activation energy would be larger, effecting far greater improvements at high temperature. This explanation would require significant coupling between layers. In view of this, both the calculation of Gerhauser et al.[7] (that the correlation length along the vortices is equal to the separation between CuO_2 planes) and the lack of unidirectional pinning reported by Thompson et al.[8] are perplexing. While it is certainly not suggested that vortices are confined along lengths approaching sample dimensions, if these greatly improved critical currents result from increased longitudinal correlation lengths, one would expect some directional pinning such as was observed by Klein et al.[9] In any event, intrinsic bulk pinning is clearly negligible compared to columnar pinning, with pinning by our (probably) cluster-type defects falling inbetween. This suggests that vortices have at least some

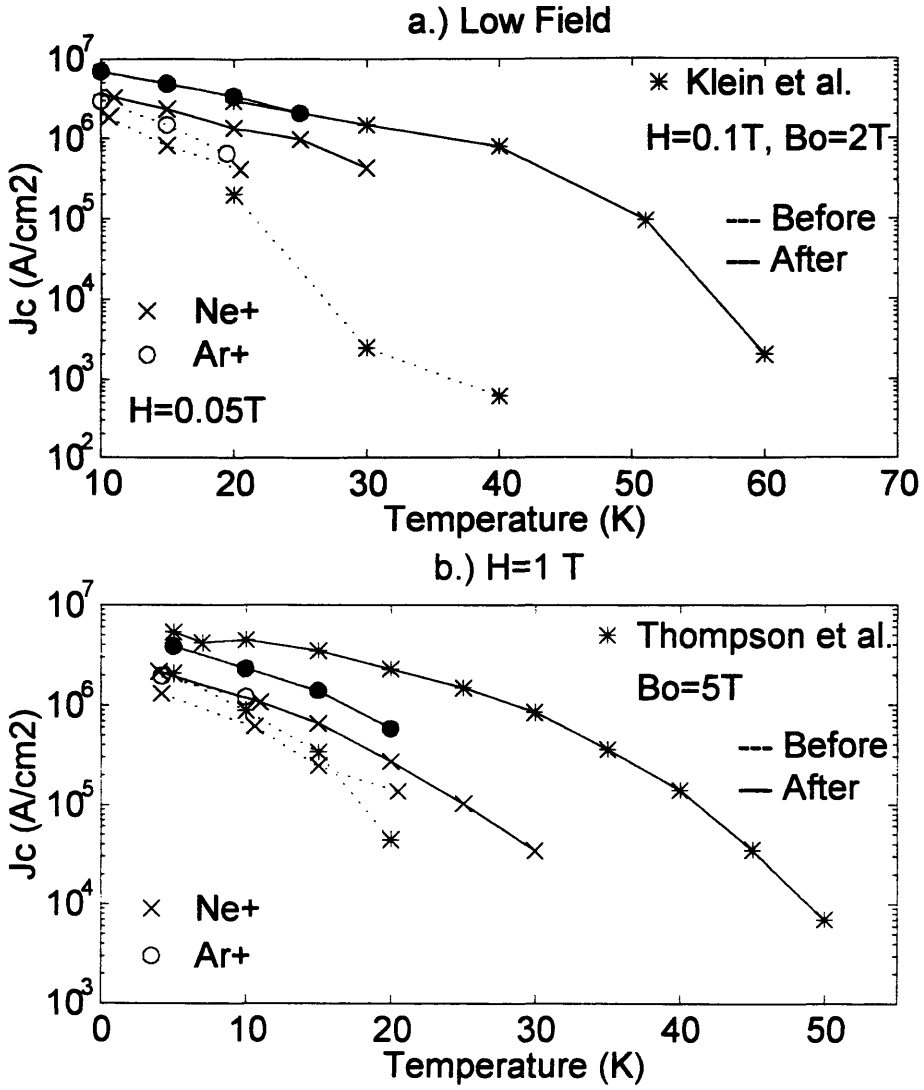

Figure 6-2: $Bi_2Sr_2CaCu_2O_8$ crystals before and after the introduction of columnar defects by fast (GeV) heavy ions plotted on the same graph with samples of this thesis before and after Ne^- and Ar^- irradiations in the MeV range. a.) low field (Klein et al.[9]). b.) H = 1 T (Thompson et al.[8]). Note that the ion fluences for columnar damage are expressed according to an established convention, using the dose equivalent field parameter, $B_\Phi = 2\Phi_0/\sqrt{3}a^2$, where a is the average distance between columns. In this manner the areal column density is treated as though it were the equivalent areal vortex density.

line nature (coupling) in these samples.

There are many unanswered questions concerning the decoupling of vortices. The criterion of decoupling by superentanglement is that for strong enough thermal fluctuations, the interplanar coupling is overcome at a given field for which the vortex segment between adjacent planes wanders a sideways distance exceeding the average intervortex spacing. This implies that coupling is destroyed at high enough fields and temperatures, below which the vortices are three dimensional. Klein et al.,[9] on the other hand found evidence (unidirectional pinning) for increased Josephson coupling as a function of increasing temperature, complicating the issue of exactly what conditions decouple the vortices. It should be pointed out that coupling is likely to be influenced by the defect structure itself, especially if it perturbs the anisotropy by way of a local destruction of the planar structure. Recently it was reported that the interlayer coupling is significantly enhanced by the presence of columnar pins even at fields above the matching field.[27] The melting transition may be similarly shifted by the presence of defects. In the next section we discuss how the results of Fig. 6.2 could alternatively be explained as an upward shift of the melting line.

6.3.3 Induced Defects and Melting

In the absence of a comprehensive theory of three dimensional vortex melting, the melting line is usually determined by the Lindemann criterion for thermal fluctuations, $<r^2> \approx c_L^2 a_0^2$. In a lattice of rigid lines the melting temperature is related to the lattice stiffness constant, k. In strongly layered superconductors, however, vortex lines may also tilt. Nelson[13] has used a "cage" model (classical Einstein model of phonons in an atomic box) to describe flexible line melting, in which $<r^2>=kT/\sqrt{gk}$ and therefore the melting temperature, $T_m \propto \sqrt{gk}$, where g is the local tilt modulus. It is easy to imagine how the presence of columnar defects would inhibit tilting and therefore melting for fields aligned or nearly aligned with the columns. In the extreme case of line vortices (YBCO-like) at low temperatures, vortices become completely localized on the columnar pins, leading to the replacement of the vortex glass by a Bose glass. At higher temperatures, even for a weakly coupled line, the force exerted by a longitudinal pin

would increase the distance necessary to travel along the field direction before thermal excursions are sufficient to satisfy the melting criterion (effectively increasing the tilt modulus). For weakly coupled BSCCO-like vortices, the excitations which mediate melting and/or depinning are more complex and speculative than in YBCO, including tilt, decoupling or a step-wise kinking process. Yet it seems plausible that any one or all of these processes would be inhibited by a longitudinal pinning structure oriented along the field, resulting in an upward shift of the melting line. For that matter the defect clusters in our heavy ion irradiated sample could have this effect on a diminished scale. These processes are still under avid investigation and are not well understood at this time. For example, Zech et al.[11] recently investigated the irreversibility line in single crystal BSCCO as shifted by irradiation induced columnar pins. They found the shifted line to be more consistent with a transition between the single vortex pinning regime and the collective weak pinning regime than with a shifted melting line.

In terms of depinning, one additional consideration that has been overlooked regarding improvements in our MeV heavier ion-irradiated samples is the concept of thermal depinning. The relatively random low density blob-like damage in these samples would retard the gradual process of thermal depinning of vortices as it would require a larger amplitude of thermal fluctuations to effect a smoothing of the pinning potential.

6.3.4 Thermally Activated Flux Creep, Vortex Melting and Collective Pinning

At the time we conducted our irradiation experiments, vortex melting and thermally activated flux creep were considered to be competing models of the irreversibility line, as described in Chapter 3. Today, arguments are more generally over where in the phase diagram the great variety of possible phases reside, which pinning mechanisms prevail there, and the thermodynamic nature of the transitions between them. As mentioned in Chapter 3, results of Gammel et al.'s[21] vibrating reed measurements implied a melting transition in single crystal BSCCO (assumed to be from a vortex glass) around 30 K. Notably, Zeldov[18] recently found direct evidence in BSCCO for a first order melting transition, specifically, a discontinuity in the local

magnetic induction (vortex density), at a temperature of 43.25 K for a local field in the several hundred gauss range. This suggests that the liquid freezes to an ordered lattice in a clean sample. It is worth pointing out by comparison that the in-field thermally activated resistance at that temperature and field is far below measurement thresholds. This may be clearly seen in Figures 5.3 and 5.4 of this thesis, which show the Arrhenius plot of the resistive transition at a field of 500 Gauss. This would seem to suggest that as the temperature is lowered, the resistivity falls below measurement thresholds long before the elastic properties of the lattice are detectable. (In our samples this occurred between 60 K - 70 K at 500 G). Therefore we measure the low resistance portion of the in-field transition totally in the thermally activated flux creep regime. This would explain why we did not observe any evidence of freezing in current-voltage measurements, as was found by Koch[22] in YBCO.

Furthermore, models of the vortex glass transition were based upon collective pinning, which was generally accepted to be the case in YBCO, but of which we found no evidence in our samples. In fact we found our results to be consistent with the single-vortex strong pinning limit, as was implied by the temperature independence of the matching field, as shown in Figs. 5.13 and 5.14. We may speculate on these differences between observations in YBCO and BSCCO in the following terms. At low enough fields and temperatures is a regime in which the vortices are pinned individually (small thermal fluctuations, large intervortex distances). Above the temperature at which a single vortex depins, the pinning of vortices must involve flux bundles, i.e. a collective pinning regime is entered and the interaction between vortices is relevant. At still higher temperatures, thermal fluctuations overcome intervortex forces and the lattice melts. The regime of single vortex pinning cannot by definition touch the melting line and the collective pinning regime must lie inbetween. As previously stated, our low field transport measurements of BSCCO appear to lie completely in the thermally activated pinned liquid phase. Yet, if melting occurs at low field at 43 K (as measured by Zeldov[18]) then our measurements of the magnetization J_c, all of which were conducted at temperatures below 30 K, would lie below the melting line and could lie below the collective pinning regime as well. (The effect of irradiation, if any, would be to shift the melting line further upwards.) To summarize, we suggest that our low field transport measurements were conducted above the melting temperature and

our magnetization measurements were conducted below the melting temperature, in the single vortex strong pinning regime. Hence we saw no evidence of melting.

Our high field transport measurements, on the other hand, would probably have probed the solid regime, particularly in the very low temperature, high current portions of the I-V curves. (In the measurement of the resistive transition, currents are too low to detect voltage at temperatures below approximately 30 K) This would be consistent with the observations in some examples of more threshold-like behavior in this regime. Finally note that in any analysis of the high field behavior of these samples, that the non-linearity of the Arrhenius plots at 5 T in the thermally activated regime must be considered.

6.3.5 Matching Effects

In the preceding section we suggested that our magnetization measurements were conducted below the melting line. We now consider the question of decoupling. From Figure 6.1a, B_{2D} defines the decoupling field, which is calculated in BSCCO to be approximately 1 T. The two-dimensional (vertical) melting line is asymptotic to the three dimensional curve and is placed at about 25 K for the strongly layered superconductors. Below approximately 25 K, then, except for the reentrant low field liquid phase, the lattice is in either a 3D or 2D frozen state, depending upon the field. Since our highest measurement field for the magnetization J_c was 1 T, the three dimensional frozen lattice phase is more likely, although the case has been made for decoupling in this regime.[7,8] Referring again to Figure 5.13 (matching effect) recall that for an increase in the field of a factor of twenty (from 0.05 T to 1 T), the peak moves from 1.2 x 10^{12} Ar^-/cm^2 to 2.4 x 10^{12} Ar^-/cm^2, that is, double the fluence. While we hesitate to draw conclusions in the absence of TEM results of the actual defect density, an increase in the pinning efficiency at higher field is suggested, which would be difficult to account for with a decoupling transition. Involvement of the reentrant liquid phase is possible at H=0.05 T ($H \approx 2H_{c1}$) and might explain a lower pinning efficiency at low field, but is rather unlikely because this phase occupies only a narrow field region above H_{c1}. Thus the strongest possibility by far is that the magnetization J_c's were measured in the 3D vortex lattice phase. This explains why we could observe a well

behaved classical matching effect such as is reported for conventional superconductors.

6.3.6 Current-Voltage Results

The current-voltage characteristics in BSCCO are still not quantitatively understood at this time. Neither is the precise underlying structure of the static and dynamic phase diagrams sufficiently well determined to support detailed analysis. As previously mentioned it might be possible to more carefully probe regions in phase space where the melting transition is expected. Under most of the conditions probed in this thesis an appropriate model would have to incorporate the dynamics of the flux liquid. Along these lines, Kuncher et al.[42,43] have recently reported evidence of the unpinned liquid regime, i.e. true Stephen-Bardeen-like behavior, at very high dissipation levels using a novel pulse current technique (generating up to 10^9 W/cm^2). They found a flux flow resistivity that scales linearly with H_{c2} only at very high dissipation levels, but not at the lower dissipation levels of typical current-voltage measurements. Ohmic resistivities are observed (with different slopes) in both regimes but at low currents linearity is associated rather with thermally activated flux creep, i.e. a pinned liquid state.

With regard to the thermally unstable behavior that we observed in the I-V characteristics at very low temperature and high field, it is worth noting that flux jumps have been observed in large crystals of $Bi_2Sr_2CaCu_2O_8$[44] at 4.2 K and 10 K as well as in $La_{1-x}Sr_xCuO_4$.[45,46] Flux jumps are a thermodynamic instability which occurs in a magnetic field as a result of positive thermal feedback under conditions of low heat capacity. (Formation of a local hot spot reduces the critical current, allowing an increment of flux into the sample, and this dissipative flux motion produces more heat, etc.) It is likely that this phenomenon is related to the rapid voltage increases inconsistently observed while measuring the current-voltage characteristics in high fields at temperatures below 10 K.

6.3.7 Context of the Early Work on Anisotropy

The results reported in Chapter 2 are remarkably current today in the sense of identifying major issues in the high temperature superconductors which continue to be investigated. Clearly the main points, that we were not measuring the anisotropy of a classical H_{c2} phase boundary, and that the angular dependence was associated rather with anisotropic flux "flow" of an unprecedented magnitude, have had far reaching implications for HTC vortex behavior that have been discussed throughout this thesis. While our observations may be more correctly described in terms of flux creep, as opposed to flux flow, the association with the crystal structure of anisotropic flux motion as described in Fig 2.5 is still accurate. For fields applied perpendicular to the **c**-axis it is indeed true that the layered crystal structure inhibits the motion of flux normal to the a-b plane. This phenomenon is now referred to as "intrinsic pinning", in that it does not depend on the existence of any artificially introduced defects. Due to the very short coherence length, the insulating layers between the CuO_2 planes act as core pinning sites.* Furthermore, for fields applied at small angles with respect to the a-b plane it is energetically favorable for flux lines to align themselves to take advantage of the interplanar intrinsic pinning, and a kinked formation of vortices is favored over alignment with the applied field. This is known as a "lock-in" transition,[47] and is consistent with our observation that the shape of the field-induced resistive transition changes rapidly only when the field is within 10^o of the a-b planes.

6.3.8 Future Work

The consideration of further enhancement of flux pinning in the strongly layered HTSC materials is rather different in 1997 than it was in 1991. Six years ago, calculations of recoil energy spectra led in the direction of further microstructural characterization of MeV ion-irradiated samples, and the use of still heavier ionic species at higher incident energies, or alternatively, fast neutrons. Clearly, however, results of superior improvements to the critical current in samples with columnar defects induced by very heavy ions at GeV energies, as presented in section

*This also explains why grain boundary pinning in the thin film was not effective; in this case the coherence length is small compared to the thickness of the grain boundary walls.

6.3.2, have radically changed the landscape of future work.

At this time, the goal of obtaining higher critical currents at elevated temperature and field would be better served by further investigation of the detailed effects of columnar damage upon the static and dynamic phase diagrams. In particular, a more quantitative understanding of the increases in the longitudinal vortex correlation lengths, Josephson inter-layer coupling, and melting temperature in the presence of columnar damage is needed, especially in the more strongly anisotropic materials. Better interplanar coupling promises to lead to further upward shifts of the irreversibility line, perhaps even for very dilute columnar densities.[27]

Closely related to coupling issues in the strongly layered materials are the depinning mechanisms, which are not well understood at this time. However, the hypothesis of a mechanism of off-axis excitations of pancake vortex sections is consistent with the success of alternative defect structures such as splayed columnar defects[31] and crossing tracks of fission fragments.[33] The range of the lengths of coupled vortex sections are, however, not precisely known under various conditions of temperature, field and current. Techniques of intermediate energy (MeV $< E <<$ GeV) irradiations, such as neutron bombardment of samples doped with elements having large neutron scattering cross-sections,[32] seem to be largely unexplored, in favor of the known success of columnar damage. It would also be interesting to investigate relatively heavy (e.g. Xe^{+}) ion irradiation at several MeV or 10's of MeV in thin films of $Bi_2Sr_2CaCu_2O_8$, under conditions of complete penetration. The work of this thesis suggests that defect geometries that are shorter than columns but bigger than point defects result in pinning and critical currents which are inbetween those existing in as-grown material and samples with columnar defects. It would seem to be worth exploring an intermediate regime of defects that could effectively pin vortex sections over distance scales considerably shorter than the sample thickness but large compared to the interplanar spacing, and see if the columnar results can be approached using more accessible experimental tools.

In more theoretical terms, future challenges include not only the more precise determination of the phase diagrams, both with and without quenched disorder, but also an understanding of

how the phase diagrams of the different HTC cuprates are related. Another quickly developing area of theoretical study is vortex dynamics,[23,24] which promises to shed light in the future upon depinning mechanisms and also vortex behavior at higher applied currents. The incorporation of HTC phenomena such as vortex entanglement and decoupling into these models should prove to be very informative in modifying vortex dynamics at higher temperatures, fields and currents.

It is interesting to note in the consideration of future work to improve the flux pinning in strongly layered superconductors, that the concept of spatially extended defects is central to these efforts in the foreseeable future. As a final comment on the historical context of this thesis, the work presented here is one of the earliest demonstrations known to the author that induced defects of a spatially extended nature can raise the irreversibility line in $Bi_2Sr_2CaCu_2O_8$.

6.4 References

1. G. Blatter, M.V. Feigel'man, V.B. Geshkenbein, A.I. Larkin, and V.M. Vinokur, Rev. Mod. Phys. **66**, 1125 (1994), and references therein.

2. P.G. de Gennes, *Superconductivity of Metals and Alloys*, (Addison-Wesley, Reading, MA, 1986).

3. O. Pla and F. Nori, Phys. Rev. Lett. **67**, 919 (1991).

4. P. Bak, C. Tang, and K. Wiesenfeld, Phys. Rev. A **38**, 364 (1988).

5. V.M. Vinokur, M.V. Feigel'man, and V.B. Geshkenbein, Phys. Rev. Lett. **67**, 915 (1991).

6. L. Civale, A. D. Marwick, T. K. Worthington, M. A. Kirk, J.R. Thompson, L. Krusin-Elbaum, Y. Sun, J. R. Klem, and F. Holtzberg, Phys. Rev. Lett. **67**, 648 (1991).

7. W. Gerhauser, G. Ries, H.W. Neumuller, W. Schmidt, O. Eibl, G. Saemann-Ischenko, and S. Klaumunzer, Phys. Rev. Lett. **68**, 879 (1992).

8. J.R. Thompson, Y.R. Sun, H.R. Kerchner, V.K. Christen, B.C. Sales, B.C. Chakoumakos, A.D. Marwick, L. Civale, and J.O. Thomson, Appl. Phys. Lett. **60**, 2306 (1992).

9. L. Klein, E.R. Yacoby, Y. Yeshurun, M. Konczykowski, and K. Kishio, Phys. Rev. B **48**, 3523 (1993).

10. V. Hardy, D. Groult, J. Provost, M. Hervieu, and B. Raveau, Physica C **178**, 255 (1991).

11. D. Zech, S.L. Lee, H. Keller, G. Blatter, P.H. Kes, and T.W. Li, Phys. Rev. B **54**, 6129 (1996).

12. M.E. McHenry and R.A. Sutton, Prog. Mater. Sci. **38**, 159 (1994), and references therein.

13. G. W. Crabtree and D. R. Nelson, Physics Today, p. 38, April, 1997.

14. Y. Yeshurun, A. P. Malozemoff, and A. Shaulov, Rev. Mod. Phys. **68**, 911 (1996).

15. R. Griessen, J.G. Lensink, and H.G. Schnack, Physica C **185-189**, 337 (1991).

16. A.C. Mota, G. Juri, P. Visani, A. Pollini,T. Teruzzi, K.Aupke, and B. Hilti, Physica C **185-189**, 343 (1991).

17. D. Lopez, E.F. Righi, G. Nieva, F. de la Cruz, W.K. Kwok, J.A. Fendrich, G.W. Crabtree, and L. Paulius, Phys. Rev. B **53**, 8895 (1996); D. Lopez, E.F. Righi, G. Nieva, F. de la Cruz, Phys. Rev. Lett. **76**, 4034 (1996).

18. E. Zeldov, D. Majer, M. Konczykowski, V.B. Geshkenbein, V.M. Vinokur, Nature **375**, 373 (1995).

19. A. Schilling, R.A. Fisher, N.E. Phillips, U. Welp, D. Dasgupta, W.K. Kwok, and G.W. Crabtree, Nature **382**, 791 (1996).

20. M. P. A. Fisher, Phys. Rev. Lett., **62**, 1415 (1989).

21. P.L. Gammel, L.F. Schneemeyer, J.V. Waszczak, and D.J. Bishop, Phys. Rev. Lett. **61**, 1666 (1988).

22. R.H. Koch, V. Foglietti, W.J. Gallagher, G. Koren, A. Gupta, and M.P.A. Fisher, Phys. Rev. Lett., **63**, 1511 (1989).

23. F. Nori, Science **271**, 1373(1996); M.J. Higgins, S. Bhattacharya, Physica C **257**, 232 (1996).

24. A.E. Koshelev, V.M. Vinokur, Phys. Rev. Lett. **73**, 3580 (1994); T. Giamarchi, P. Le Doussal, Phys. Rev. Lett. **76**, 3408 (1996).

25. D.R. Nelson and V.M. Vinokur, Phys. Rev. Lett. **68**, 2398 (1992); Phys. Rev. B **48**, 13060 (1993).

26. L. Krusin-Elbaum, L. Civale, G. Blatter, A.D. Marwick, F. Holtzberg, and C. Feild, Phys. Rev. Lett. **72**, 1914 (1994).

27. T. Hanaguri, Y. Tsuchiya, S. Sakamoto, A. Maeda, and D.G. Steel, High T_c Update E-Mail Version, Vol. 11, No. 8, April 15, 1997, To be published in Phys. Rev. Lett. (1997).

28. T. Matsushita, M. Kiuchi, H. Yamato, T. Hirano, and N. Koshizuka, High T_c Update E-Mail Version, Vol. 11, No. 8, April 15, 1997, To be published in Physica C (in press, 1997).

29. D.R. Nelson and S. Seung, Phys. Rev. B **39**, 9153 (1989); M.C. Marchetti and D.R. Nelson, Physica C **174**, 40 (1991).

30. T. Hwa, P. Le Doussal, D.R. Nelson, and V.M. Vinokur, Phys. Rev. Lett. **71**, 3545 (1992).

31. W. K. Kwok, L. M. Paulius, V. M. Vinokur, A. M. Petrean, R. M. Ronningen, and G. W. Crabtree, High T_c Update E-Mail Version, Vol. 11, No. 8, April 15, 1997, Submitted to Phys. Rev. Lett. (1997).

32. J.O. Willis, K.E. Sickafus, and D.E. Peterson, *Advances in Superconductivity IV. Proc. 4th Int. Symp. Superconductivity*, Tokyo, 323 (1991).

33. L. Krusin-Elbaum, J.R. Thompson, R. Wheeler, A.D. Marwick, Appl. Phys. Lett. **64**, 3331 (1994); H. Safar, J.H. Cho, S. Fleshler, M.P. Maley, J.O. Willis, J.Y. Coulter, J.L. Ullmann, P.W. Lisowski, G.N. Riley Jr., M.W. Rupich, J.R. Thompson, and L. Krusin-Elbaum, Appl.

Phys. Lett. **67**,130 (1995).

34. M. Murakami, Mod. Phys. Lett. **4**, 163 (1990).

35. B. Ni, M. Kobayashi, K. Funaki, K. Yamafuji, and T. Matsushita, Jpn. J. Appl. Phys. **30**, L1861 (1991).

36. R. Ramesh, S. Jin, S. Nakahara, and T.H. Tiefel, Appl. Phys. Lett. **57**, 1458 (1990).

37. Y.M. Chiang, D.A. Rudman, D.K. Leung, J.A.S. Ikeda, A. Roshko, and B.D. Fabes, (unpublished data, 1988).

38. D.L. Shi, M.S. Boley, U. Welp, J.G. Chen, and Y. Liao, Phys. Rev. B **40**, 5255 (1989).

39. K.S. Harshavardan, M. Rajeswari, D.M. Hwang, C.Y. Chen, T. Sands, T. Venkatesan, J.E. Tkaczyk, K.W. Lay, A. Safari, Appl. Phys. Lett. **60**, 1902 (1992); M. Rajeswari, A.W. Smith, S.N. Mao, X.X. Xi, Physica B **194-196**, 2269 (1994).

40. M. McElfresh, T. Miller, D. Schaefer, R. Reifenberger, R.E. Munchausen, M. Hawley, S.R. Foltyn, and X.D. Wu, J. Appl. Phys. **71**, 5099 (1992).

41. M. A. Kirk and H. W. Weber, in *Studies of High Temperature Superconductors* (ed. Narlikar, A. V.), Vol. **10**, 253-315, (Nova Science Publishers, New York, 1992).

42. M.N. Kuncher, D.K. Christen, and J.M. Phillips, Phys. Rev. Lett. **70**, 998 (1993).

43. M.N. Kuncher, D.K. Christen, C.E. Klabunde, and J.M. Phillips, Phys. Rev. Lett. **72**, 752 (1994).

44. M. Guillot, J.L. Tholence, O. Laborde, M. Patel, P. Gougeon, H. Noel, and J.C. Levet, Physica C **162-164**, 361 (1989).

45. A. Gerber, J.N. Li, Z.Z. Tarnawski, J.J.M. Franse, and A.A. Menovsky, Phys. Rev. B **49**, 6047 (1993).

46. M.E. McHenry, H.S. Lessure, M.P. Maley, J.Y. Coulter, I. Tanaka, and H. Kojima, Physica C **190**, 403 (1992).

47. D. Feinberg and C. Villard, Phys. Rev. Lett. **65**, 919 (1993).

Appendix A

Neutron and Proton Irradiation

The success of fast neutron irradiation is interesting to compare with later results of the calculated primary recoil spectrum in YBCO.[1] First let us review that unlike ion irradiation, the primary recoils are governed by nearly isotropic nuclear scattering (primarily elastic), hard-sphere like with all recoil energies equally probable up to the maximum. For fission neutrons a high fraction of recoil events occur at very high energies (half of them are above 1 KeV). At the opposite extreme are electrons which, for a typical energy of 1 MeV, have a recoil distribution with virtually all events well below 100 eV. Between the primary recoil distributions for MeV electrons and fission neutrons lie all the distributions for the various ion irradiation conditions.

The scattering cross section for ions in solids can generally be described as Rutherford-like in a screened Coulomb potential. One result of this type of scattering is that the low energy recoils are dominant. High energy events (above several KeV) are relatively rare. In the irradiation of conventional superconductors it was often convenient to try to simulate damage from a particular portion of the fast neutron recoil spectrum by introducing ions incident at that energy, and examining the induced microstructure within several mean free paths of the surface. While this had the disadvantage of also introducing the low energy portion of the ion's primary recoil spectrum and the resultant damage caused by a high fraction of low energy recoils, ion beams were considerably more convenient, available and easy to monitor.

[1] Private Communication, 1991 and M. A. Kirk and H. W. Weber, in *Studies of High Temperature Superconductors* (ed. Narlikar, A. V.), Vol. **10**, 253-315, (Nova Science Publishers, New York, 1992)

At first glance the striking success of neutron irradiation would seem to suggest that it was the high energy events, so much more probable in neutron spectra, that produced the pinning centers. This conclusion turns out to be too simplistic in light of the results of proton irradiation discussed in section 3.3.5. While the neutron spectra are weighted towards the high energy events, fully half of all events occur below 1 KeV, and the fluences necessary to achieve enhancements of J_c similar to those produced by proton irradiation are about an order of magnitude higher (10^{17} neutrons/cm^2 neutrons vs. 10^{16} protons/cm^2). This higher neutron fluence would increase the density of low energy recoils relative to those produced by the smaller proton doses used. Another indication of the significance of these lower energy recoils in both types of irradiation is the role they play in the depression of T_c, associated with the displacement or disordering of oxygen. Doses of 10^{16}/cm^2 protons and 10^{17}/cm^2 neutrons result in T_c depressions of 1 K and 0.5 K respectively. The depression of T_c in YBCO does show a trend, for light ion irradiation, of scaling linearly with numbers of induced displacements.[2] Therefore, a factor of 2 difference in the depression of T_c indicates, in the rough estimate, comparable numbers of these smaller defects for both the neutron and proton cases. So, while some influence of the higher energy recoils is likely, especially in the neutron case, it seems that in both cases the more significant role in the enhancement of the J_c in YBCO is played by point defects which result from the low energy recoil events.

[2] G.P. Summers, E.A. Burke, D.B. Chrisey, M.Nastasi, and J.R. Tesmer, Appl. Phys. Lett. **55**, 1469 (1989).

Appendix B

Sample Heating After He^+ Irradiation

Before irradiation, contact resistances of all samples were in the range 2 Ω - 20 Ω. While all other samples remained in this range over the course of the measurements, the resistance after helium irradiation of sample J38 was, at the time of the last Arrhenius measurement, in excess of 400 Ω, and approximately tripled overnight prior to most of the current-voltage measurements. Due to the resultant heating of this sample, the I-V data after irradiation were generally limited to currents below 1 mA. The criterion established for gathering "good" data at higher currents was that the measured sample temperature not rise by more than 0.1 K during the measurement, at which point the ramped current input was manually aborted.

It was not possible to alleviate this heating problem by using the pulse technique, due to an experimental artifact observed during measurement of this sample even before irradiation. It was later found that this artifact, which was an irregularity in the transient response of the sample to pulse input, was most probably also associated with the contacts. (However, there was no initial indication that the contact resistance might worsen as it did.) More specifically, the shapes of the sample voltage and current pulses, as monitored on the oscilloscope (refer to Fig. 1.1, the block diagram of the pulse I-V measurement) for this sample were not square. Instead of the typically observed square wave pulse shapes, there appeared to be a lag (decay)

in the rise and fall of the current accompanied by a spike in the voltage, consistent with a large ($\approx 10^{-4}$ henries) inductance in series with the sample. This transient response to the pulse was further investigated and was found to persist in the normal state, thereby ruling out the possibility that these effects were associated with superconducting phenomena. The contact resistance appeared to be only slightly erratic prior to irradiation, but repair work on the contacts did result in changes in the size of the bump in the transient voltage response. While these changes did not follow any predictable pattern or correlate to the contact resistance, they suggest an association of some kind between the contact quality and the observed artifact. It would have been possible to adjust the pulse length and the window of the boxcar to exclude the transient response, but as the origin of the effect was not well understood, it seemed preferable to avoid the pulse measurement altogether and proceed with dc measurements instead.

There was an additional reason to switch to a dc measurement, which was the appearance of a rolling baseline in the current-voltage characteristic. A negative voltage response was observed for currents as high as ten or twenty milliamps (worst case, before irradiation) which then increased to positive voltages, i.e. exhibited typical behavior at higher currents. It was necessary to check whether this effect would be reproducible using the simple dc measurement. In fact, it was reproducible, and was therefore considered to be "real", possibly the effect of current redistribution around "hotspots" caused by regions of poor contact quality. Critical currents were accordingly based in these cases upon negative voltages corresponding to the electric field criterion of -1μV/mm, and these are plotted in Fig. 5.7b, the temperature dependence of the critical current.

Shown in Figure B.1 are the detailed current-voltage characteristics of the sample before and after irradiation by 6.4 x 10^{14} He^{-}/cm^{2} . The pre-irradiated results at H=0, 0.05 T, and 5 T are plotted in Figs. B.1a - B.1c respectively. Because the measurements after irradiation were restricted by heating to very low currents (< 1 mA in most cases), the post-irradiated results are plotted separately on a smaller current scale ($\div 10$) in Figs. B.1d - B.1f. As in the case of H^{-} irradiation, T_c degradation dominates the I-V characteristics in the high temperature regime. There is perhaps some hint of very slightly suppressed voltages after irradiation

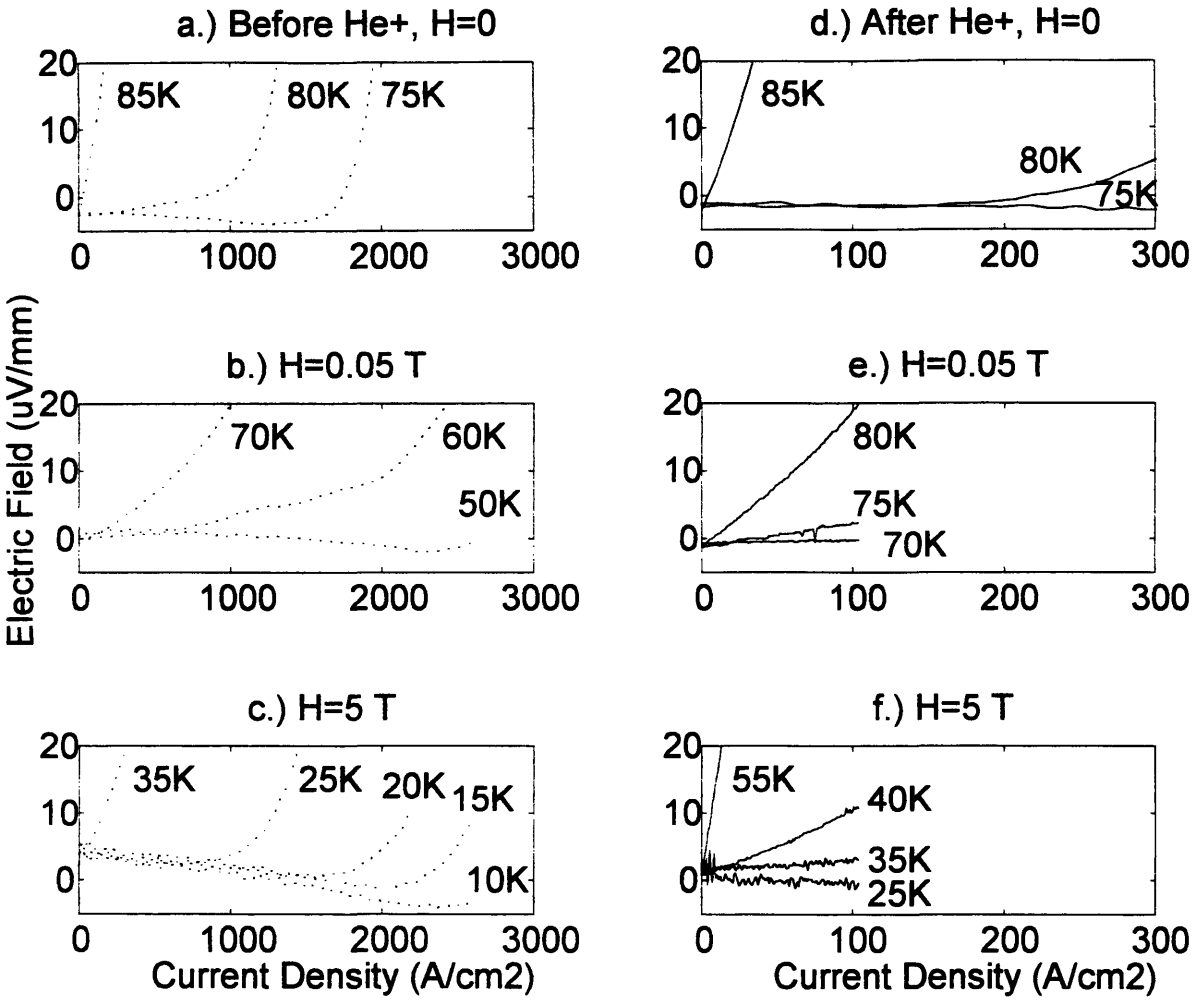

Figure B-1: Electric field vs. current density (dc measurement) before irradiation at a.) H=0 b.) H=0.05 T c.) H=5 T, and after irradiation with He^+ at d.) H=0 e.) H=0.05 T and f.) H=5 T. Note that $I \approx J \cdot 10^{-5}$ cm^2 and $V \approx E \cdot 1$ mm.

around 70 K at low field and 35 K at high field, as was reflected in the critical current results presented in Fig. 5.7b. It was, however, impossible to further explore these (slight) changes in lower temperature regimes because the measurements would have required the use of higher applied currents. Even for currents below 1 mA, the rise in the sample temperature during the current ramp was approaching 0.1 K. For higher currents, the sample temperature could not have been accurately specified or maintained over the course of the measurement, and would likely have eventually burned out the contacts. At the lower currents measured, however, there is no evidence of major changes to the sample after He^- irradiation.

It is interesting to speculate that if current redistribution caused by poor contact quality were responsible for the initial negative dc voltage response, then perhaps a convoluted current path within the sample could also account for the apparent inductance observed in the transient response. There was no external physical evidence as obvious as a loop of wire to account for the inductance, yet within the sample itself, given the known dimensions (0.126 cm x 0.048 cm x 0.0002 cm), it would require a complicated path indeed to give rise to an inductance as large as 10^{-4} henries. For comparison, a few turns of wire wound in a coil of cross sectional area, A = 1 cm has an inductance on the order of a few microhenries. This artifact cannot therefore be readily explained in this manner.

While the issues of high contact resistance, the anomalous transient response and the negative slope of the baseline might still quite easily all have been related, the important point is that these considerations do not change the overall picture of the results. In addition to the results of the I-V characteristics at low currents, the lack of enhanced pinning is indicated by the relatively minor increase in the activation energy after irradiation (also measured at low current and before the tripling of the contact resistance). Also consistent is the post-irradiated result of the magnetization critical current. Specifically, the magnetization J_c of the He^+ irradiated sample did not have a temperature dependence different from that of a typical unirradiated sample, as was discussed in Section 5.5 and shown in Fig. 5.11. This indicates that the heating problem in the transport measurement was not masking significant improvements in the critical current.

Coincidentally, this sample had lower critical currents relative to the other samples even before irradiation, in part reflecting the high normal state resistivity ($\rho_n(95K) = 87\ \mu\Omega$-cm), which was approximately five times greater than that of the H^+ sample before irradiation ($\rho_n(95K) = 18\ \mu\Omega$-cm). In any event, neither the He^+ nor the H^+ sample show significant improvement in the critical current or the pinning energy after irradiation. In contrast, the results of the Ne^+ and Ar^+ irradiated samples unambiguously show enhancement of the critical current for all fields and temperatures as well as significantly higher pinning energies. Whatever speculations one makes about the experimental difficulties, these conclusions remain the same.

Appendix C

Related Publications

The journal articles and conference presentations associated with this thesis are listed below, and are reproduced as appropriate in the following pages of this appendix.

- J. A. Cutro, D. A. Rudman, T. P. Orlando, R. B. van Dover, L. F. Schneemeyer, A. E. White, E. M. Gyorgy, J. V. Waszczak, and R. J. Felder, "Increased Pinning Energies and Critical Current Densities in Heavy-Ion-Irradiated $Bi_2Sr_2CaCu_2O_8$ Single Crystals", Appl. Phys. Lett. **62**, 759 (1993).

- J. A. Cutro, R. B. van Dover, L. F. Schneemeyer, A. E. White, T. P. Orlando, and D. A. Rudman, "Modification of the Flux Pinning in Single Crystal $Bi_{2.2}Sr_2Ca_{0.8}Cu_2O_{8+\delta}$ by Irradiation with Various Ions", *Mater. Res. Soc., Fall Meeting*, Boston, December 2-6, 1991, Session A12.4/H10.4.

- J. Y. Juang, J. A. Cutro, D. A. Rudman, R. B. van Dover, L. F. Schneemeyer, and J. V. Waszczak, "Angular Dependence of the Magnetic-Field-Induced Resistive Transition in Single Crystal $Bi_{2.2}Sr_2Ca_{0.8}Cu_2O_{8+\delta}$", Phys. Rev B **38**, 7045, (1988).

- J. A. Cutro, J. Y. Juang, D. A. Rudman, R. B. van Dover, L. F. Schneemeyer, and J. V. Waszczak, *Mater. Res. Soc., Fall Meeting*, Boston, Nov. 28-Dec. 2, 1988, Session F6.5.

- J. A. Cutro, J. Y. Juang, and D. A. Rudman, "Angular Dependence of the Current-Voltage Characteristics of Single Crystal $Bi_{2.2}Sr_2Ca_{0.8}Cu_2O_{8+\delta}$ in a Magnetic Field", *Int. Conf. on Critical Currents in High-T_c Superconductors*, Snowmass, Colorado, August 16-19, 1988.

Increased pinning energies and critical current densities in heavy-ion-irradiated $Bi_2Sr_2CaCu_2O_8$ single crystals

J. A. Cutro,[a] D. A. Rudman,[b] and T. P. Orlando
Massachusetts Institute of Technology, Cambridge, Massachusetts 02139

R. B. van Dover, L. F. Schneemeyer, A. E. White, E. M. Gyorgy, J. V. Waszczak, and R. J. Felder
AT&T Bell Laboratories, Murray Hill, New Jersey 07974

(Received 10 December 1991; accepted for publication 8 April 1992)

We report a significant increase in the pinning energy of vortices in single-crystal $Bi_2Sr_2CaCu_2O_8$ when irradiated with heavy ions such as Ar^+. This is in contrast with the results of light ion (H^+, He^+) irradiations which give pinning energies comparable with those of unirradiated crystals. The stronger pinning is attributed to defects larger than point defects, e.g., clusters or amorphized regions. As a result of higher pinning energies, critical currents persist at markedly higher temperatures and fields.

It is widely recognized[1] that the critical current of the 85 K superconductor $Bi_2Sr_2CaCu_2O_8$ is generally insignificant at temperatures above 20 K and fields greater than a few hundreths of a tesla. This is important because $Bi_2Sr_2CaCu_2O_8$ is unique among the high-temperature superconducting cuprates in its ready fabrication in the form of long wires that support high current densities at 4 K.[2,3] Studies of the temperature and field sensitivity in single crystal $Bi_2Sr_2CaCu_2O_8$ indicate that these limitations reflect the extremely weak intrinsic flux pinning in this material.[4,5] Introduction of defects by light ion irradiation has produced small increases in pinning energies which suggests[6] that the physics of pinning in this material is dominated by the high anisotropy of $Bi_2Sr_2CaCu_2O_8$ leading to a small correlation length along the vortex axis (i.e., pancake vortices).[7] To overcome this materials limitation we have examined the generation of defect structures other than point defects to act as pinning centers. This approach parallels recent efforts using fast neutron irradiation[8-10] and extremely high energy ion irradiation[11,12] (at fractions of GeV), which produced shifts in the irreversibility line, but up until now no data exist on heavy ion irradiation in the MeV energy range.

We report results on the resistive transition and both transport and magnetization J_c of single-crystal samples measured before and after irradiation by H^+, He^+, Ne^+, and Ar^+. The crystals were sufficiently thin as to assure nearly complete penetration of the ions through the sample. The irradiation conditions were chosen to hold the total vacancy production by each ionic species approximately constant, in order to more clearly resolve the effects on flux pinning of the different types of defects introduced by various ions. Higher ion masses lead to increased pinning energies and critical current densities, suggesting that the damage cascades induced by the heavier ions result in more effective pinning centers than the point defects likely to be created by the lighter ions.

Single-crystal[13] samples of $Bi_2Sr_2CaCu_2O_8$ were measured by dc and pulsed dc transport techniques and a vibrating sample magnetometer ($H \| \hat{c}$). Critical currents were inferred using the critical state model with appropriate geometrical corrections.[14] Damage profiles were calculated by the program TRIM[15] according to a Kinchin–Pease model of vacancy production and fluences and energies of He^+, Ne^+, and Ar^+ were selected to approximately match the density of vacancies produced by 1×10^{16} cm^{-2} H^+ at 2 MeV, (about 5×10^{19} vacancies cm^{-3}). With energies in this range, damage can be expected to vary from point defects to clusters or amorphized regions of various sizes, but should not result in the long straight columnar damage tracks observed at very high energies.[16] The appropriate doses for the other ions were determined to be 6.4×10^{14} cm^{-2} He^+, 2×10^{12} cm^{-2} Ne^+ and 6×10^{11} cm^{-2} Ar^+.

Figure 1 shows an Arrhenius plot of the resistive transition at 0.05 T before and after irradiation by H^+ and Ar^+. The resistance has been normalized to R_{n0}, the resistance at 93 K before irradiation. The calculation of activation energies, determined by drawing the best line through the linear section of the data, provides a useful means of comparing the relative pinning energies before and after irradiation. In the as-grown crystals at 0.05 T these energies are roughly within ± 10% of 1500 K. After irradiation with Ar^+, the activation energy increases by a factor of 2.3, as compared to only 1.4 for H^+. Thus, higher pinning energies result from the heavier ion irradiations. Results obtained for He^+ and Ne^+ (factors of 1.40 and 1.55, respectively) support this interpretation and are consistent with results reported for He^+ irradiation of $Bi_2Sr_2CaCu_2O_8$ by Palstra *et al.*[6] Interestingly, the effects of vacancy-equivalent doses of light versus heavy ions also differ with respect to T_c degradation which is greater by a factor of four for H^+ and He^+, ($\Delta T_c \approx 2.3$ K) than for Ne^+ and Ar^+ ($\Delta T_c \approx 0.5$ K). This effect is noticeable in Fig. 1 in that the temperature at which the postirradiated resistance falls below that of the as-grown crystal is considerably higher for Ar^+ than for H^+. Whatever the exact nature of the induced defects, an attractive explanation for both of these trends is that heavier ions produce, in addition to small or point defects, significant numbers of large

[a] Present address: IBM, Yorktown Heights, NY 10536.
[b] Present address: Nat. Inst. Sci. Tech., Boulder, CO 80303.

 0003-6951/93/070759-03$06.00

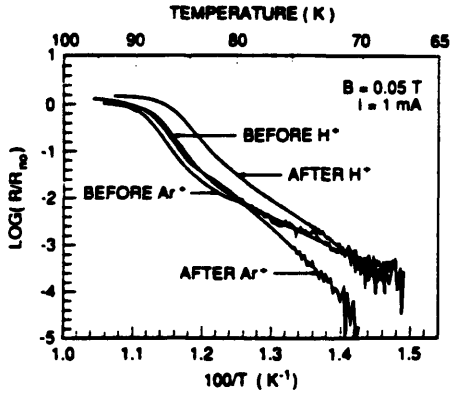

FIG. 1. Arrhenius plot of the electrical resistivity of a $Bi_2Sr_2CaCu_2O_8$ single crystal at $H=0.05$ T before and after irradiation with H^+ and Ar^+ ions. Curves are normalized to $R(93\ K)$. The marked suppression of the resistive tail resulting from Ar^+ irradiation is attributed to an increased pinning energy.

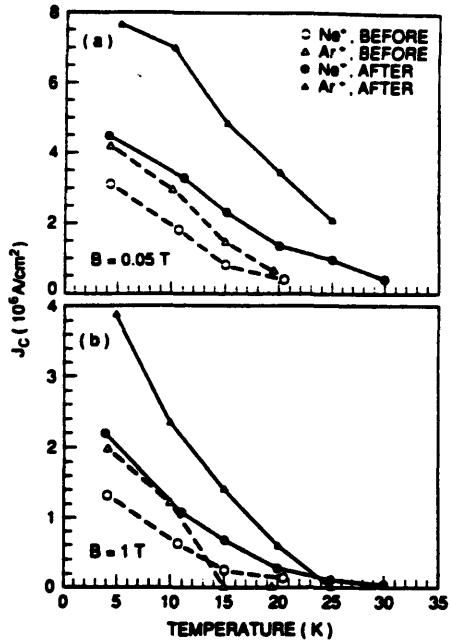

FIG. 2. Temperature dependence of the magnetization J_c of $Bi_2Sr_2CaCu_2O_8$ at $H=1$ T before and after irradiation with Ne^+ and Ar^+ ions. The characteristic temperature at which the critical current diminishes to zero is strongly increased by heavy-ion irradiation.

or clustered defects resulting from damage cascades of high energy recoils of primary knockon atoms.[17] In contrast, the dominance of low energy recoils in light ion bombardment is more likely to result in a predominance of point defects, as was inferred for $Ba_2YCu_3O_7$.[18] Spatially extended defects would interact with longer segments of the vortices, resulting in the observed higher pinning energies. In the most simplistic approximation, clusters would also be less destructive to the superconductivity than an equivalent number of point vacancies randomly distributed, thus explaining the relatively smaller reduction in T_c. Finally, the trends are qualitatively similar at high fields, although nonlinearity of the Arrhenius plot makes the determination of activation energies less meaningful.

Figure 2 shows the temperature dependence of J_c, inferred from magnetization, before and after irradiation by Ne^+ and Ar^+ at a field of 1 T. There is marked improvement in both samples with generally better results occurring for Ar^+. Similar results were obtained at an applied field of 0.05 T. At low temperature and field the apparent improvements in J_c are on the order of factors of two, but more impressive is the decreasd sensitivity of J_c to elevated temperature and field. Before irradiation, J_c of a typical sample is immeasurably small at 1 T ($<10^4$ A cm^{-2}) above roughly 15 K, but after Ar^+ irradiation, the critical current at 20 K is nearly 10^6 A cm^{-2} and only approaches zero near 30 K. Similarly, the J_c of the Ne^+ irradiated sample is above 10^4 A cm^{-2} at 30 K after irradiation. These results are consistent with the observation of increased pinning energies in the Arrhenius plots of activated resistivity. Results on H^+ and He^+ irradiated samples show essentially no change in the temperature at which J_c diminishes to zero, an indication that the pinning energy has not changed significantly. This is again consistent with the behavior of the activated resistivity. Pre- and post-irradiated measurements of the transport J_c's indicated that improvements resulting from Ne^+ and Ar^+ irradiation are of the same order of magnitude as for the magnetization critical currents. For example, at 5 T and 20 K the critical current (based on a field criterion of 1 μV/mm) increased from 2.43×10^3 to 3.75×10^3 A cm^{-2} after irradiation with Ar^+. By comparison, J_c decreased after H^+ irradiation.

The dose dependence of the magnetization J_c for Ar^+ in the temperature range 6–28 K at fields of 0.05 and 1 T is shown in Figs. 3(a) and 3(b). For all temperatures, the maximum J_c at low field is obtained at a dose of 1.2×10^{12} Ar^+, while the maximum at the higher field is clearly obtained at twice that fluence at all temperatures (the anomalous peak at 17 K is attributed to experimental difficulties). The fact that J_c (or equivalently the pinning force density $F_p\equiv J_cB$) peaks at a field dependent but temperature independent fluence is a strong indication that this is associated with a classical "matching effect"[19] where the highest J_c is obtained at the field for which the average defect spacing is equal to the vortex spacing. In the samples which experienced the highest fluences, the critical current inevitably must decrease due to the fact that the superconducting order parameter in the region between defects will begin to diminish as the defect spacing approaches $\xi_{ab}(T)$. The overall transition temperature is found to be essentially unaffected below the peak in J_c, but at 4.8×10^{12} Ar^+, for example, T_c drops from 90 to 72 K as measured by low-field ac susceptibility.

A simple interpretation of the vacancy density produced by Ar^+ is not consistent with the observed peak

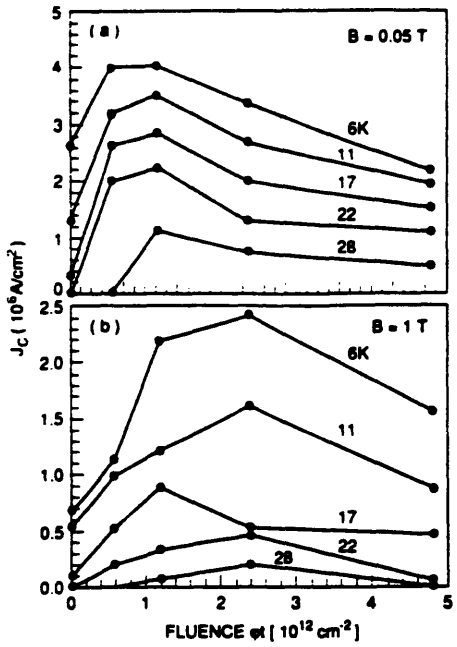

FIG. 3. (a) Ar^+ dose dependence of the magnetization J_c of $Bi_2Sr_2CaCu_2O_8$ at $H=0.05$ T for temperatures between 6 and 28 K showing matching effect at fluence of 1.2×10^{12} cm^{-2}. (b) The peak in J_c (ϕt) moves to higher fluence at $H=1$ T.

effect. The intervortex spacing is $a=1.075(\phi_0/B)^{1/2}$ which is $\simeq$48 nm at 1 T. TRIM calculations give a total vacancy density of 2×10^{20} cm^{-3} for a fluence of 2.4×10^{12} cm^{-2} or, if a random distribution is assumed, a defect separation of $(2\times10^{20})^{1/3}=1.7$ nm. We can hypothesize that it is mainly clustered or extended defects, resulting from a relatively small fraction of recoil events occurring at high energies, that contribute to the increase in the pinning, and that these are considerably further apart than the calculated vacancy spacing. More realistic calculations of defect density and size can be made, based on the recoil energy distributions for different ions[17] and are underway. While the model is appealing and accounts for the general trend we observe, quantitative agreement will require incorporating complications such as the range of cluster sizes produced and details of vortex interactions, vortex correlation lengths and possible cooperative phenomena. The effects we see for light ion irradiation are consistent with results reported by Palstra *et al.*,[6] that is, fluences up to 4×10^{14} cm^{-2} He^+ at 2 MeV on single crystals produced only modest improvements in the pinning energy. Extended defects can interact more strongly with vortices and lead to a higher pinning energy. Civale *et al.*, have produced columnar defects in $Ba_2YCu_3O_7$ by GeV Sn^+ irradiation which illustrate this effect.[16] It is most likely that our $\sim$3 MeV Ne^+ or Ar^+ irradiation of $Bi_2Sr_2CaCu_2O_8$ would produce cluster-type defects rather that columnar defects. HRTEM might resolve questions concerning the precise defect structure in our crystals; in any case we have shown that heavy ion irradiation does result in a significantly increased pinning energy and a peak effect which is qualitatively consistent with the existence of clusters.

These results demonstrate the potential to improve pinning in $Bi_2Sr_2CaCu_2O_8$ with spatially extended defects in order to overcome two-dimensional (pancake) vortex effects. Effective pinning centers need not be radiation induced; other promising structures include grain boundaries and precipitates.[20] We are optimistic that novel microstructures in $Bi_2Sr_2CaCu_2O_8$ can lead to increased vortex-defect interaction energies and thus higher critical currents at high temperatures and fields.

We thank Mark Kirk, Argonne National Laboratory, and Alan Marwick, IBM, for helpful discussions on ion irradiation damage. J.A.C. acknowledges funding support from the MIT Center for Material Science and Engineering, NSF Grant No. DMR-9022933.

[1] R. B. van Dover, L. F. Schneemeyer, E. M. Gyorgy, and J. V. Waszczak, Appl. Phys. Lett. 52, 1910 (1988).
[2] K. Heine, J. Tenbrick, and M. Thoner, Appl. Phys. Lett. 55, 2441 (1989).
[3] K. H. Sandhage, G. N. Riley, Jr., and W. L. Carter, J. Mater. 43, 21 (1991).
[4] T. T. M. Palstra, B. Batlogg, L. F. Schneemeyer, and J. V. Waszczak, Phys. Rev. Lett. 61, 1662 (1988).
[5] P. L. Gammel, L. F. Schneemeyer, J. V. Waszczak, and D. J. Bishop, Phys. Rev. Lett. 61, 1666 (1988).
[6] T. T. M. Palstra, B. Batlogg, L. F. Schneemeyer, and J. V. Waszczak, Phys. Rev. B 43, 3756 (1991).
[7] D. R. Nelson and S. Seung, Phys. Rev. B 39, 9153 (1989).
[8] W. Kritscha, F. M. Sauerzopf, H. W. Weber, G. W. Crabtree, Y. C. Chang, and P. Z. Jiang, Europhys. Lett. 12, 179 (1990).
[9] W. Gerhauser, H. W. Neumuller, W. Schmidt, G. Ries, G. Saemann-Ischenko, H. Gerstenberg, and F. M. Sauerzopf, Physica (Amsterdam) C 185-189, 2273 (1991).
[10] H. W. Weber and G. W. Crabtree, in *Studies of High Temperature Superconductors*, edited by A. V. Narlikar (Nova Science, New York, 1991), Vol. 9, and references therein.
[11] W. Gerhauser, G. Ries, H. W. Neumuller, W. Schmidt, O. Eibl, G. Saemann-Ischenko, and S. Klaumunzer, Phys. Rev. Lett. 68, 879 (1992).
[12] J. R. Thompson, Y. R. Sun, H. R. Kerchner, V. K. Christen, B. C. Sales, B. C. Chakoumakos, A. D. Marwick, L. Civale, and J. O. Thomson, Appl. Phys. Lett. 60, 2306 (1992).
[13] L. F. Schneemeyer, R. B. van Dover, S. H. Glarum, S. A. Sunshine, R. M. Fleming, B. Batlogg, T. Siegrist, J. H. Marshall, J. V. Waszczak, and L. W. Rupp, Jr., Nature 332, 422 (1988).
[14] E. M. Gyorgy, R. B. van Dover, K. A. Jackson, L. F. Schneemeyer, and J. V Waszczak, Appl. Phys. Lett. 55, 283 (1989).
[15] J. Biersack and L. Haggmark, Nucl. Instrum. Methods, 174, 257 (1980); J. F. Ziegler, J. P. Biersack, and U. Littmark, *The Stopping and Range of Ions in Solids* (Pergamon, New York, 1985).
[16] L. Civale, A. D. Marwick, T. K. Worthington, M. A. Kirk, J. R. Thompson, L. Krusin-Elbaum, Y. Sun, J. R. Klem, and F. Holtzberg, Phys. Rev. Lett. 67, 648 (1991).
[17] M. A. Kirk and H. W. Weber (unpublished).
[18] R. B. van Dover, E. M. Gyorgy, A. E. White, L. F. Schneemeyer, R. M. Fleming, R. J. Felder, and J. V. Waszczak, *Advances in Superconductivity III*, edited by K. Kajimura and H. Hayakawa (Springer, Berlin, 1991), p. 467.
[19] A. M. Campbell and J. E. Evetts, Adv. Phys. 21, 199 (1972).
[20] D. Shi, M. S. Boley, U. Welp, and J. G. Chen, Phys. Rev. B 40, 5255 (1989).

ABSTRACT MODEL 1991 FALL MEETING
ABSTRACT DEADLINE: JULY 1, 1991

Submitted to: Symposium H (Letter) JOINT SESSION WITH SYMPOSIUM A
Symposium Title: HIGH TEMP SUPERCONDUCTORS
Second Choice Symposium A (Letter) (JOINT SESSION WITH SYMPOSIUM H
Symposium Title: BEAM-SOLID INTERACTIONS

MODIFICATION OF THE FLUX PINNING IN SINGLE CRYSTAL $Bi_{2.2}Sr_2Ca_{0.8}Cu_2O_{8+\delta}$ BY IRRADIATION WITH VARIOUS IONS. J.A. Cutro, Dept. of Physics, M.I.T., Cambridge, MA; R.B. van Dover, L.F. Schneemeyer, A.E. White, AT&T Bell Laboratories, Murray Hill, NJ; T.P. Orlando, EECS, M.I.T., Cambridge, MA; and D.A. Rudman, N.I.S.T., Boulder, CO.

The low intrinsic flux pinning in $Bi_{2.2}Sr_2Ca_{0.8}Cu_2O_{8+\delta}$ limits the technological potential of weak-link-free wires based on this material, and is of scientific interest as well. Previous experiments on $Ba_2YCu_3O_{7-\delta}$ have shown that ion-beam-induced defects can serve as effective pinning centers, so we have investigated the effect on flux pinning of different types of extrinsic defects introduced by irradiation with various ions. Changes in the pinning were examined by comparing the resistive transition, current-voltage characteristics, and magnetization in zero, low (0.05 Tesla) and high (> 1.5 Tesla) magnetic fields before and after irradiation. Fluences of H^+, He^+ and Ne^+ were selected to produce equivalent damage (vacancy production) according to the TRIM91 program. The crystals were sufficiently thin so as to assure nearly complete penetration of the sample by the ions. We find that defects introduced by irradiation result in higher pinning energies (as inferred from the slope of *log* ρ *vs.* $1/T$) for higher ion masses. This is also reflected in a decrease in the temperature and field sensitivity of the critical current as inferred from magnetization measurements. Based on this trend, irradiations with a yet heavier ion (Ar^+) are currently being performed and will be reported.

Angular dependence of the magnetic-field-induced resistive transition in single-crystal $Bi_{2.2}Sr_2Ca_{0.8}Cu_2O_{8+\delta}$

J. Y. Juang,* J. A. Cutro,† and D. A. Rudman*
Massachusetts Institute of Technology, Cambridge, Massachusetts 02139

R. B. van Dover, L. F. Schneemeyer, and J. V. Waszczak
AT&T Bell Laboratories, Murray Hill, New Jersey 07974
(Received 22 June 1988)

We report here detailed measurements of the angular and temperature dependence of the magnetic-field-induced resistive transition in single-crystal $Bi_{2.2}Sr_2Ca_{0.8}Cu_2O_{8+\delta}$. Resistance is observed in the sample for small values of applied field (≈ 100 Oe) even at low current densities (< 10 A/cm^2). This suggests that the resistive transition does not reflect the upper-critical field of the superconductor in a simple manner, but is complicated by flux-flow effects. Consequently, the angular dependence of the resistive transition cannot be fit by any standard model for anisotropic critical fields in superconductors. We find anisotropic ratios as large as 50 for fields applied perpendicular and parallel to the $\hat{c}$ axis of the crystal, indicating large differences in the viscosity for flux motion in the two directions.

The recent discovery of high-temperature superconductivity in the nonrare-earth-based compound $Bi_{2.2}Sr_2Ca_{0.8}Cu_2O_{8+\delta}$ (Refs. 1–3) has provided another member of the cuprate family to study. Structurally, this compound differs from the $YBa_2Cu_3O_7$ superconductors in several respects.[4,5] The Cu-O chains found in $YBa_2Cu_3O_7$ are replaced by Bi-O edge-shared tetrahedra in $Bi_{2.2}Sr_2Ca_{0.8}Cu_2O_{8+\delta}$, perhaps leading to more two-dimensional-like behavior in the latter system. The pair of Cu-O planes believed to be central to superconductivity in these materials are apparently more weakly coupled than in $YBa_2Cu_3O_7$, as suggested by the higher anisotropy in the resistivity of this material.[6] Finally, unlike $YBa_2Cu_3O_7$, there is no twinning in the a-b plane in this system.

In this study we have measured the angular and temperature dependence of the "critical field" on a single-crystal sample of $Bi_{2.2}Sr_2Ca_{0.8}Cu_2O_{8+\delta}$. Our results, while extremely interesting, are not easily interpreted in terms of the conventional definition of the critical field. We find instead that there is an onset of resistance across the sample for fields as low as 100 Oe, even for current densities as small as 10 A/cm^2 and for temperatures as low as 77 K. The shape of the resistive transition depends strongly on the orientation of the crystal in the magnetic field, leading to anisotropy ratios as large as 50 for fields applied perpendicular and parallel to the $\hat{c}$ axis of the crystal. These results reflect the anisotropic nature of the flux-flow resistivity in these materials, and are not a direct measure of the upper critical field of the material.

Single-crystal samples for this study were grown from alkali chloride fluxes, as described previously.[7] The indicated stoichiometry, $Bi_{2.2}Sr_2Ca_{0.8}Cu_2O_{8+\delta}$, was determined from x-ray structure refinement. The crystals form as thin rectangular plates, typically $1\times2\times0.001$ mm^3, with the $\hat{c}$ axis normal to the plate. Low resistance contacts for transport measurements were made using Ag contact pads and silver cement.[8] Measurements of the resistive transition as a function of the applied magnetic field were made at the Francis Bitter National Magnet Laboratory using a standard four-point technique with a constant current density of approximately 10 A/cm^2. The sample temperature was measured in zero field using both platinum and carbon-glass resistance thermometers, and was controlled in field with a capacitance thermometer. Temperature control of better than 0.1 K can be achieved with this technique. The cryostat was placed on a rotating table to vary the direction of the applied field relative to the $\hat{c}$ axis of the sample. The angular resolution was better than half a degree. As will be seen in the following discussion, the large anisotropies in these samples makes this degree of angular resolution necessary.

Figure 1 shows the temperature dependence of resistivity as a function of magnetic field for fields parallel and perpendicular to the $\hat{c}$ axis of the crystal. The zero-field curve shows the high quality of the sample; the sample resistance goes to zero at 84 K. However, in the presence of a small applied magnetic field the sample exhibits nonzero resistance even for temperatures far below T_c. Details of the low-field current-voltage characteristics of these samples are reported elsewhere,[9] and verify the absence of any threshold current for the onset of resistance in this temperature regime for fields greater than 100 Oe.

The angular dependence of the field-induced resistive transition is shown in Fig. 2 for a sample temperature of 83 K. The resistance is normalized to the extrapolated normal-state resistance of the sample at the measurement temperature, as indicated by the dashed line in Fig. 1. As described above, resistance is immediately developed upon application of the field. Similar effects were seen for temperatures down to 77 K. The shape of the transition remains essentially unchanged until the field is oriented to within 30° of the a-b planes, and the shape changes rapidly only when the field is within 10° of the a-b plane. The transition shape is distinctly different from the field-broadened transitions typically observed in $YBa_2Cu_3O_7$ single-crystal samples,[10] and supports our view that the

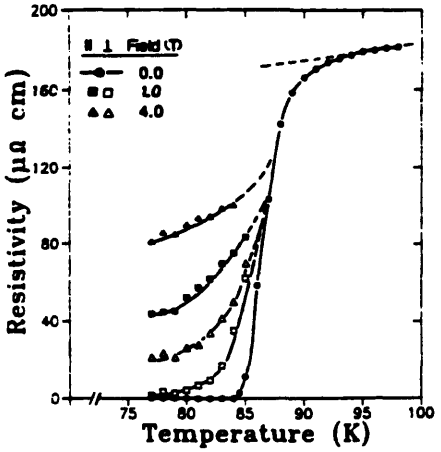

FIG. 1. Change in the temperature dependence of the resistive transition as a function of applied magnetic field for single crystal $Bi_{2.2}Sr_2Ca_{0.8}Cu_2O_{8+\delta}$. Field is applied both parallel to (solid points) and perpendicular to (open points) the ĉ axis of the crystal. Lines are to guide the eye only.

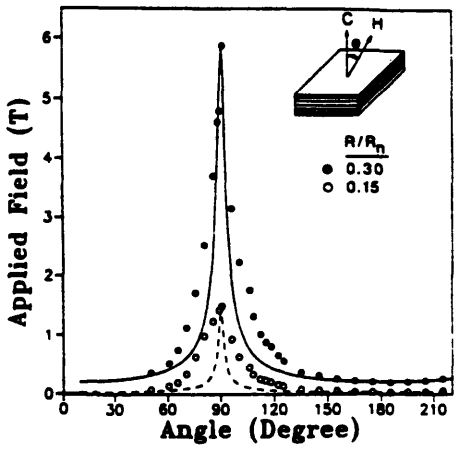

FIG. 3. Angular dependence of the field-induced resistive transition for two values of the normalized resistance measured at 83 K. Lines represent fits to the data using the effective-mass model for anisotropic superconductivity.

resistive transition represents a flux-flow-induced voltage regime, and is not a direct measurement of the critical field transition of the superconductor.

The detailed angular dependence of the applied field anisotropy for the resistive transition is shown in Fig. 3. Here we plot the field required to return the sample to 15% (open circles) and 30% (closed circles) of the normal-state resistance as a function of the field direction. This is equivalent to taking a horizontal cut in Fig. 2 at R/R_n values of 0.15 and 0.30, and is the standard criterion used to define the upper critical field in traditional

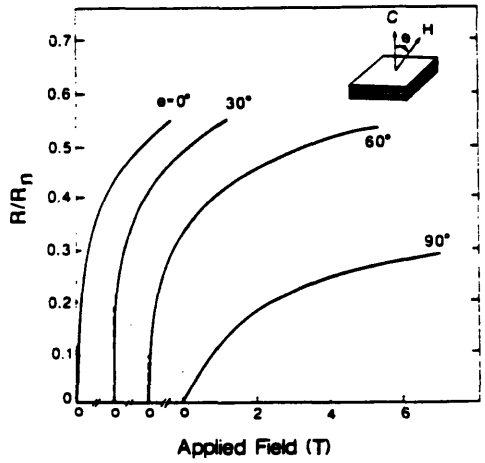

FIG. 2. Resistive transition as a function of applied field for various field orientations relative to the crystal ĉ axis. Measurement temperature was 83 K. Resistance has been normalized to the extrapolated normal-state resistance at that temperature.

anisotropic superconductors.[11] The anisotropies between perpendicular and parallel orientations (with respect to the ĉ axis of the crystal) are 50 and 30, respectively, for these two definitions. This is a much larger anisotropy than has been reported for either the critical field or critical current of other high-temperature superconductors.[12] Note that the narrowness of the angular dependence emphasizes the need for accurate field alignment in any measurement of the anisotropic properties of this material.

We have attempted to fit this angular-dependent data with both the effective-mass model[13] and Tinkham's thin-film formula[14] for critical field anisotropy of superconductors. The curves shown in Fig. 3 are fits to the data using the effective-mass model with the anisotropy ratio as the only input parameter. (For such large values of anisotropy the effective-mass model and Tinkham's model are indistinguishable on this scale.) While neither model accounts for the data well, the agreement between the fit and the data improves for larger R/R_n values. Recent results by Palstra, Batlogg, Schneemeyer, and Cava[15] on $Bi_{2.2}Sr_2Ca_{0.8}Cu_2O_{8+\delta}$ single crystals show similarly poor fits to the effective-mass model when the criterion for the transition is chosen as $R/R_n=0.3$, but show greatly improved fits for $R/R_n=0.5$, continuing the trend we have observed. For comparison, in both traditional superconductors[11] and $YBa_2Cu_3O_7$ single crystals[12,16] the angular dependence of the resistive transition in an applied field can be fit with the effective-mass model relatively independent of the value of R/R_n chosen, indicating that the upper critical field phase boundary is being measured directly. Our results for $Bi_{2.2}Sr_2Ca_{0.8}Cu_2O_{8+\delta}$ indicate that the resistive transition at the phase boundary is modified by flux-flow effects. We speculate that at low values of R/R_n the onset of resistance may result primarily from flux flow, while higher values of R/R_n may probe the phase boundary.

The observed anisotropy shown in Fig. 3 corresponds to

large differences in the flux-flow viscosity for the two field directions. In the simple model for flux flow the viscosity parameter β is defined by

$$\frac{\rho_f(t,B,\theta)}{\rho_n} = \frac{1}{\beta(t)} \frac{B}{H_{c2}(t,\theta)} \quad (1)$$

where ρ_f is the flux-flow resistivity, ρ_n is the normal-state resistivity, B is the flux density in the superconductor (corresponding to the applied magnetic field), H_{c2} is the upper critical field, and $t = T/T_c$. In the Bardeen-Stephen[17] model $\beta(t) = 1$, while a more sophisticated dirty limit calculation by Gor'kov and Kopnin[18] (based on the kinetic equation of Eliashberg) yields a more complicated temperature and field dependence. While the full temperature and field dependence of ρ_f has not been calculated, it is clear that the flux-flow resistivity is at least indirectly related to the upper critical field H_{c2}. Work is currently underway to extract information about $H_{c2}(T)$ in this system from the flux-flow resistivity data.

Figure 4 shows the temperature dependence of three different R/R_n values for fields parallel and perpendicular to the $\hat{c}$ axis of the crystal. There is a strong negative curvature for the perpendicular field direction in all cases. This result is different from other reports of the critical field in this material, where a linear temperature dependence was found for both field orientations.[15,19] Although the curve shape is suggestive of two-dimensional effects for which $H_{c2} \propto (1-t)^2$, the curves cannot be fit by a parabolic temperature dependence.

In summary, we have measured the detailed angular dependence of the resistive transition in a magnetic field of single-crystal $Bi_{2.2}Sr_2Ca_{0.8}Cu_2O_{8+\delta}$. We find the anisotropy to be much larger than reported values for other high-temperature superconductors. The observed field-induced resistance in the sample is attributed to flux flow, which begins at fields as low as 100 Oe in this temperature regime. The large anisotropy is attributed to a correspondingly large difference in the viscosity for flux motion in the a-b plane relative to motion normal to the a-b plane. Determination of the upper critical field from these data should be possible, but extreme caution should be used in interpreting the magnetic-field-induced resistivity as directly reflecting the upper critical field of the material.

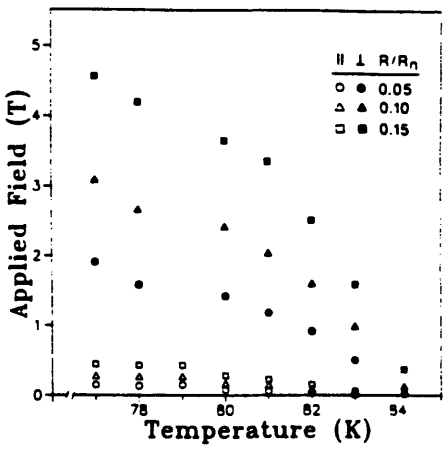

FIG. 4. Temperature dependence of the field-induced resistive transition for three different values of R/R_n. Field direction is parallel to (open symbols) and perpendicular to (closed symbols) $\hat{c}$ axis of crystal.

We would like to thank T. P. Orlando, T. Palstra, and B. Batlogg for useful discussion. We gratefully acknowledge the help of the National Magnet Laboratory in performing these experiments. The MIT portion of this work was supported by the Center for Materials Science and Engineering (NSF Grant No. DMR 87-19217).

*Department of Materials Science and Engineering.
†Department of Physics.

[1]H. Maeda, Y. Tanaka, M. Fukutomi, and T. Asano, Jpn. J. Appl. Phys. 27, L209 (1988).
[2]R. M. Hazen, C. T. Prewitt, R. J. Angel, N. L. Ross, L. W. Finger, C. G. Hadidiacos, D. R. Veblen, P. J. Heaney, P. H. Hor, R. L. Meng, Y. Y. Sun, Y. Q. Wang, Y. Y. Xue, Z. J. Huang, L. Gao, J. Bechtold, and C. W. Chu, Phys. Rev. Lett. 60, 1174 (1988).
[3]C. W. Chu, J. Bechtold, L. Gao, P. H. Hor, Z. J. Huang, R. L. Meng, Y. Y. Sun, Y. Q. Wang, and Y. Y. Xue, Phys. Rev. Lett. 60, 941 (1988).
[4]S. A. Sunshine, T. Siegrist, L. F. Schneemeyer, D. W. Murphy, R. J. Cava, B. Batlogg, R. B. van Dover, R. M. Fleming, S. H. Glarum, S. Nakahara, R. Farrow, J. J. Krajewski, S. M. Zahurak, J. V. Waszczak, J. H. Marshall, P. Marsh, L. W. Rupp, Jr., and W. F. Peck, Phys. Rev. B 38, 893 (1988).
[5]J. M. Tarascon, Y. Le Page, P. Barboux, B. G. Bagley, L. H. Greene, W. R. McKinnon, G. W. Hull, M. Giroud, and D. M. Hwang, Phys. Rev. B 37, 9382 (1988).
[6]S. Martin, A. T. Fiory, R. M. Fleming, L. F. Schneemeyer, and J. V. Waszczak, Phys. Rev. Lett. 60, 2194 (1988).
[7]L. F. Schneemeyer, R. B. van Dover, S. H. Glarrum, S. A. Sunshine, R. M. Fleming, B. Batlogg, T. Siegrist, J. H. Marshall, J. V. Waszczak, and L. W. Rupp, Jr., Nature 332, 422 (1988).
[8]R. B. van Dover, L. F. Schneemeyer, E. M. Gyorgy, and J. V. Waszczak, Appl. Phys. Lett. 52, 1910 (1988).
[9]R. B. van Dover, L. F. Schneemeyer, E. M. Gyorgy, and J. V. Waszczak (unpublished).
[10]Y. Iye, T. Tamegai, H. Takeya, and H. Takei, Jpn. J. Appl. Phys. Lett. 26, L1850 (1987); T. Sakakibara, T. Goto, Y. Iye, N. Miura, H. Takeya, and H. Takei, Jpn. J. Appl. Phys. Lett. 26, L1892 (1987).
[11]D. A. Rudman, J. Y. Juang, R. B. van Dover, S. Nakahara, D. W. Capone II, and J. Talvacchio, IEEE Trans. Magn. MAG-23 831 (1987).
[12]T. K. Worthington, W. J. Gallagher, D. L. Kaiser, F. H. Holtzberg, and T. R. Dinger, in *Proceedings of the International Conference on High-T_c Superconductors and Materials and Mechanisms of Superconductivity, Interlaken, Switzerland, 1988*, edited by J. Müller and J. L. Olsen [Physica C 153–155, 32 (1988)].
[13]D. R. Tilley, Proc. Phys.-Soc. (London) 86, 289 (1965); 86,

678 (1965).
[14]M. Tinkham, Phys. Lett. 9, 217 (1964).
[15]T. M. Palstra, B. Batlogg, L. F. Schneemeyer, and R. J. Cava (unpublished).
[16]J. A. Cutro, J. Y. Juang, D. A. Rudman, R. B. van Dover, L. F. Schneemeyer, and J. V. Waszczak (unpublished).
[17]J. Bardeen and M. J. Stephen, Phys. Rev. 140, A1197 (1965).
[18]L. P. Gor'kov and M. B. Kopnin, Zh. Eksp. Teor. Fiz. 64, 356 (1973), [Sov. Phys. JETP 37, 183 (1973)]; Zh. Eksp. Teor. Fiz. 65, 396 (1974) [Sov. Phys. JETP 38, 195 (1974)]; Usp. Fiz. Nauk 116, 413 (1975) [Sov. Phys. Usp. 18, 496 (1975)].
[19]J. H. Kang, R. T. Kampwirth, and K. E. Gray (unpublished).

ANGULAR DEPENDENCE OF THE CURRENT-VOLTAGE CHARACTERISTICS OF SINGLE CRYSTAL $Bi_{2.2}SR_2CA_{0.8}CU_2O_8$ IN A MAGNETIC FIELD.*

J. A. Cutro, J. Y. Juang, and D. A. Rudman, MIT, Cambridge, MA. 02139.

We report on the detailed angular dependence of the onset of resistance in single crystal $Bi_{2.2}Sr_2Ca_{0.8}Cu_2O_8$. We measure the current-voltage characteristics as a function of the angle between the applied field and the crystal c-axis at various fields and temperatures. The observed onset of resistance for small values of the applied field (<100 Oe) even at low current densities (<10 A/cm^2) suggests that the transition is more representative of flux flow effects than of the upper critical field. For temperatures above 77K and for fields applied parallel to the c-axis the current-voltage characteristics are linear for low currents, suggesting that it may be possible to extract critical field information using a Bardeen-Stephen model. We find anisotropic ratios as large as 50 for fields applied perpendicular and parallel to the c-axis of the crystal, indicating large differences in the viscosity for flux motion in the two directions. The shape of the current-voltage characteristic remains relatively unchanged until the field is within about 20^o of the a-b planes, where there is a sudden change to a more standard threshold-like behavior.

*Supported by the Center for Material Science and Engineering, MIT, NSF DMR87-19217.

Mailing Address of Author: J. A. Cutro
MIT, 13-2057
77 Massachusetts Ave.
Cambridge, MA. 02139 USA
Phone: (617) 253-4213